University of Alberta

Synthesis and Catalytic Applications of Iron-Palladium Nanostructures

by

Shuai Zhou

A thesis submitted to the Faculty of Graduate Studies and Research
in partial fulfillment of the requirements for the degree of

Master of Science

Department of Chemistry

Fall 2011
Edmonton, Alberta

Abstract

This thesis focuses on synthesis, characterization and catalytic applications of iron-based nanoparticles (NPs) in Suzuki-Miyaura cross-coupling reactions.

Palladium "decorated" Fe@Fe_xO_y NPs (Fe@Fe_xO_y/Pd NPs) were prepared making use of established reducing nature and coordinating ability of the Fe@Fe_xO_y NPs. Fe@Fe_xO_y/Pd NPs were evaluated and found to exhibit high catalytic activity in a series of Suzuki-Miyaura cross-coupling reactions in aqueous solution at room temperature in air. The Fe@Fe_xO_y/Pd system was reused efficiently and only a slight loss of activity was observed after the third reaction. Furthermore, Fe@Fe_xO_y/Pd has special retention ability for Pd species making leached Pd negligible. The effect of Fe@Fe_xO_y on the catalytic activity for Suzuki coupling was investigated and no visible effect was found.

Three Fe-Pd nanostructures—"nanodendrites" (ND), nanoparticles (NP1 and NP2) were synthesized by simultaneous thermal decomposition of $Fe(CO)_5$ and reduction of $Pd(acac)_2$. ND exhibit a dendritic structure with an average diameter of 51.6 nm, while NP1 and NP2 exhibit a pseudospherical morphology with average diameters of 12.8 nm and 17.7 nm, respectively. The three nanostructures all contain crystalline FePd alloy and iron oxides were formed due to exposure to air. They have high catalytic activities toward Suzuki cross-coupling reactions, and ND have the highest activity among them. ND were recycled by applying a magnet and reused three times with some loss of activity which is readily attributed to material handling limitations.

Acknowledgements

This thesis is not only from my own contribution, but also from contribution of those people who helped me in every way. It is a pleasure to express my gratitude to all of the people for helping me go through three-year graduate studies in a variety of aspects. I could not have done this if it were not with your help and support.

First and foremost I would like to thank my supervisor Dr. Jonathan Veinot, for his immense guidance and support throughout my graduate studies. I would have been lost without him. His passion and expertise in Chemistry, creative ideas, insightful advice, exciting encouragement and patient assistance in writing manuscripts and thesis have made my research work keep going forward. He allowed me to try things on my own, which sometimes wasted money and time. Jon is also a great friend out of lab, thank you for helping and supporting me during the most difficult times.

Members of the Veinot Group are thanked for stimulating discussions, suggestions, encouragement and all the fun we have had in the last three years. You guys are awesome and provide such an amazing and dynamic environment in which to learn and grow as a chemist. You are always there whenever I need help in the lab. Many thanks go in particular to Melanie Johnson for her work on Chapter 2, Zhenyu Yang for doing most of TEM in this thesis and Steve Barry for his help with XRD.

I want to thank Chemistry staff in administration, analytical & instrumentation laboratory, machine shop and glass shop for their professional support and help, Guangcheng Chen at Earth and Atmospheric Sciences for ICP-MS, staff at Alberta Center for Surface Engineering and Science (ACSES) for XPS, Diane Caird at Earth and Atmospheric Sciences for XRD.

I wish to thank my supervisory committee members Drs. Steven Bergens and Julianne Gibbs-Davis for their supervision, great advice and insightful comments.

Last but never the least, I need to thank my family and friends. I am indebted to my parents for everything they have done for me. My dad makes me feel confident in my research, and my mom always provides me useful life advice. Despite the geographical distance from China to Canada, they are always nearby. It is hard using words to express my gratitude to them. None of this could have happened without my wife, Manhui Liu. You encouraged, supported, understood, and loved me at every moment, and I am intellectually indebted to your ideas and your conversations. You are always with me no matter happy or difficult times.

Table of Contents

List of Tables

List of Figures

List of Schemes

List of Symbols and Abbreviations

Å	angstrom
°C	degree Celsius
λ	wavelength
μm	micrometre
μL	microlitre
μg	microgram
atm	atmosphere
acac	acetylacetonate
AB	ammonia borane
Ar	aryl
ACA	1-adamantanecarboxylic acid
a.u.	arbitrary units
bcc	body centered cubic
bpd	barrels per day
DMF	dimethylformamide
E	electrochemical potential
EDX	energy dispersive X-ray spectroscopy
Et	ethyl
eV	electron volt
Fe@Fe_xO_y	iron oxide capped iron nanoparticles
FTS	Fischer-Tropsch synthesis
FWHM	full width at half maximum
GC-MS	gas chromatography-mass spectrometry
g	gram

h	hour
HR	high resolution
ICP-MS	inductively coupled plasma-mass spectrometry
M	molar
M	metal atom
ml	millilitre
min	minute
mol	mole
mmol	millimole
mg	milligram
MHz	megahertz
MΩ·cm	maga-Ohms-centimetre
MNP	magnetic nanoparticle
MRI	magnetic resonance imaging
NP	nanoparticle
NC	nanocrystal
nm	nanometer
ND	Fe-Pd nanodendrites
NP1	Fe-Pd nanoparticles, average diameter: 12.8 nm
NP2	Fe-Pd nanoparticles, average diameter: 17.7 nm
NMR	nuclear magnetic resonance
P	pressure
psi	pound per square inch
ppm	parts per million
PEG	polyethylene glycol
PRB	permeable reactive barrier
RT	room temperature
SAED	selected area electron diffraction

SEM	scanning electron microscopy
SASOL	South African Synthetic Oil Limited
T	temperature
TEM	transmission electron microscopy
TOF	turnover frequency
THF	tetrahydrofuran
TBP	tri-n-butylphosphine
wt.	weight
X	halogens (Cl, Br, I)
XPS	X-ray photoelectron spectroscopy
XRD	X-ray diffraction
ZVI	zero valent iron

Chapter 1: Introduction

Iron is an essential element for life on earth. It is the fourth most abundant element in the Earth's crust (i.e., 4.5%) and it is widely used in industry. Humankind started using metallic iron to fashion tools and weapons in ancient times (i.e., The Iron Age)[1] and now carbon containing iron alloys (steels) and low carbon iron alloys with other metals (alloy steels) are the most common metal materials in modern industrial use. This popularity is partly due to the hardness and strength of these materials. Iron also plays an important role in human physiology and it is present in many proteins and enzymes, such as hemoglobin, myoglobin and cytochromes.[2] Hemoglobin is the primary protein found in red blood cells and represents about two thirds of the body's iron. The vital role of hemoglobin is transporting oxygen from the lungs to the rest of the body, which is derived from its unique ability of binding to molecular oxygen via iron. Not having enough iron can lead to anemia. The most common symptoms of anemia are weakness and fatigue, which is because cells don't get enough oxygen. Iron exists in a wide range of oxidation states, −2 to + 6, of which +2 and +3 are the most common. Elemental iron reacts with oxygen in the air and water to form various oxide and hydroxide compounds and the most common are iron (II, III) oxide (Fe_3O_4) and iron (III) oxide (Fe_2O_3).

Over the past two decades, the tremendous developments in nanotechnology

are reflected in our expanded ability to design and control nanomaterials, their size, shape, chemical composition, and assembly that could lead to advanced applications.[3,4] A vast array of nanoscale objects and proto-type devices have been fabricated, such as nanospheres, nanorods, nanowires, nanorings, nanosensors and nanomotors.[3,4] These advances in nanotechnology have promoted new research in traditional disciplines involving the incorporation of nanoscale materials into established processes. Increasing attention has been paid to nanoscale materials based upon iron because of their unique magnetic and electronic properties. Iron and iron oxides can be manipulated by external magnetic fields and metallic iron has very strong electron-donating (i.e., reducing) ability. These magnetic nanoaprticles have tremendous advantages for many applications, including environmental remediation, catalyst support, contrast agents in magnetic resonance imaging (MRI), targeted drug delivery, biosensing applications and magnetic storage media.[5] This chapter will briefly review synthetic methods and catalytic applications of iron-containing nanoparticles (NPs).

1.1 Synthesis of Iron-Containing NPs

1.1.1 Synthesis of Iron and Iron Alloy NPs

The synthesis of iron nanoparticles (NPs) can be achieved via a variety of mechanical (i.e., "top-down") and chemical (i.e., "bottom-up") methods, however in all cases care must be exercised to ensure the particles do not oxidize. If oxidation occurs, particle surfaces are often terminated by an ill-defined oxide layer.

Mechanical ball milling has been widely employed by industry to yield ultrafine powders, metal alloys, paints and pigments. In contrast to chemical reduction (vide infra), ball milling is relatively straightforward: heavy, inert milling balls are used to strike and break bulk starting materials. Zhang and coworkers demonstrated precision ball milling,[6] with micro iron powder as the starting material produced zero valent iron (ZVI) NPs exhibiting specific surface area and reducing activity similar to those of the NPs synthesized by sodium borohydride reduction. The milling method is fully scalable and delivers nearly 100% yield of iron using no hazardous materials. However, it is very difficult to control particle size, and products are highly deformed with irregular shapes and contain many defects.

Zhang et al. developed a solution based procedure that yields metallic iron NPs that employs Fe (III) salts as an iron source and sodium borohydride as a reductant (Equation 1-1).[7,8,9] NPs generated using this approach are pseudospherical and size polydisperse. As a consequence of their inherent ferromagnetism, the Fe NPs form chain-like aggregates evident in TEM analysis (Figure 1-1).[10] Variations of this procedure employ inverse micelles containing the iron salt. Subsequent reduction of the salt inside the micelle leads to improved size control.[11,12]

$$4Fe^{3+} + 3BH_4^- + 9H_2O \longrightarrow 4Fe^0 + 3H_2BO_3^- + 12H^+ + 6H_2 \qquad \text{Equation 1-1}$$

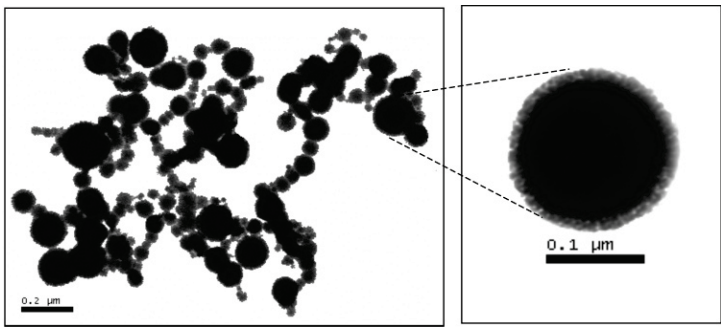

Figure 1-1. TEM images of iron NPs synthesized by sodium borohydride reduction, reproduced from ref. 10.

Reducing iron oxide NPs to metallic iron by H_2 at high temperature is another common method used by industry. This process begins with the precipitation of iron hydroxide from hydrolysis of Fe (III) salts that are dehydrated to yield iron oxide (hematite, α-Fe_2O_3). The hematite particles are subsequently reduced to the metallic state by hydrogen gas (Scheme 1-1).[13]

$$Fe^{3+} + 3OH^- \longrightarrow Fe(OH)_3 \xrightarrow{-H_2O} Fe_2O_3 \xrightarrow{H_2} Fe$$

Scheme 1-1. Iron NPs synthesized from iron oxide reduction by H_2

Thermal decomposition of iron pentacarbonyl (i.e., $Fe(CO)_5$) also provides metallic iron nanoparticles. Despite the well-established toxicity of $Fe(CO)_5$ and the CO by-product of this reaction, this approach provides small (i.e. $\lesssim$ 20 nm) uniform-sized metallic Fe NPs. Sun and co-workers synthesized amorphous monodisperse Fe NPs via a facile one-pot thermal decomposition of $Fe(CO)_5$ in octadecene in the presence of oleylamine.[14] TEM imaging (Figure 1-2a) showed the as-synthesized particles bear a core/shell structure with 8 nm diameter Fe core and 2.5 nm thick Fe_3O_4 oxide shell. The Fe_3O_4 oxide layer is formed as a result of exposure to air. More recently, the same research group reported the synthesis of

15 nm body centered cubic (bcc) Fe NPs via the decomposition of $Fe(CO)_5$ in the presence of oleylamine, oleic acid, and hexadecylammonium chloride (Figure 1-2b,c).[15] When exposed to ambient environments, the surface layers of the bcc-Fe were oxidized to crystalline Fe_3O_4. These bcc-Fe@Fe_3O_4 NPs exhibit substantially improved stability and an increased magnetic moment compared to amorphous Fe@Fe_3O_4 NPs, and exhibit an enhanced magnetic imaging contrast effect and have been proposed as robust probes for magnetic resonance imaging (MRI).

Many factors such as surfactant choice, concentration ratios, reaction times and temperature have been identified to influence particle size and morphology in the synthesis of iron NPs using thermal decomposition of $Fe(CO)_5$.[16] Our group found the presence of water increases nucleation events by lowering the activation energy for $Fe(CO)_5$ decomposition through water-gas-shift chemistry, which produces smaller particles.[17]

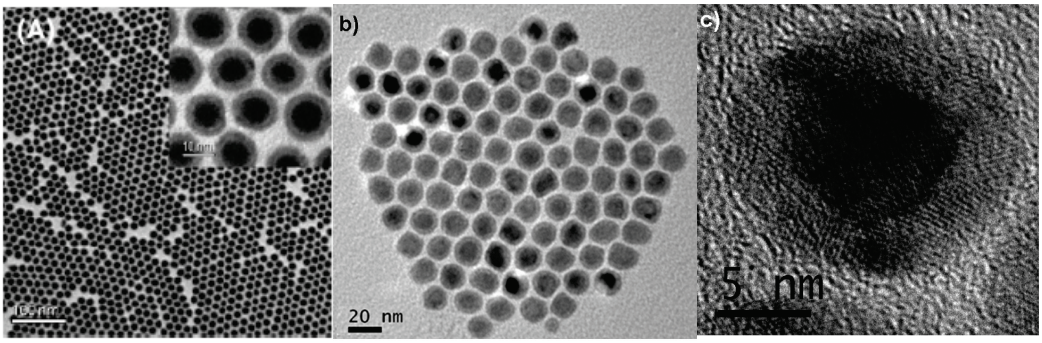

Figure 1-2. (a) TEM image of 4 nm/2.5 nm (radius) Fe@Fe_3O_4 NPs, (Inset) HRTEM image of the Fe@Fe_3O_4 NPs. (b) TEM image of the 15 nm bcc-Fe@ Fe_3O_4 NPs. (c) HRTEM image of a single bcc-Fe@Fe_3O_4 NP revealing the metallic bcc-Fe core and Fe_3O_4 shell with Fe (110) and Fe_3O_4 (222) planes indicated. Reproduced from refs. 14 and 15.

Building on their Fe nanoparticle work, Sun et al. reported the first synthesis of monodisperse FePt alloy NPs which employed the simultaneous reduction of platinum acetylacetonate ($Pt(acac)_2$) and thermal decomposition of $Fe(CO)_5$ in a mixture of oleic acid and oleylamine.[18] The size and composition of the resulting NPs were controlled via rational variation of synthetic parameters such as molar ratio of stabilizers to metal precursors and the molar ratio of two metal precursors (Figure 1-3).[18,19]

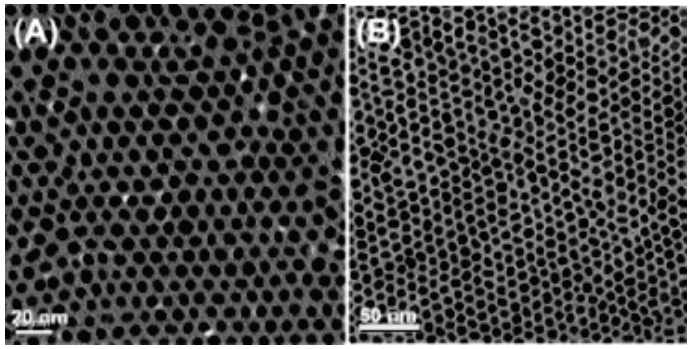

Figure 1-3. TEM bright field images of (A) 6 nm $Fe_{53}Pt_{47}$, (B) 9 nm $Fe_{44}Pt_{56}$. Reproduced from ref. 19.

1.1.2 Synthesis of Iron Oxide and Ferrite NPs

Among the iron oxides, γ-Fe_2O_3 (maghemite) and Fe_3O_4 (magnetite) nanomaterials have received far more attention than FeO. This is because FeO is prone to decompose into α-Fe and Fe_3O_4 via disproportionation or oxidize to form Fe_3O_4, γ-Fe_2O_3, and/or α-Fe_2O_3. These materials are of interest because of their magnetic response and intensive studies have been devoted to their colloidal synthesis. A wide variety of methods including coprecipitation, microemulsion synthesis, hydrothermal synthesis, and thermal decomposition have been employed.

Coprecipitation is a facile synthetic method that affords iron oxide NPs (i.e., Fe_3O_4 or γ-Fe_2O_3) from aqueous Fe^{2+}/Fe^{3+} salt solutions by the addition of a base (e.g., ammonia) under inert atmosphere at room temperature or at elevated temperature. The chemical reaction of Fe_3O_4 formation via coprecipitation is shown in Equation 1-2. Fe_3O_4 is transformed to γ-Fe_2O_3 in the presence of oxygen as shown in Equation 1-3. The size, shape, and composition of the magnetic NPs very much depend on the salt anions (e.g., chloride, sulfate, nitrate), the Fe^{2+}/Fe^{3+} ratio, the nature of the base, reaction temperature, pH, and ionic strength of the reaction media. Massart first performed the controlled preparation of Fe_3O_4 particles, which was precipitated out from a alkaline solution of $FeCl_3$ and $FeCl_2$.[20] When all of parameters mentioned above are modulated, it is possible to obtain polydisperse particles with a size ranging from 4.2 to 16.6 nm.[21] Other studies demonstrated the modulation of pH and ionic strength enables tailoring of particle size in the range of 2-15 nm. Recently, advances in preparing monodisperse magnetite NPs, of different sizes, have been realized by introducing organic additives such as oleic acid to the reaction mixture as stabilization agents.[22] The advantages of coprecipitation method lie in its simplicity, readily available cost-effective precursors, the use of aqueous solutions, and high overall yields. Despite these advantages, challenges associated with controlling particle size distribution remain.

$$Fe^{2+} + 2Fe^{3+} + 8\ OH^- \longrightarrow Fe_3O_4 + 4H_2O \qquad \text{Equation 1-2}$$

$$4Fe_3O_4 + O_2 \longrightarrow 6\gamma\text{-}Fe_2O_3 \qquad \text{Equation 1-3}$$

Given particles obtained from the coprecipitation method exhibit broad size distributions, alternative methods are being developed in efforts to realize NPs with more uniform sizes. Microemulsion methods are a promising approach as they employ aqueous nanodroplets in oil (i.e., inverse micelles) to constrain particle growth.[23] In this approach, aqueous iron salt solutions are encapsulated in surfactants that partition them from a surrounding organic solution. The size of the nanodroplet reactors is governed by the molar ratio of water to surfactant. An emulsion of cyclohexane/Brij-97/aqueous phase was used to form uniform γ-Fe_2O_3 NPs with size ranging from 2-8 nm by the coprecipitation reaction of ferrous and ferric salts with the organic base cyclohexylamine.[24] NPs of more complex iron oxides such as the spinel ferrite $MnFe_2O_4$ were synthesized using a similar approach that employed water-in-toluene inverse micelles with sodium dodecylbenzenesulfonate (NaDBS) surfactant.[25] Although particle size and shape are well controlled using the microemulsion method, this synthetic method suffers from low yield compared to the coprecipitation method due to low concentration of aqueous iron salt solution in nanodroplets.

Hydrothermal synthesis is yet another promising alternative that is performed in aqueous media under high pressure and temperature. Li et al. prepared Fe_3O_4 and $CoFe_2O_4$ NPs with uniform sizes of about 9 and 12 nm, respectively, by a liquid-solid-solution phase transfer and separation strategy.[26] The system consists of metal linoleate (solid), an ethanol-linoleic acid liquid phase, and a water-ethanol solution at different reaction temperatures under hydrothermal conditions. A phase transfer and separation occurs at the interfaces of the liquid, solid, and

solution phases present during the synthesis.

Monodisperse magnetic iron oxide NPs of small dimensions (i.e., ≤20 nm) may be synthesized through the thermal decomposition of a variety of organometallic precursors (e.g., iron pentacarbonyl, iron acetylacetonate, and iron N-nitrosophenylhydroxylamine (cupferron) complexes) in high-boiling organic solvents containing stabilizing surfactants. Alivisatos and co-workers prepared near-monodispersed γ-Fe_2O_3 nanocrystals (6-7 nm) through the solution-based pyrolysis of an iron-cupferron complex in trioctylamine at 200-300°C.[27] Similarly, Sun et al. used the high-temperature reaction of iron(III) acetylacetonate ($Fe(acac)_3$) with 1,2-hexadecanediol in phenyl ether in the presence of oleic acid and oleylamine to obtain monodisperse magnetite NPs with sizes variable from 3 to 20 nm in diameter.[28] An extension of this approach to the reaction of $Fe(acac)_3$ and $Co(acac)_2$ or $Mn(acac)_2$ with 1,2-hexadecanediol provides monodisperse $CoFe_2O_4$ or $MnFe_2O_4$ NPs.[29] Particle dimensions may be tuned from 3 to 20 nm by varying reaction temperatures or by employing seed-mediated growth (Figure 1-4). Hyeon et al. prepared monodisperse γ-Fe_2O_3 nanocrystals using $Fe(CO)_5$ decomposition in a mixture of octyl ether and oleic acid at 100°C.[30] While it is well established that the decomposition of $Fe(CO)_5$ generates metallic iron NPs, oxidation with trimethylamine oxide was used to further generate γ-Fe_2O_3 nanocrystals with trimethylamine as a gas by-product.

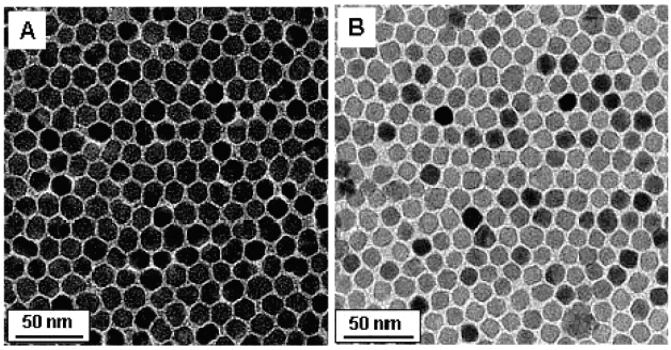

Figure 1-4. TEM images of (A) 14 nm $CoFe_2O_4$ and (B) 14 nm $MnFe_2O_4$ NPs, reproduced from ref. 29.

1.2 ZVI NPs for Environmental Remediation

Zero-valent iron nanoparticle technology is becoming a viable alternative for remediation of hazardous contaminants (e.g., heavy metals and chlorinated organics) from soil and groundwater. As a result of low cost, large surface-to-volume ratio, and high surface reactivity (i.e., reduction) of ZVI NPs, these materials are ideal for such applications. Granular ZVI was first employed in permeable reactive barrier (PRB) systems in early 1990s.[31] A PRB is an engineered zone of reactive material for water flowing-through, extending below the water table, designed to intercept and treat contaminated groundwater. Contaminants passing through the PRB are either degraded by and/or retained in the reactive barrier material. A variety of PRBs have been developed and installed at contaminated sites to treat a range of inorganic, organic, and radioactive contaminants.[31] However, these systems are costly and often difficult to construct. Injectable forms of ZVI NPs were developed to mitigate these problems. As a result of their small dimensions, it is possible to prepare ZVI NP slurries in water that can be injected under pressure and/or gravity flow into a contaminated

aquifer. ZVI NPs remain in suspension and flow with water for extended periods to establish an *in situ* treatment zone (Figure 1-5).[7]

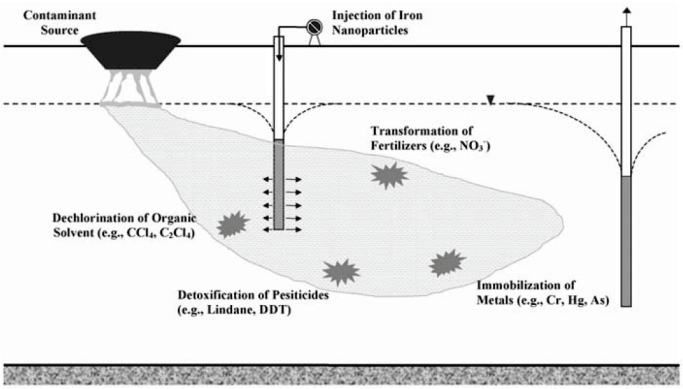

Figure 1-5. ZVI NPs for *in situ* remediation, reproduced from ref. 7.

ZVI NPs have a core-shell structure with a thin electrically conductive, passivating oxide shell of ca. 2-3 nm (see Figure 1-6).[32,33] The core consists of metallic iron that provides electrons that are responsible for the reactions that lead to remediating environmental contaminants. The passivating shell is composed of iron oxides (i.e., Fe_3O_4 and Fe_2O_3) and hydroxide (FeOOH) formed through the oxidation of metallic iron.[32,33] Zhang et al. determined oxide shell thickness of "freshly prepared" ZVI NPs is typically ~3 nm by using high-resolution transmission electron microscopy (TEM), high-resolution X-ray photoelectron spectroscopy (XPS) and complete oxidation reaction of the ZVI NPs by Cu(II).[34]

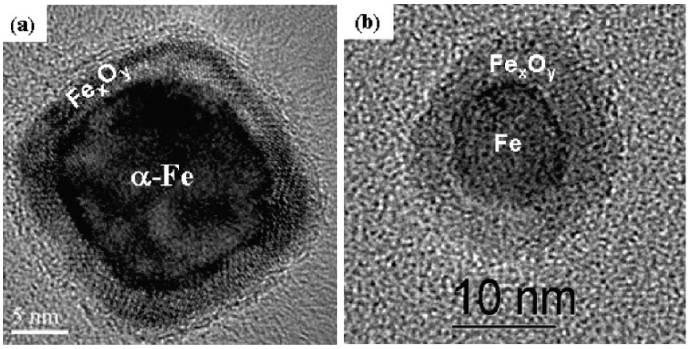

Figure 1-6. HRTEM images showing two types of Fe NPs with core-shell structure: (a) faceted core-shell particle; (b) spherical core-shell particle. Reproduced from ref. 32.

ZVI NPs are effective for the treatment of many pollutants commonly identified in groundwater, including chlorinated hydrocarbons, such as perchloroethene (PCE), trichloroethene (TCE) and carbon tetrachloride (CT), and residual organochlorine pesticides such as lindane and DDT (dichloro-diphenyl-trichloroethane), as well as heavy metals (Figure 1-7).[7-10, 35-38]

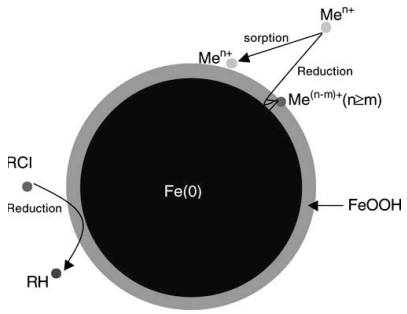

Figure 1-7. The model of ZVI NPs for pollutant treatment, reproduced from ref. 35.

The chemical principles underlying the transformation of halogenated hydrocarbons have been well investigated given their prevalence in soil and groundwater. ZVI NPs are an electron donor and participate in redox reactions that degrade certain contaminants (for example see Equation 1-4).

$$Fe^0 \longrightarrow Fe^{2+} + 2e^- \quad E^0 = -0.44\ V$$
$$3Fe^0 + 4H_2O \longrightarrow Fe_3O_4 + 8H^+ + 8e^- \qquad \text{Equation 1-4}$$
$$C_2Cl_4 + 4H^+ + 8e^- \longrightarrow C_2H_4 + 4Cl^-$$

As indicated by these half-cell reactions, ZVI NPs can be oxidized to ferrous iron or to Fe_3O_4, and the latter is more thermodynamically favoured above pH 6.1. As the reaction proceeds, ZVI NPs can become coated with a shell of oxidized

iron that renders them inactive.

The addition of catalytic transition metals suitable for promoting hydrogenation reactions enhances the rate and efficiency of remediation process. ZVI NPs decorated with palladium (ZVI/Pd NPs) are prepared by dispersing freshly prepared ZVI NPs in aqueous palladium nitrate. The Pd^{2+} is initially coordinated to particle surface through hydroxyl groups and subsequently reduced to Pd^0 by electrons supplied by metallic Fe core. Pd decorated ZVI NPs generally exhibit greater reactivity in the reduction of chlorinated hydrocarbons than their non-decorated counterparts. Under environmental conditions, reactions of chlorinated organic compounds (e.g., TCE) with ZVI/Pd NPs yield more saturated products (e.g., C_2H_6) and generate fewer toxic intermediates, such as dichloroethenes and vinyl chloride. These results are consistent with known palladium metal catalytic chemistry. Palladium metal is a well-known heterogeneous catalyst for gas-phase dehalogenation and hydrogenation reactions. Mechanistic studies of the degradation of simple aliphatic chlorinated compounds in water suggest the iron component of the ZVI NPs provides electrons to water to form hydrogen and the palladium decoration facilitates activation of chlorinated compounds and formation of atomic hydrogen that act as the reducing agent responsible for dechlorination and hydrogenation reactions.[39]

In addition to the remediation of chlorinated organics from the environment, a range of iron-based technologies have been developed to address the problems of heavy metal contamination (e.g., arsenic, chromium and lead) in drinking water. This remediation process also relies on the reductive capabilities of the metallic

Fe core and coordinative abilities of Fe-OH surface moieties of the ZVI NPs responsible for the Pd deposition process described above.

1.3 Iron-Containing NPs as Catalyst Supports and Catalysts

Advances in our understanding and ability to prepare materials at the nanoscale have facilitated rational design and control of catalysts and catalytic processes.[40] A key goal in designing a useful catalyst is the realization of satisfactory activity and reaction selectivity. Two broad classes of catalysts are often identified, homogeneous and heterogeneous. Homogeneous catalysts possess the distinct advantages of being well-defined and readily dissolved in the reaction medium in question. Therefore, catalytic sites are readily accessible to reactants and reaction mechanisms are generally well understood. As a result, many homogeneous catalysts show high activity and selectivity.[41-44] Unfortunately, some of the advantages of homogeneous catalytic systems are also their shortcomings. In light of their solubility, removal of expensive catalysts from reaction products is far from trivial leading to contamination and loss of expensive noble metals.[45,46] To overcome these problems, many different approaches have been used to generate effective and recyclable catalysts.[47,48] Nanoscale metal-based catalysts and supports can improve catalyst recovery while retaining the high activity of homogeneous catalysts. Unlike conventional micrometer-sized supports, NPs may be readily dispersed in solvents to yield non-opalescent solution-like suspensions. In this regard NP catalysts may be viewed as pseudo-homogeneous systems. Moreover if the nanoscale support is magnetic (e.g., Fe_3O_4 NPs), effective

separation may be achieved upon exposure to a magnetic field. As a result, the design and application of catalysts supported on magnetic nanoscale supports has been the subject of substantial research.[49,50]

Catalytic species can be immobilized onto magnetic NP surfaces by a variety of methods, such as direct deposition or immobilization through surface bonded chelating moieties. However, magnetic NPs (MNPs) tend to aggregate in solution to form clusters when treated without any protection agents, thus negating their unique properties derived from their small size.[51,52] Therefore, maintaining the stability of these particles for a long time without aggregation and acid erosion is an important issue that must be addressed in the material design. In the case of iron oxide NPs, surface coatings of organic stabilizers (e.g., surfactants and polymers) or silica, carbon or metal oxides are employed.[53-62] These surface treatments not only stabilize the MNPs, but also allow further modification of the surface with other functional groups. Among MNPs, magnetite (Fe_3O_4) and maghemite (γ-Fe_2O_3) are commonly used as catalyst supports.

1.3.1 Heterogenization of Homogeneous Catalysts Using MNPs

Heterogenization (i.e., rendering a well-defined homogeneous catalyst less compatible with reaction media) of the efficient homogeneous catalysts by tethering them to magnetic nanoscale supports has received considerable interest because the resulting catalytic systems can be efficiently reused whilst keeping the inherent activity of the original catalytic center.[54,55,59,60] Generally, these catalytic systems can be well dispersed in the reaction media to retain the original catalytic activity. Magnetic and chemically innocent supports have been

frequently prepared by coating MNPs with a layer of silica.[63-65] This approach affords a platform for effective particle surface functionalization while maintaining the favourable magnetic properties. Some relevant examples are discussed below.

Gao and co-workers immobilized palladium complex with N-heterocyclic carbene ligand (Pd-NHC complex) onto the surface of polymer coated γ-Fe_2O_3 NPs.[66] 1-Methylimidazole was first tethered to poly(4-vinylbenzyl chloride) terminated surface of γ-Fe_2O_3 NPs, and a subsequent deprotonation of the imidazolium group in the presence of Na_2CO_3 generated the NHC ligand that form strong complex with $Pd(OAc)_2$ to give the desired catalyst (Scheme 1-2). These heterogenized palladium catalyst exhibited superior activity (70-89%) to the Suzuki cross-coupling of aryl bromides and iodides with arylboronic acids, and could be recycled by magnetic decantation and used for five consecutive times without significant loss in activity.

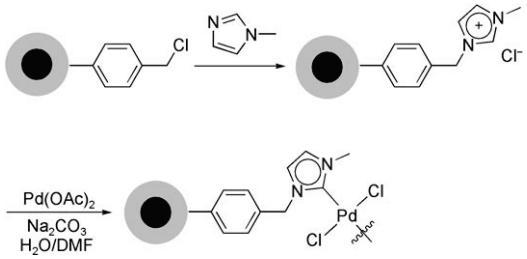

Scheme 1-2. Synthesis of iron oxide NP-supported Pd-NHC complex, reproduced from ref. 66.

Jin et al. demonstrated Fe_3O_4 NP-supported (methyl)(triphenylphosphine)(4-amino-3-pentene-2-one)palladium complex is an efficient catalyst for coupling reactions of aryl chlorides in aqueous conditions.[67] In their report, commercially available Fe_3O_4 NPs with an average diameter of 20 nm were coated with a thin

layer of silica using a sol-gel process to give silica-coated Fe_3O_4. Surface hydroxyl groups were subsequently reacted to tether triethoxysilyl-functionalized (methyl)(triphenylphosphine)(4-amino-3-pentene-2-one)palladium complex onto the surface of the silica (Scheme 1-3).

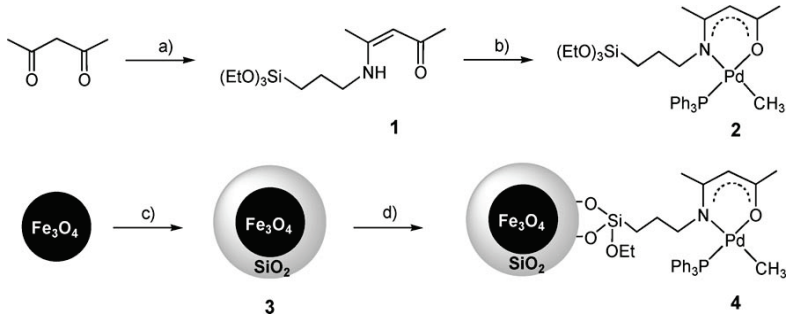

Scheme 1-3. Synthesis of Fe_3O_4 NP-supported (methyl)(triphenylphosphine)(4-amino-3-pentene-2-one)palladium complex **4**. a) $NH_2(CH_2)_3Si(OEt)_3$, microwave heating; b) EtOTl, $[Pd_2(\mu\text{-}Cl)_2Me_2(PPh_3)_2]$, THF, RT; c) tetraethyl orthosilicate; d) **2**, toluene, 100 ^oC, 12 h. Reproduced from ref. 67.

The resulting catalyst was highly active in the Suzuki, Sonogashira, and Stille reactions when employing "unreactive" aryl chlorides under relatively mild conditions, and yields range from 71% to 96% with 0.5 mol% of catalyst relative to aryl chlorides. In addition, catalyst recovery was achieved by straightforward decanting while catalyst particles were retained using a magnet. The catalyst performance remained constant over ten reaction cycles. The analysis of Pd in supernatant indicated less than 0.06% of the starting catalyst leached out.

Similarly, Zhu et al. anchored a second-generation Hoveyda-Grubbs catalyst onto surface modified MNPs (Fe_3O_4 NPs) (Scheme 1-4).[68] In their procedure, commercially available starch functionalized MNPs were first coated with *ortho*-isopropoxystyrene ligands by covalent bonds. Subsequent reaction of the supported ligands with the second-generation Grubbs catalyst produced the MNP

supported Hoveyda-Grubbs catalyst, which displayed high activity for both self- and cross-metathesis of methyl oleate. In addition, the catalyst can be easily separated by using a magnet and reused several times with sustained activity.

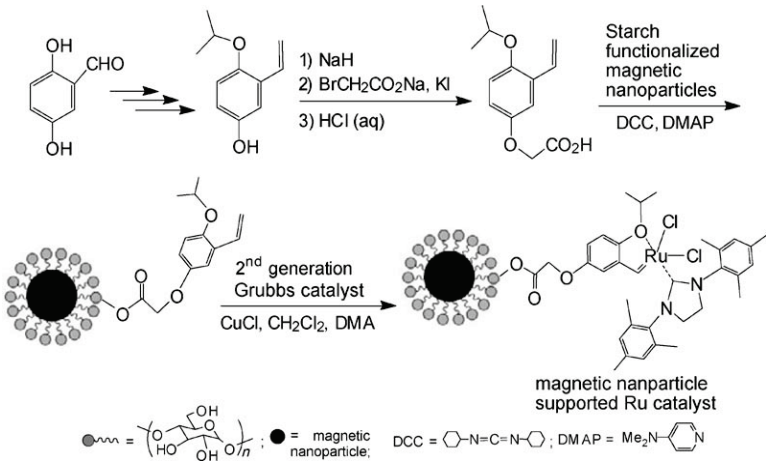

Scheme 1-4. Synthesis of MNP-supported Hoveyda-Grubbs catalyst, reproduced from ref. 68.

MNPs have also been used as supports to prepare "heterogenized" asymmetric catalysts that exhibit superior reusability than their homogeneous equivalents. Hu et al. surface bonded a binaphthyl-based Ru catalyst established by Noyori onto magnetite (Fe_3O_4) NPs via the phosphonate functionality.[69] $[Ru(BINAP{-}PO_3H_2)(DPEN)Cl_2]$ was synthesized by treating $[Ru(benzene)Cl_2]_2$ with (*R*)-2,2'-bis(diphenylphosphino)-1,1'-binaphthyl-4-phosphonic acid ($BINAP{-}PO_3H_2$) followed by (*R*,*R*)-1,2-diphenylethylenediamine ((*R*,*R*)-DPEN) in DMF at elevated temperatures. Then the chiral Ru catalyst $[Ru(BINAP{-}PO_3H_2)(DPEN)Cl_2]$ was immobilized onto magnetite NPs by surface bonding. The synthesis is summarized in Scheme 1-5.

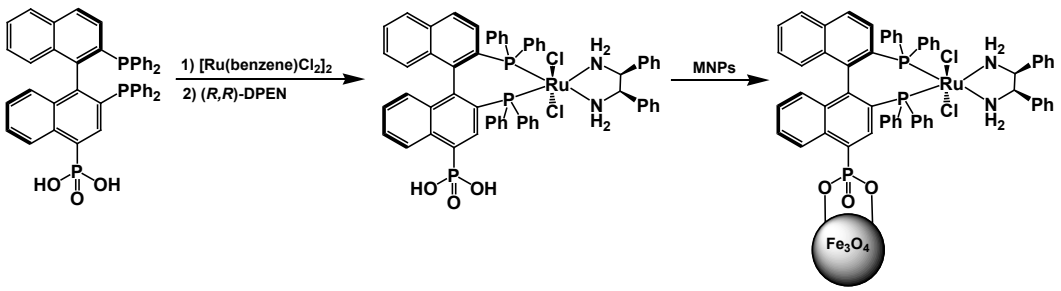

Scheme 1-5. Immobilization of chiral Ru catalyst on magnetite NPs.

The Fe_3O_4 NP-supported chiral catalyst catalyzed asymmetric hydrogenation of aromatic ketones with remarkably high activity and enantioselectivity. In particular, the enantiomeric excess values reported (i.e., 77% to 98.0%) are comparable to those of the parent homogeneous catalyst. The immobilized catalysts were readily recycled by magnetic decantation and reused for up to 14 times for hydrogenation of 1-acetonaphthone without obvious loss of activity and enantioselectivity with a total turnover number (TON) of ca. 14,000 (Figure 1-8), whereas the parent homogeneous catalyst [Ru(BINAP−$(PO_3H_2)_2$)(DPEN)Cl_2] has a TON of 13,000 under identical conditions.[70] Unfortunately catalyst leaching was not investigated.

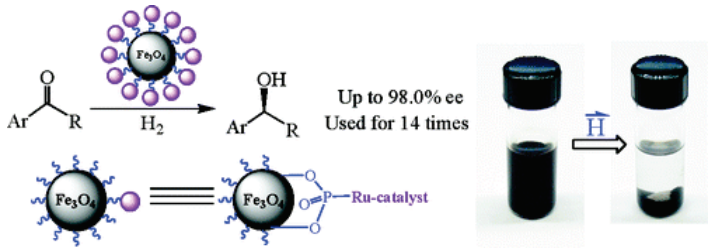

Figure 1-8. Asymmetric hydrogenation of aromatic ketones using Fe_3O_4 NP-supported chiral Ru catalyst and catalyst recycle, reproduced from ref. 69.

1.3.2 Immobilization of Catalytic Metals onto MNPs

Immobilization of catalytic metals onto MNPs is another popular strategy to render magnetic particles catalytic. A particularly interesting example involved

formation of palladium particles on dopamine-modified $NiFe_2O_4$ NPs ($NiFe_2O_4$-DA-Pd) by reducing Na_2PdCl_4 with hydrazine (Scheme 1-6).[71,72] The resulting $NiFe_2O_4$-DA-Pd NPs showed high activity toward hydrogenation as well as Suzuki and Heck coupling reactions. The authors claimed the catalyst was recoverable by magnetic extraction, and the catalytic activity remained unaltered after 10 cycles for hydrogenation reactions and 3 cycles for coupling reactions.

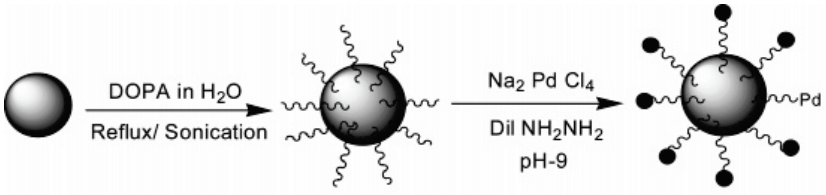

Scheme 1-6. Synthesis of $NiFe_2O_4$-DA-Pd, reproduced from ref. 71.

Yi et al. employed silica-coated Fe_2O_3 NPs (SiO_2/Fe_2O_3 NPs) as a catalyst support.[73] The SiO_2/Fe_2O_3 NPs were functionalized with mercapto and amino groups, which were able to bind strongly with Pd^0 nanoclusters (ca. 2-3 nm) producing Pd/HS-SiO_2/Fe_2O_3 and Pd/H_2N-SiO_2/Fe_2O_3 nanocomposite catalysts (Figure 1-9). These catalysts exhibited higher turnover frequencies (TOFs) than commercial Pd/C in the catalysis for hydrogenation of nitrobenzene to form aniline. These magnetic catalysts were easily collected by a magnet for reuse, which gave 99% yield for 5 consecutive repeat reactions.

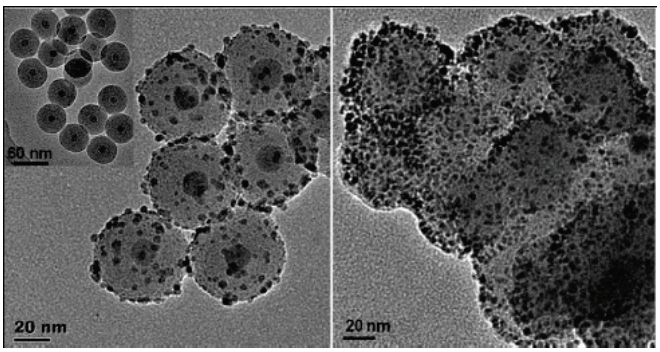

Figure 1-9. TEM images of as-prepared SiO_2/Fe_2O_3 (left inset), Pd/HS-SiO_2/Fe_2O_3 (left), and Pd/H_2N-SiO_2/Fe_2O_3 (right). Reproduced from ref. 73.

Liu et al.[74] reported palladium could be directly deposited onto the surface of Fe_3O_4 through chemical reduction of palladium (II) salt by KBH_4. The generated Pd/Fe_3O_4 catalyst catalyzed the carbonylative Sonogashira coupling reaction of aryl iodides with terminal alkynes under phosphine-free conditions with yield from 71% to 95% (Scheme 1-7).

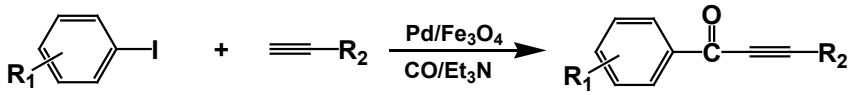

Scheme 1-7. Sonogashira carbonylative coupling of alkynes and aryl iodides.

The catalyst could be readily separated from the reactant with the simple application of an external magnetic field, and its catalytic efficiency for coupling of iodobenzene and phenylacetylene almost remained unaltered even after recycling seven times (Figure 1-10).

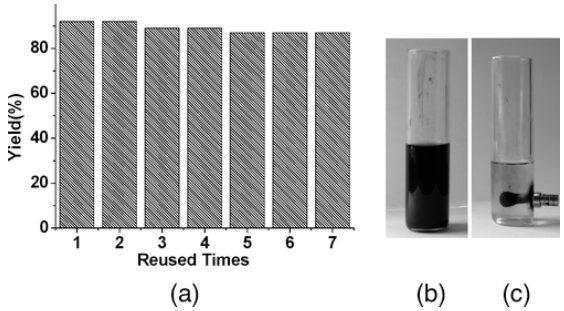

Figure 1-10. Recycle of the Pd/Fe_3O_4 catalyst for coupling of iodobenzene and phenylacetylene. Reproduced from ref. 74.

1.3.3 Iron NPs as Catalysts

Iron NPs themselves also show some catalytic activity in reactions such as hydrolytic dehydrogenation, alkene and alkyne hydrogenation, and Fischer-

Tropsch synthesis.

A key example of hydrolytic dehydrogenation reactions was reported by Xu et al. who have developed a straightforward *in situ* method for preparing amorphous Fe NPs with high catalytic activity for the hydrolytic dehydrogenation of ammonia borane (AB) to generate H_2.[75] The as-prepared Fe catalyst can be readily recycled by magnetic decantation and reused up to 20 times with no obvious loss of activity in air. Compared to the pre-synthesized Fe NPs obtained by reduction of $FeSO_4$ with $NaBH_4$, the catalytic activity of *in situ* synthesized particles is approximately 20-times higher (Figure 1-11). X-ray diffraction analysis indicated pre-synthesized Fe particles were composed of α-Fe crystallites, whereas *in situ* prepared Fe existed as an amorphous phase. The authors concluded the amorphous character is essential to the high activity of Fe NPs for catalytic H_2 generation from AB aqueous solution, and that the presence of AB is helpful for the preparation of amorphous Fe NPs.

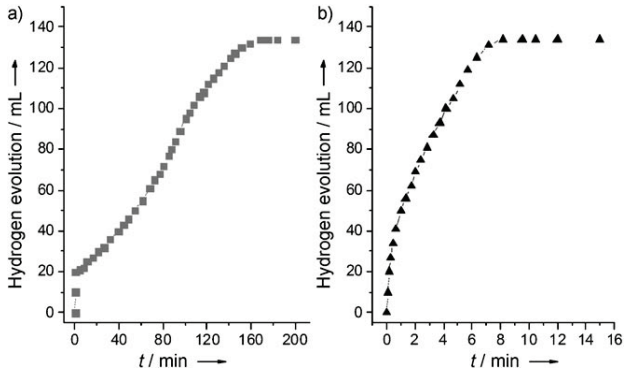

Figure 1-11. Hydrogen generation by hydrolysis of aqueous AB (0.16m, 10 ml) in the presence of a) the pre-synthesized and b) *in situ* synthesized Fe catalysts (Fe/AB = 0.12) at room temperature under argon. Reproduced from ref. 75.

The application of Fe NP catalysts in the hydrogenation of unsaturated C-C bonds has advantages over other metals more commonly used in hydrogenation

such as Pd, Pt, Rh or Ir. First, iron is an abundant element and consequently iron-containing reagents are substantially more cost effective than those of other transition metals. Second, iron-containing chemicals are usually nontoxic and can be handled and disposed of with ease. de Vries et al.[76,77] found iron NPs prepared via reduction of $FeCl_3$ with alkyl Grignard and alkyl lithium reagents in THF were active catalysts in the hydrogenation of a range of alkenes and alkynes under moderate conditions (Scheme 1-8).

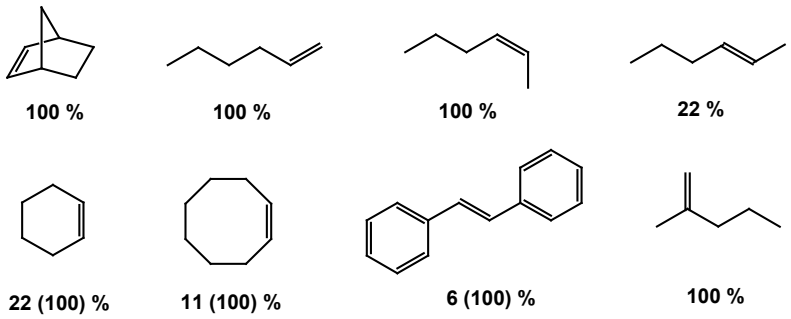

Scheme 1-8. Scope of the $FeCl_3$/EtMgCl hydrogenation catalyst (reaction conditions: 5 mol% Fe, [Alkene] = 0.33 M, THF, 20 bar H_2, R.T. except values in parentheses at 100 °C, 18 h).

The Fischer-Tropsch synthesis (FTS) offers the possibility of converting a mixture of carbon monoxide and hydrogen (syngas) into a series of hydrocarbons (Equations 1-5, 6).[78,79] Syngas is readily produced from natural gas,[80] coal[81] and biomass,[82] and its conversion to hydrocarbons is an attractive alternative to petroleum-derived fuels and chemicals if suitable cost-effective catalysts can be developed. The historic development in the FTS will be discussed in detail in Chapter 4.

$$nCO + (2n + 1)\,H_2 \longrightarrow C_nH_{2n+2} + nH_2O \qquad \textbf{Equation 1-5}$$

$$nCO + 2nH_2 \longrightarrow C_nH_{2n} + nH_2O \qquad \textbf{Equation 1-6}$$

Iron and cobalt have been used as FTS catalysts in industry for hydrocarbon synthesis for a long time. Kou et al. prepared Fe NPs by the reduction of iron (II) chloride with sodium borohydride in ethylene glycol solvent, and found these Fe NPs catalyzed FTS in polyethylene glycol (PEG) at mild conditions (150 °C, 2.0 MPa H_2, 1.0 MPa CO) with an activity as high as 1.5 mol_{CO} mol_{Fe}^{-1} h^{-1}.[83] The iron NP catalyst was magnetically separable, and the hydrocarbon products were insoluble in PEG and could be easily separated from the reaction mixture. This work opens a new window for the applications of Fe NPs as FTS catalysts.

1.4 Scope of The Thesis

Clearly the chemistry of iron-based nanostructures and their catalytic activity is vast and the potential offered by exploring the reactivity of such nanostructures could lead to substantial advances in catalytic applications. This thesis describes a series of investigations aimed at interfacing iron-based nanomaterials with various known catalytic metals and evaluating the catalytic activity of these designer materials in relevant reactions. Chapter 2 describes the synthesis and characterization of Pd decorated iron/iron oxide NPs prepared via surface coordination of Pd ions followed by metallic iron core mediated reduction. These NPs were characterized by TEM and XPS and their catalytic activities toward Suzuki cross-coupling reactions of different substrates were evaluated in aqueous solution under ambient conditions. In addition, the effect of iron/iron oxide NPs on the activities of Suzuki cross-coupling reactions was also investigated.

In Chapter 3 the scope of the iron-based catalysts is expanded to FePd alloy NPs that were prepared by concomitant thermal decomposition of $Fe(CO)_5$ and

reduction of $Pd(acac)_2$ in oleylamine with or without additional reducing agents. These as-synthesized FePd alloy NPs were characterized by TEM, XPS and XRD, and they serve as a robust catalyst for Suzuki cross-coupling reactions of chlorobenzene with phenylboronic acid.

Finally, in Chapter 4 general conclusions and potential opportunities for future work are discussed. Some preliminary investigations of Fischer-Tropsch synthesis and hydrogenation of aromatics using various iron-based NP catalysts are presented and some ongoing studies are outlined.

1.5 References

1. Melvin, E.G. *The Junior Encyclopedia Britannica: A reference library of general knowledge*. **1897**, Chicago.
2. Wood, R.J.; Ronnenberg, A. G. *Modern Nutrition in Health and Disease*. 10th ed. Philadelphia: Lippincott Williams & Wilkins; **2006**: 248-270.
3. Linkov, I. *Nanomaterials*; Springer: New York, 2008.
4. Vollath, D. *Nanomaterials: an introduction to synthesis, properties and application*; Wiley-VCH: Weinheim, 2008.
5. Laurent, S.; Forge, D.; Port, M.; Roch, A.; Robic, C.; Vander Elst, L.; Muller, R. N. *Chem. Rev.* **2008**, *108*, 2064 and references therein.
6. Li, S.; Yan, W.; Zhang, W. *Green Chem.* **2009**, *11*, 1618-1626.
7. Zhang, W. *J. Nanopart. Res.* **2003**, *5*, 323-332.
8. Wang, C.; Zhang, W. *Environ. Sci. Technol.* **1997**, *31*, 2154-2156.
9. Elliott, D. W.; Lien, H.; Zhang, W. *J. Environ. Eng.* **2009**, *135*, 317.
10. Li, X.; Zhang, W. *Langmuir*, **2006**, *22*, 4638-4642.
11. Carpenter, E.; Sims, J.; Wiemann, J.; Zhou, W.; O'Connor, C. *J. Appl. Phys.* **2000**, *87*, 5615-5617.
12. Li, F.; Vipulanandan, C.; Mohanty, K. *Colloids Surf. A* **2003**, *223*, 103-112.
13. Hisano, S.; Saito, K. *J. Magn. Magn. Mater.* **1998**, *190*, 371-381.
14. Peng, S.; Wang, C.; Xie, J.; Sun, S. *J. Am. Chem. Soc.* **2006**, *128*, 10676-10677.
15. Lacroix, L.; Huls, N. F. Ho, D.; Sun, X.; Cheng, K.; Sun, S. *Nano Lett.* **2011**, *11*, 1641-1645.
16. Teng, X. W.; Yang, H. *J. Mater. Chem.* **2004**, *14*, 774-779.
17. Macdonald, J. E.; Brooks C. J.; Veinot, J. G. C. *Chem. Commun.* **2008**, 3777-3779.
18. Sun, S.; Murray, C. B.; Weller, D.; Folks, L.; Moser, A. *Science* **2000**, *287*, 1989-1992.
19. Chen, M.; Liu, J. P.; Sun, S. *J. Am. Chem. Soc.* **2004**, *126*, 8394-8395.
20. Massart, R. *IEEE Trans. Magn.* **1981**, *17*, 1247.
21. Massart, R.; Cabuil, V. *J. Chim. Phys.* **1987**, *84*, 7.
22. Cushing, B. L.; Kolesnichenko, V. L.; O'Connor, C. J. *Chem. Rev.* **2004**, *104*, 3893.
23. Inouye, K.; Endo, R.; Otsuka, Y.; Miyashiro, K.; Kaneko, K.; Ishikawa, T. *J. Phys. Chem.* **1982**, *86*, 1465.
24. Lopez-Perez, J. A.; Lopez-Quintela, M. A.; Mira, J.; Rivas, J.; Charles, S. W. *J. Phys. Chem. B* **1997**, *101*, 8045.
25. Liu, C.; Zou, B.; Rondinone, A. J.; Zhang, Z. J. *J. Phys. Chem. B* **2000**, *104*, 1141.
26. Wang, X.; Zhuang, J.; Peng, Q.; Li, Y. *Nature* **2005**, *437*, 121.
27. Rockenberger, J.; Scher, E. C.; Alivisatos, A. P. *J. Am. Chem. Soc.* **1999**, *121*, 11595 -11596.
28. Sun, S.; Zeng, H. *J. Am. Chem. Soc.* **2002**, *124*, 8204.
29. Sun, S.; Zeng, H.; Robinson, D. B.; Raoux, S.; Rice, P. M.; Wang, S. X.; Li, G. *J. Am. Chem. Soc.* **2004**, *126*, 273-279.

30. Hyeon, T.; Lee, S. S.; Park, J.; Chung Y.; Bin Na, H. *J. Am. Chem. Soc.* **2001**, *123*, 12798.
31. Gavaskar, A. R.; Gupta, N.; Sass, N. M.; Janoy, R. J.; O'Sullivan, D. *Permeable Barriers for Goundwater Remediation-Design, Construction, and Monitoring*; Battelle Memorial Institute, Columbus, OH, **1998**.
32. Wang, C.; Baer., D. R.; Amonette, J. E.; Engelhard, M. H.; Antony, J.; Qiang, Y. *J. Am. Chem. Soc.* **2009**, *131*, 8824-8832.
33. Wang, C.; Baer, D. R.; Thomas, L. E.; Amonette, J. E.; Antony, J.; Qiang, Y.; Duscher, G. *J. Appl. Phys.* **2005**, *98*, 094308.
34. Martin, J. E.; Herzing, A. A.; Yan, W.; Li, X.; Koel, B. E.; Kiely, C. J.; Zhang, W. *Langmuir* **2008**, *24*, 4329-4334.
35. Li, X.; Elliott, D. W.; Zhang, W. *Crit. Rev. Solid State Mater. Sci.* **2006**, *31*, 111-122.
36. He, F.; Zhao, D. Y. *Environ. Sci. Technol.* **2005**, *39*, 3314.
37. Sohn, K.; Kang, S. W.; Ahn, S.; Woo, M.; Yang, S. K. *Environ. Sci. Technol.* **2006**, *40*, 5514.
38. Elliott, D. W.; Zhang, W. *Environ. Sci. Technol.* **2001**, *35*, 4922.
39. Lien, H.; Zhang, W. *App. Catal. B: Environ.* **2007**, *77*, 110-116.
40. Bell, A. T. *Science* **2003**, *299*, 1688.
41. Littke, A. D.; Dai, C.; Fu, G. C. *J. Am. Chem. Soc.* **2000**, *122*, 4020.
42. Yin, J.; Rainka, M. P.; Zhang, X.-X.; Buchwald, S. L. *J. Am. Chem. Soc.* **2002**, *124*, 1162.
43. Martin R.; Buchwald, S. L. *Acc. Chem. Res.* **2008**, *41*, 1461.
44. Navarro, O.; Kelly, R. A.; III; Nolan, S. P. *J. Am. Chem. Soc.* **2003**, *125*, 16194.
45. Hagen, J. *Industrial Catalysis: A Practical Approach*, 2nd Edition, Wiley-VCH, Weinheim, 2006.
46. Sheldon, R. A.; van Bekkum, H. *Fine Chemicals through Heterogeneous Catalysis*, Wiley: Weinheim, 2001.
47. Yin, L,; Liebscher, J. *Chem. Rev.* **2007,** *107*, 133 and references therein.
48. Astruc, D.; Lu, F.; Aranzaes, J. R. *Angew. Chem. Int. Ed.* **2005**, *44*, 7852 and references therein.
49. Shylesh, S.; Schünemann, V.; Thiel, W. R. *Angew. Chem. Int. Ed.* **2010**, *49*, 3428-3459.
50. Zhu, Y.; Stubbs, L. P.; Ho, F.; Liu, R. Ship, C. P.; Maguire, J. A.; Hosmane, N. S. *ChemCatChem* **2010**, *2*, 365- 374.
51. Shen, L.; Laibinis, P. E.; Hatton, T. A. *Langmuir* **1999**, *15*, 447- 453.
52. Shen, X.; Fang, X.; Zhou, Y.; Liang, H. *Chem. Lett.* **2004**, *33*, 1468-1469.
53. Cushing, B. L.; Kolesnicheno, V. L.; O'Connor, C. J. *Chem. Rev.* **2004**, *104*, 3893-3946.
54. White, M. A.; Johnson, J. A.; Koberstein, J. T. Turro, N. J. *J. Am. Chem. Soc.* **2006**, *128*, 11356-11357.
55. Wan, S.; Zheng, Y.; Liu, Y.; Yan, H.; Liu, K. *J. Mater. Chem.* **2005**, *15*, 3424-3430.
56. Bruce, I. J.; Sen, T. *Langmuir* **2005**, *21*, 7029-7035.
57. Caruso, F. *Adv. Mater.* **2001**, *13*, 11-22.

58. Lu, Y.; Yin, Y.; Mayers, B. T.; Xia, Y. *Nano Lett.* **2002**, *2*, 183-186.
59. Lu, A.; Salabas, E. L.; Schüth, F. *Angew. Chem. Int. Ed.* **2007**, *46*, 1222-1244.
60. Kohler, N.; Fryxell, G. E.; Zhang, M. *J. Am. Chem. Soc.* **2004**, *126*, 7206-7211.
61. Nikitenko, S. I.; Koltypin,Y.; Palchik, O.; Felner, I.; Xu, X. N.; Gedanken, A. *Angew. Chem. Int. Ed.* **2001**, *40*, 4447-4449.
62. Geng, J.; Jefferson, D. A.; Johnson, B. F. G. *Chem. Commun.* **2004**, 2442-2443.
63. Deng, Y.; Qi, D.; Deng, C.; Zhang, X.; Zhao, D. *J. Am. Chem. Soc.* **2008**, *130*, 28.
64. Ge, J.; Huynh, T.; Hu, Y.; Yin, Y. *Nano Lett.* **2008**, *8*, 931.
65. Schtz, A.; Hager, M.; Reiser, O. *Adv. Funct. Mater.* **2009**, *19*, 2109.
66. Stevens, P. D.; Fan, J.; Gardimalla, H. M. R.; Yen, M.; Gao, Y. *Org. Lett.* **2005**, *7*, 2085-2088.
67. Jin, M.; Lee, D. *Angew. Chem. Int. Ed.* **2010**, *49*, 1119-1122.
68. Zhu, Y.; Loo, K.; Ng, H.; Li, C.; Stubbs, L. P.; Chia, F. S.; Tan, M.; Peng, S. C. *Adv. Synth. Catal.* **2009**, *351*, 2650-2656.
69. Hu, A.; Yee, G. T.; Lin, W. *J. Am. Chem. Soc*. **2005**, *127*, 12486.
70. Hu, A.; Ngo, H. L.; Lin, W. *Org. Lett.*, **2004**, *6*, 2937-2940.
71. Guin, D.; Baruwati, B.; Manorama, S. V. *Org. Lett*., **2007**, *9*, 1419-1421.
72. Baruwati, B.; Guin, D.; Manorama, S. V. *Org. Lett*., **2007**, *9*, 5377-5380.
73. Yi, D. K.; Lee, S. S.; Ying, J. Y. *Chem. Mater.* **2006**, *18*, 2459.
74. Liu, J.; Peng, X.; Sun, W.; Zhao, Y.; Xia, C. *Org. Lett.* **2008**, *10*, 3933.
75. Yan, J.-M.; Zhang, X.-B.; Han, S.; Shioyama, H.; Xu, Q. *Angew. Chem., Int. Ed.* **2008**, *47*, 2287-2289.
76. Rangheard, C.; de Julián Fernández, C.; Phua, P.; Hoorn, J.; Lefort L.; de Vries, J. G. *Dalton Trans.* **2010**, *39*, 8464-8471.
77. Phua, P.; Lefort L.; Boogers, J. A. F.; Tristany, M.; de Vries, J. G. *Chem. Commun.* **2009**, 3747-3749.
78. Khodaov, A. Y.; Chu, W.; Fongarland, P. *Chem. Rev.* **2007**, *107*, 1692-1744.
79. de Klerk, A. *Green Chem.* **2008**, *10*, 1249-1279.
80. Schulz, H. *Appl. Catal., A* **1999**, *186*, 3-12.
81. Dry, M. E. *Catal. Today* **2002**, *71*, 227-241.
82. Tijmensen, M. J. A.; Faaij, A. P. C.; Hamelinck, C. N.; van Hardeveld, M. R. M. *Biomass Bioenergy* **2002**, *23*, 129-152.
83. Fan, X.-B.; Tao, Z.-Y.; Xiao, C.-X.; Liu, F.; Kou, Y. *Green Chem.* **2010**, *12*, 795-797.

Chapter 2: Synthesis of Pd Decorated Iron/Iron Oxide NPs and Their Catalytic Application in Suzuki Cross-Coupling Reactions*

2.1 Introduction

The 2010 Nobel Prize in Chemistry was awarded to Drs. Richard F. Heck, Ei-ichi Negishi and Akira Suzuki for the development of palladium-catalyzed couplings in organic synthesis.[1] Palladium-catalyzed coupling reactions, in which palladium is used to catalyze the formation of carbon-carbon bonds, are widely used to make complex molecular structures. The discoveries have been used in academic research and many industrial chemical processes for the synthesis of functional materials, medicines, and other biologically active compounds.

In 1979, Suzuki and co-workers reported organoboron compounds could be coupled with alkenyl and aryl halides in the presence of tetrakis(triphenylphosphine) palladium ($Pd(PPh_3)_4$) under basic conditions.[2,3] This reaction has since been extended to include couplings with alkyl groups.[4] A further significant development is aryl boronic acids can participate as coupling partners. In 1981 the "classic" Suzuki-Miyaura reactions of aryl halides with aryl boronic acid were reported (Scheme 2-1).[5] This chemistry has been greatly

*A part of this chapter has been published in Zhou, S.; Johnson, M.; Veinot, J. G. C. *Chem. Commun.* **2010**, *46*, 2411-2413.

extended and elaborated over the years.[6] Today, the Suzuki coupling reaction is among the most important methods for synthesizing biaryl derivatives of all kinds, because the required arylboronic acids or borates are readily synthesized from trialkylborates with Grignard or organolithium reagents. Furthermore, arylboronic acids and borates are stable toward air and moisture, tolerate a wide range of functional groups, and exhibit low toxicity, which make the coupling reaction very practical. Since biaryls are ubiquitous substructures in natural products,[7-9] pharmaceuticals,[10,11] agrochemicals,[12-14] and new electronic materials,[15] it is not surprising the Suzuki reaction is used not only in academic research but also for the industrial production of fine chemicals.

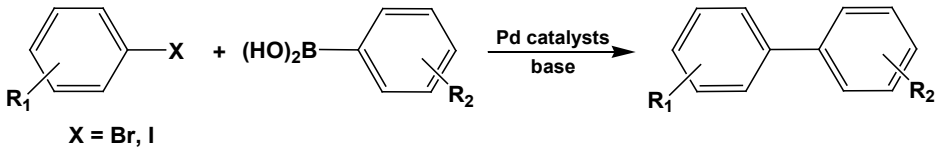

Scheme 2-1. Suzuki-Miyaura reactions of aryl halides with aryl boronic acids.

There are a number of natural product syntheses reported in the literature that rely on the Suzuki coupling for carbon-carbon bond formation.[16] One example is the efficient synthesis of the antiviral bromoindole alkaloid dragmacidin F. This synthesis involved two key carbon-carbon bond forming steps using Suzuki coupling (Figure 2-1).[7] Suzuki coupling has been used for a number of industrial scale syntheses, including the preparation of the fungicide Boscalid developed by BASF (Figure 2-1).[12-14]

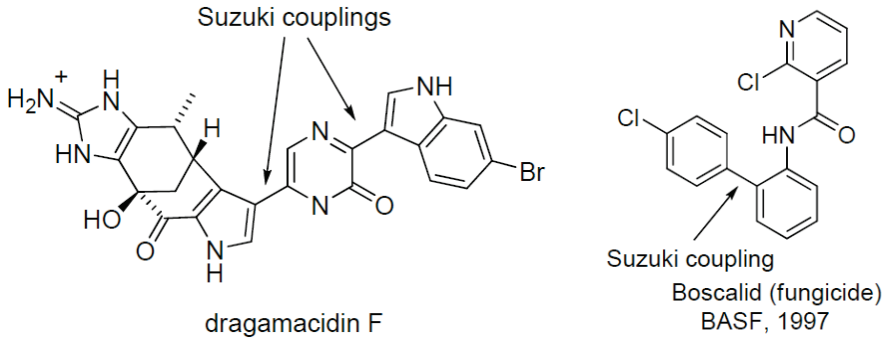

Figure 2-1. Suzuki coupling reactions used in the syntheses of dragmacidin F. and Boscalid.

Homogeneous palladium complexes have been widely explored as catalysts for Suzuki coupling.[17-20] Despite the high activity and selectivity of these systems, they have limited utility in industrial processes because of challenges associated with catalyst removal, recovery, and recycling.[21] Complicating matters, many ligands used in catalyst design (e.g., phosphines) are air sensitive, challenging to prepare and/or costly, limiting suitability of such materials for large-scale application.[21] To overcome these issues, many heterogeneous catalysts have been developed, such as inorganic solid (e.g., charcoal, zeolites and metal oxides) supported and polymer-stabilized systems.[22,23] However, heterogeneous catalysts usually have lower activity compared to their homogeneous counterparts because they have far fewer accessible catalytic sites.

With the development of methods to prepare engineered nanomaterials, a new class of materials has been fabricated whose members find application as catalysts or catalyst supports for chemical transformations. Their impact is seen in the fields including the petrochemical industry,[24,25] pollutant removal,[26-28] and production of fine chemicals.[29] Generally, engineered nanomaterial catalysts possess nanoscale active components (typically metals or metal oxides) dispersed

onto a solid support material. Unlike conventional micrometer-sized supports, nanomaterials are readily dispersed in reaction media to form suspensions that approach the homogeneity of solutions. Owing to their nanometer scale sizes, nanomaterials exhibit very high surface area-to-volume ratios that offer high loadings of catalytically active sites.[26] Recently, transition metals supported on magnetic nanoparticles (MNPs) have emerged as promising catalysts because of the combined advantages of high specific surface area and facile magnetic recovery.[30-35] Magnetic separation has the potential of being a straightforward alternative to filtration or centrifugation as it minimizes loss of catalyst and increases the reusability for cost-saving.

Catalytic species can be immobilized onto magnetic NP surface by a variety of methods, such as direct deposition and immobilization through cheating group coordination. However, examples of catalytic metals being deposited onto magnetic nanoparticles in the literature require surface modification and addition of external reducing agents to realize deposition of the metals.[32-35] Our group found iron oxide capped iron nanoparticles ($Fe@Fe_xO_y$ NPs) sequestered transition metal ions from aqueous and organic media, as well as coordinating environments.[36,37] Sequestrations were conducted in basic media. Under these conditions surface –OH groups are deprotontated making them more suitable for catalytic metal ion binding. The generally accepted sequestration mechanism involves coordination of metal ions to the iron oxide surface followed by reduction of these coordinated ions to their metallic state by the iron core (Scheme 2-2).[36-38]

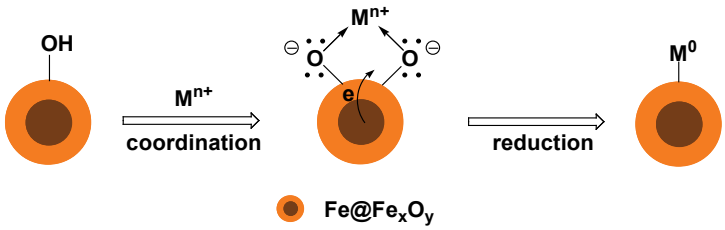

Scheme 2-2. The deposition of metallic domains onto the surface of $Fe@Fe_xO_y$ NPs.

This process gives rise to $Fe@Fe_xO_y$ particle surfaces bearing spectroscopically detectable zero valent metals. Uniquely, our approach does not use any external reducing reagents or post-synthetic NP surface modification because of the established reducing nature and coordinating ability of the $Fe@Fe_xO_y$ support. Highlighting the versatility of our method, in principle it is possible to deposit any metal with a reduction potential more positive than that of iron (e.g., Co, Ni, Cu, Pd, Ag, Pt, Rh and Ru, Table 2-1).[36,37] This straightforward method enables the preparation of catalytic metal "decorated" $Fe@Fe_xO_y$ NPs.

Table 2-1. Sequestration of metal ions in basic aqueous solutions using $Fe@Fe_xO_y$[a]

Metal	Source	$E°$ (V)	Original [M] (mM)	Final [M] (mM)	Sequestered %
Co	$Co(NO_3)_2•xH_2O$	-0.28	18	8.01	54.524
Ni	$Ni(NO_3)_2•6H_2O$	-0.257	19	5.40	71.170
Cu	$Cu(NO_3)_2•xH_2O$	0.3419	19	0.97	94.991
Pd	$Pd(NO_3)_2•xH_2O$	0.951	27	0.0005	99.998
Ag	$AgNO_3$	0.7996	20	0.0009	99.996
Pt	$PtCl_4$	0.718	13	0.00095	99.9993
Rh	$RhCl_3•xH_2O$	0.758	17	0.000079	99.9995
Ru	$RuCl_3•xH_2O$	0.386	26	0.00001	99.99997

[a]$Fe@Fe_xO_y$ to solution ratio of 5 mg:1 ml; $E°$ are with respect to standard hydrogen electrode. Reproduced from ref. 37.

To explore catalytic capabilities of palladium "decorated" $Fe@Fe_xO_y$ NPs ($Fe@Fe_xO_y$/Pd) toward Suzuki-Miyaura cross-coupling reactions, we prepared $Fe@Fe_xO_y$/Pd via direct reduction of Pd^{2+} by size polydisperse $Fe@Fe_xO_y$ NPs.

2.2 Experimental Section

2.2.1 Chemicals

Iron (III) chloride ($FeCl_3$, 97%), palladium (II) nitrate hydrate ($Pd(NO_3)_2 \cdot xH_2O$), sodium borohydride ($NaBH_4$, 99%) and all aryl halides, aryl boronic acids were purchased from Sigma-Aldrich. K_2CO_3 was purchased from Mallinckrodt. KOH and Na_2SO_4 were obtained from Caledon. All reagents were used without further purification unless otherwise noted. In-house deionized water was employed for all syntheses and reactions and 18.2 $M\Omega \cdot cm^{-1}$ Millipore water was used for ICP-MS studies.

2.2.2 Preparation of $Fe@Fe_xO_y$ NPs

$Fe@Fe_xO_y$ NPs were prepared using a modified literature procedure.[39] Briefly, $FeCl_3$ (3.41 g, 21 mmol) was dissolved in 400 ml of deionized water. A solution of $NaBH_4$ (2.24 g, 59 mmol) in 30 ml of water was added dropwise while the iron (III) chloride solution was stirred vigorously. The orange solution became dark, and a black precipitate formed. The precipitate was vacuum-filtered in air and washed with 500 ml of deionized water followed by 50 ml of 100 % ethanol. The resulting black paste was transferred to a round-bottom flask and dried *in vacuo* for 2 days to yield a dry powder. The $Fe@Fe_xO_y$ powder was ground using a

mortar and pestle to break up large aggregates in an argon-filled glovebox (0.6 ppm H_2O, 0.6 ppm O_2). Yield: 0.98 g.

2.2.3 Preparation of Fe@Fe_xO_y/Pd NPs

0.01 mmol of $Pd(NO_3)_2$, 2 mg of Fe@Fe_xO_y, and 5 ml of aqueous KOH solution (pH 10.5) were mixed under argon and sonicated for 20 minutes. The reaction mixture was subsequently centrifuged, and the black precipitate was washed with distilled water once and directly used in the Suzuki-Miyaura coupling reactions under investigation. The Pd loading amount was determined by inductively coupled plasma mass spectrometry (ICP-MS). After filtering the reaction mixture (Whatman No. 2 filter paper), the colorless filtrate was acidified with concentrated nitric acid and analyzed by ICP-MS to determine the amount of unreacted Pd (metal content in HNO_3 was subtracted).

2.2.4 General Procedure for Suzuki Cross-Coupling Reactions

The aryl halide (2.0 mmol) and aryl boronic acid (2.4 mmol) of choice were dissolved in 5 ml ethanol (Table 2-2). K_2CO_3 (5 mmol) dissolved in 2 ml of deionized water was added to the solution. Fe@Fe_xO_y/Pd (0.01 mmol Pd, 0.5 mol% to aryl halide) were sonicated in 3 ml deionized water and added. The reaction mixture was stirred at room temperature in air for the indicated time (Table 2-2, except entry 13 at 80 °C). After reaction, the mixture was diluted with H_2O (20 ml) and diethyl ether (20 ml). The catalyst was separated by gravity filtration (Whatman No. 2 filter paper) or centrifugation (when catalyst was reused), and the mixture was extracted with diethyl ether (4 × 25 ml). The organic layers were combined, dried with anhydrous Na_2SO_4 and the solvent was removed on a rotary

evaporator to yield the crude product. If necessary, the crude product was purified by column chromatography on silica gel to give the desired products. Products were characterized by GC-MS and ^{1}H and ^{13}C NMR.

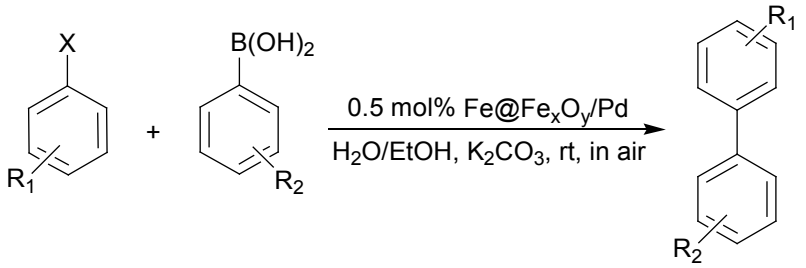

Scheme 2-3. Suzuki cross-coupling reactions

Table 2-2. A summary of Suzuki cross-coupling reactions.

Entry	R_1	X	R_2	Time (h)	Yield (%)[a]
1	H	Br	H	4	95
2	4-NO_2	Br	H	4	96
3	4-COMe	Br	H	4	96
4	4-OMe	Br	H	4	93
5	2-Me	Br	H	4	86
6	H	Br	2-OMe	4	91
7	H	Br	3-OMe	4	89
8	H	Br	4-OMe	4	94
9	H	I	H	2	98
10	4-NO_2	I	H	2	99
11	4-OMe	I	H	2	97
12	2-Me	I	H	2	84
13[b]	4-NO_2	Cl	H	36	24
14[c]	H	Br	H	4	0

[a]Isolated yield. [b]80 °C. [c]Fe@Fe_xO_y without Pd.

2.2.5 Assay of Residual Pd in Crude Products

The reaction procedures are the same as above, except membrane filters

(Millipore, 0.45 μm) were used to remove the catalyst. The crude product was heated to 625 °C for several hours to remove organic components. The residues were dissolved in concentrated nitric acid and analyzed for Pd by ICP-MS.

2.2.6 Characterization Methods

^{1}H and ^{13}C NMR spectra were recorded in $CDCl_3$ on a Varian Inova 400 spectrometer at 400 MHz and 100 MHz, respectively. Spectra were referenced to $CHCl_3$ (7.26 ppm) and $CDCl_3$ (77.06 ppm), respectively. Chemical shifts are reported in parts per million (ppm, δ).

Gas chromatography-mass spectrometry (GC-MS) was performed using a HP 5890 with a 5970 MSD electron ionization detector, helium carrier gas (1 ml/min). The injection port was at 280 °C and a linear temperature profile (50 °C - 280 °C at 10 °C/minute) was employed. 1 μL of an acetone solution of the product was injected into a DB-5MS column with a 0.25 μm film.

Transmission electron microscopy (TEM) was performed using a JEOL 2010 Transmission Electron Microscope with an accelerating voltage of 200 keV and a LaB_6 thermionic emission filament. The instrument was fitted with an Energy Dispersive X-Ray (EDX) detector for elemental analysis. TEM samples were prepared by suspending particles in distilled water by sonication and dropcoating the solution onto carbon-coated, 200-mesh Cu grids (SPI Supplies).

X-ray photoelectron spectroscopy (XPS) was performed on an AXIS-165 XPS spectrometer from Kratos Analytical. The base pressure and operating pressure in the chamber were maintained at $\leq 10^{-7}$ Pa. A monochromatic Al Kα X-ray (λ = 8.34Å) was used to irradiate the samples, and the spectra were obtained with an

electron takeoff angle of 90°. Samples were pressed into carbon tape. To control sample charging, the charge neutralizer filament was used during the experiment. The pass energy for the survey and the high-resolution spectra were 160 and 20 eV, respectively. Spectra were calibrated to the C 1s emission at 284.8 eV using CasaXPS (VAMAS) software. Following calibration, the background of each spectrum was subtracted using a Shirley-type background to remove most of the extrinsic loss structure. Fitting was carried out using 70% Lorentzian/30% Gaussian line shapes for metal zero-oxidation states, and Gaussian line shapes for higher oxidation states. Binding Energy values and orbital splitting were consistent with literature values obtained from the NIST database (http://srdata.nist.gov/xps/).

Inductively coupled plasma mass spectrometry (ICP-MS) was performed on a Perkin Elmer Elan 6000 ICP-MS. Sample solvents were evaporated and organic components were removed by heating at 625 °C for several hours. The residues were dissolved in concentrated nitric acid and analyzed by ICP-MS. The flow rate on the instrument was 1 ml/min and dual detector mode was employed. A blank was subtracted after internal standard correction and the values reported are an average of three readings (35 sweeps per reading).

2.3 Results and Discussion

2.3.1. Fe@Fe_xO_y NPs

Fe@Fe_xO_y NPs were prepared by sodium borohydride reduction of Fe^{3+} in aqueous solution. In this procedure, metallic Fe particles were formed initially because of the presence of excess sodium borohydride. When the metallic

particles were exposed to air during post-synthetic processing an oxide layer formed on and passivated their surfaces. The resulting iron oxide capped iron nanoparticles (Fe@Fe_xO_y NPs) were stored in an argon-filled glovebox to avoid loss of the core-shell structure arising from further oxidation. Fe@Fe_xO_y NPs have been well studied by high-resolution TEM (HRTEM) and XPS to exhibit a core-shell structure with a thin oxide shell of ca.2-3 nm.[40-42]

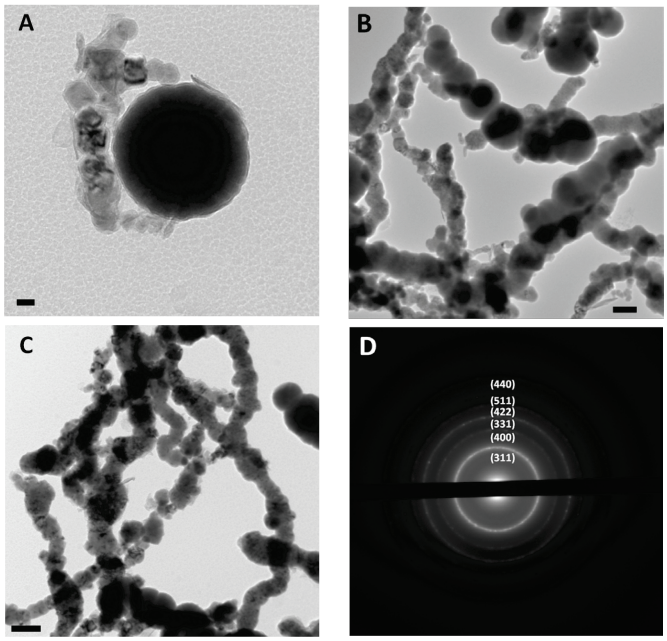

Figure 2-2. (A) **A** bright-field TEM image of a single Fe@Fe_xO_y NP, scale bar 20 nm. (B), (C) TEM images of agglomerates of Fe@Fe_xO_y NPs, scale bar 100 nm (D) SAED image showing characteristic reflections indexed to crystalline Fe_3O_4 (or γ-Fe_2O_3).

Representative bright-field transmission electron micrographs (TEM) of Fe@Fe_xO_y NPs are shown in Figure 2-2 (A, B, C). Figure 2-2 A shows a single spherical particle with a diameter of 155 nm. In Figure 2-2 B and C, the particles are pseudospherical and polydisperse with diameters of 20-150 nm. Of important note, these NPs tend to agglomerate into chains as a result of their magnetic properties.[39] Selected area electron diffraction (SAED) shows well-defined ring

patterns indexed to diffraction of the Fe_3O_4 (or γ-Fe_2O_3) crystal planes (Figure 2-2 D).[36,40,43] No reflections characteristic of metallic iron are observed, suggesting a noncrystalline metallic iron core.

XPS was used to confirm the elemental composition and oxidation states of Fe@Fe_xO_y NPs. Figure 2-3 presents the survey XP spectrum of Fe@Fe_xO_y NPs. This low-resolution scan indicates the dominant elements present in the sample. Figure 2-3 reveals that Fe@Fe_xO_y NPs contain only iron and oxygen as indicated by characteristic Fe and O emissions. The presence of the C 1s emission is expected because of the ubiquitous nature of this element in all XPS analyses.

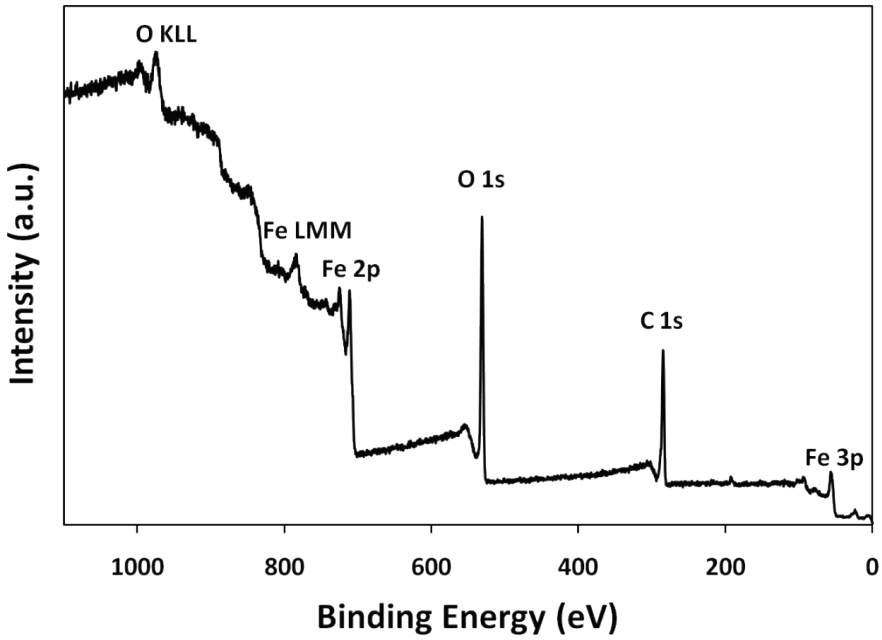

Figure 2-3. Survey XP spectrum of Fe@Fe_xO_y NPs, spectrum was calibrated to C 1s emission at 284.8 eV.

XPS in-situ sputtering was used to remove the oxide shell and confirm the Fe@Fe_xO_y structure. Figure 2-4 shows high-resolution Fe 2p region of XP spectra of Fe@Fe_xO_y NPs sputtered for 0 s, 60 s, 180 s, 360 s and 540 s, respectively.

Before sputtering (0 s), the emissions with binding energies at ca. 706.9 eV and 720.0 eV correspond to Fe $2p_{3/2}$ and $2p_{1/2}$ of zero valent iron (Fe(0)), and emissions with binding energies at ca. 710.2 eV and 723.6 eV correspond to Fe $2p_{3/2}$ and $2p_{1/2}$ of oxidized iron (Fe(II), Fe(III)).[38,39,44-46] Evaluation of the Fe $2p_{3/2}$ and O 1s spectral regions indicates the present particles contain Fe, Fe_3O_4 and FeOOH.[38,39,44-46] Prolonged sputtering of the Fe@Fe_xO_y NPs shows a loss of the oxide features and an increase in the intensity of the emissions arising from elemental iron. While this may appear to be straightforward evidence of core-shell structure of Fe@Fe_xO_y NPs, prolonged Ar sputtering can result in reduction of iron oxides to metallic iron state.[47]

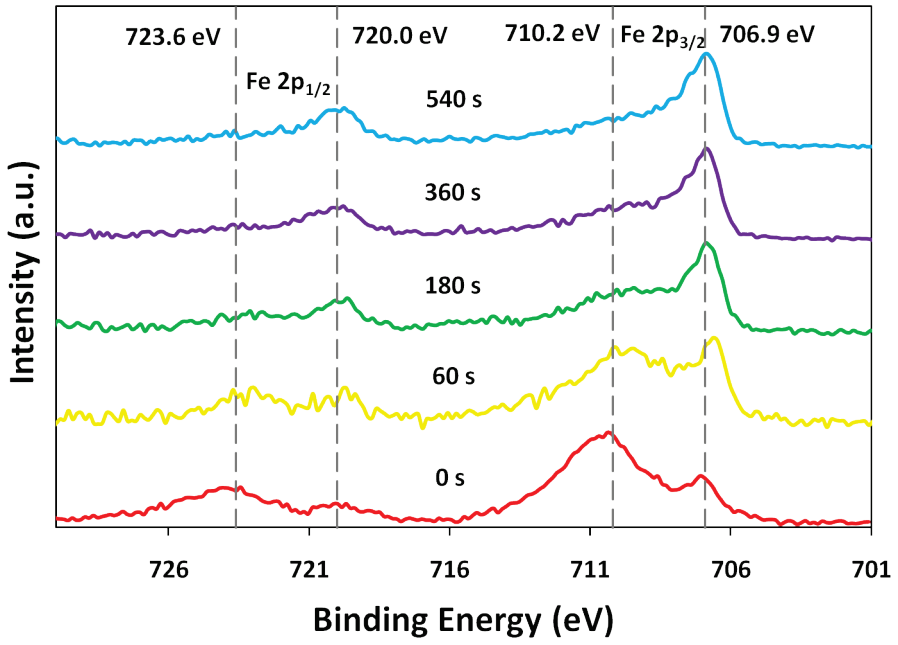

Figure 2-4. Shirley background-subtracted high-resolution Fe 2p region of the XP spectra of Fe@Fe_xO_y sputtered for 0 s, 60 s, 180 s, 360 s, 540 s. All spectra were calibrated to C 1s emission at 284.8 eV.

2.3.2. Pd "Decorated" Fe@Fe_xO_y NPs

The deposition of palladium onto the surfaces of Fe@Fe_xO_y NPs was achieved

in basic conditions (i.e., pH = 10.5). Under these conditions the surface Fe-OH groups were deprotonated to maximize surface binding to the Pd ions.[36-38] ICP-MS was used to analyze Pd content in the deposition reaction filtrate, only 0.05 % of adding $Pd(NO_3)_2$ was detected indicating $Pd(NO_3)_2$ is almost completely deposited on $Fe@Fe_xO_y$. Figure 2-5 (left) shows a representative bright-field TEM of $Fe@Fe_xO_y$/Pd NPs; particle diameters lie within the range of 3-45 nm. Individual Pd NPs were not observed during inspection using TEM, although the presence of Pd was confirmed by energy dispersive X-ray spectroscopy (EDX) (Figure 2-5, right). This observation is consistent with Pd domains being exceptionally small (i.e., <1 nm) and undetectable by standard electron microscopy imaging techniques.[34]

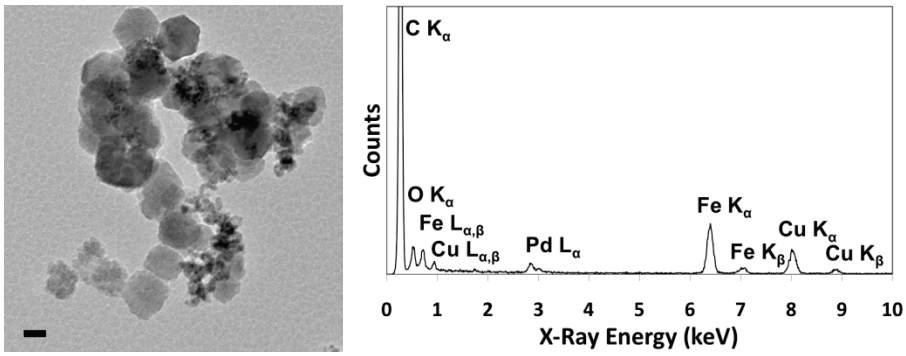

Figure 2-5. Left: A bright-field TEM image of $Fe@Fe_xO_y$/Pd, scale bar 20 nm. Right: EDX spectrum of $Fe@Fe_xO_y$/Pd.

X-ray photoelectron spectroscopy (XPS) was used to determine the oxidation state of surface bonded palladium species. Figure 2-6 shows the Pd 3d region of a typical $Fe@Fe_xO_y$/Pd XP spectrum. Emissions at 335.4 and 340.7 eV tailing to higher binding energies are characteristic of metallic Pd^0.[38,48] XPS analyses of the Fe $2p_{3/2}$ and O 1s regions indicate the particle surface iron consists of mostly

Fe_3O_4 and FeOOH after Pd was deposited (Figure 2-7).[38,39,44-46]

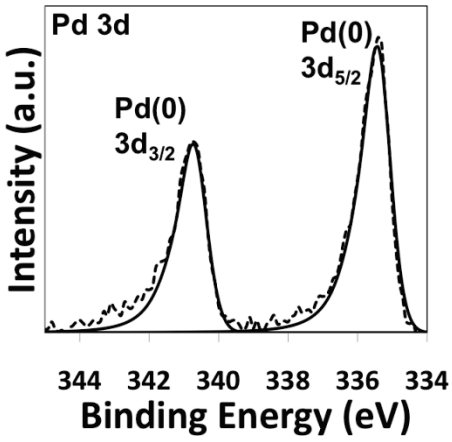

Figure 2-6. Shirley background-subtracted high-resolution Pd 3d region of the XP spectrum of Fe@Fe_xO_y/Pd (dotted line), fit solid lines indicate metallic Pd (0). Spectrum was calibrated to C 1s emission at 284.8 eV.

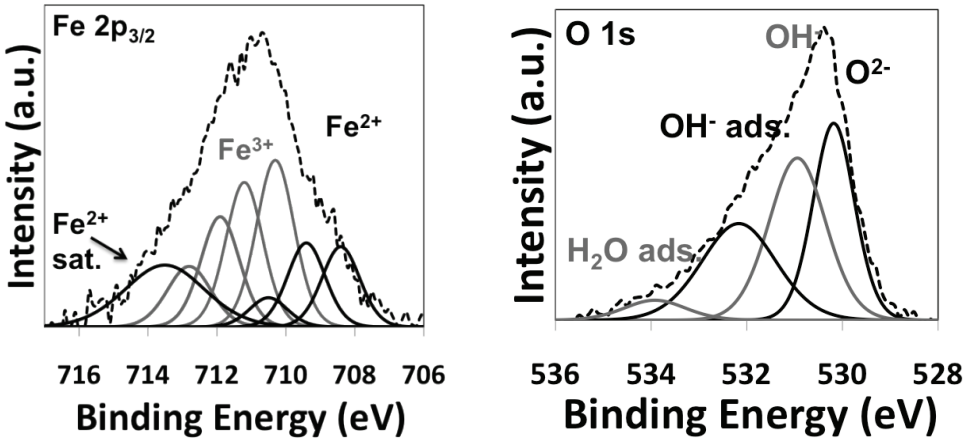

Figure 2-7. Shirley background-subtracted high-resolution Fe $2p_{3/2}$ region (left) and O 1s region (right) of the XP spectra of Fe@Fe_xO_y/Pd (dotted lines). All spectra were calibrated to C 1s emission at 284.8 eV. The fitting (solid lines) in the Fe $2p_{3/2}$ region indicates the presence of mixed oxides Fe_3O_4 and FeOOH. The peaks in O 1s region fit to crystalline OH^- confirm the presence of FeOOH alongside Fe_3O_4.

2.3.3. Catalytic Activity of Pd "Decorated" Fe@Fe_xO_y NPs

Reactions of various aryl halides with aryl boronic acids were evaluated using 0.5 mol% Fe@Fe_xO_y/Pd (Pd content relative to aryl halides) in a H_2O/EtOH

(volume ratio = 1:1) solvent mixture at room temperature in air (Table 2-3). Aryl bromides and iodides bearing electron-withdrawing or donating groups afforded cross-coupling products in high yields (entries 1-5 and 9-12, Table 2-3). As expected, electron-rich aryl boronic acids furnished coupling products in good yields (entries 6-8, Table 2-3). Steric hinderance present in the *ortho*-methylated aryl bromide and iodide influenced the reactivity resulting in a lower yield (entries 5 and 12, Table 2-3). No biphenyl was obtained from reaction of aryl chlorides when the reaction was performed at room temperature, however activated 4-nitrophenyl chloride provided the coupling product in moderate yield at 80 °C (entry 13, Table 2-3). The blank reaction of bromobenzene with phenylboronic acid using $Fe@Fe_xO_y$ without Pd resulted in no reaction (entry 14, Table 2-3). For entry 1, five-fold scale-up of the reaction of bromobenzene with phenylboronic acid did not compromise yield (i.e., 95%).

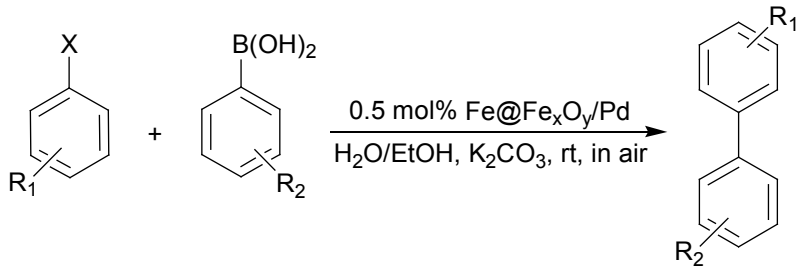

Scheme 2-4. Suzuki-Miyaura cross-coupling reactions

Table 2-3. A summary of Suzuki-Miyaura cross-coupling reactions.[a]

Entry	R_1	X	R_2	Time (h)	Yield (%)[b]	TOF (h^{-1})
1	H	Br	H	4	95	47.5
2	4-NO_2	Br	H	4	96	48
3	4-COMe	Br	H	4	96	48
4	4-OMe	Br	H	4	93	46.5
5	2-Me	Br	H	4	86	43
6	H	Br	2-OMe	4	91	45.5
7	H	Br	3-OMe	4	89	44.5
8	H	Br	4-OMe	4	94	47
9	H	I	H	2	98	98
10	4-NO_2	I	H	2	99	99
11	4-OMe	I	H	2	97	97
12	2-Me	I	H	2	84	84
13[c]	4-NO_2	Cl	H	36	24	1.33
14[d]	H	Br	H	4	0	0

[a]Reaction conditions: 2.0 mmol aryl halide, 2.4 mmol aryl boronic acid, 5.0 mmol K_2CO_3, 0.5 mol% Fe@Fe_xO_y/Pd, H_2O/EtOH (1:1), room temperature. [b]Isolated yield, average of minimum two independent reactions with deviation $\leqslant$ 2%. [c]80 °C, average of two independent reactions with 4% deviation. [d]Fe@Fe_xO_y without Pd.

It is worth mentioning the Fe@Fe_xO_y/Pd system shows improved activity over commercial Pd/C (10 wt. %, Aldrich 205699) when coupling bromobenzene with phenylboronic acid under identical reaction conditions (Table 2-4).

Table 2-4. Suzuki-Miyaura coupling reactions catalyzed by Pd/C and Fe@Fe_xO_y/Pd.[a]

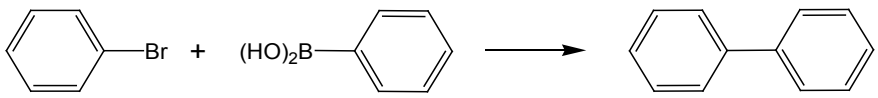

Catalyst	Time (h)	Yield (%)[b]
Pd/C	4	90
Fe@Fe_xO_y/Pd	4	95

[a]Reaction conditions: 2.0 mmol bromobenzene, 2.4 mmol phenylboronic acid, 5.0 mmol K_2CO_3, 0.5 mol % Pd, H_2O/EtOH (1:1), room temperature. [b]Isolated yield.

One of the motivations of the present study was to employ magnetic separation to recover the catalyst. While $Fe@Fe_xO_y/Pd$ NPs are paramagnetic it is reasonable to expect they can be separated from the reaction mixture upon exposure to an external permanent magnet. However, magnetic isolation of the present $Fe@Fe_xO_y/Pd$ NPs is challenging. Before Pd deposition, $Fe@Fe_xO_y$ NPs are readily recovered upon exposing the suspension to an external permanent magnet. Because $Fe@Fe_xO_y/Pd$ NPs are prepared by reducing Pd^{2+} with the electrons from the Fe core, positive charge accumulates in the NP core. As a result of electrostatic interactions, these charged NPs repel each other making straightforward magnetic isolation difficult. To minimize particle repulsion, a saturated NaCl solution was added to reaction mixture to increase ionic strength, which facilitated magnetic separation (Figure 2-8). Due to the limitation of magnetic separation, we chose to employ gravity filtration (product assay) or centrifugation (catalyst reuse) for catalyst separation rather than magnetic attraction unless otherwise noted.

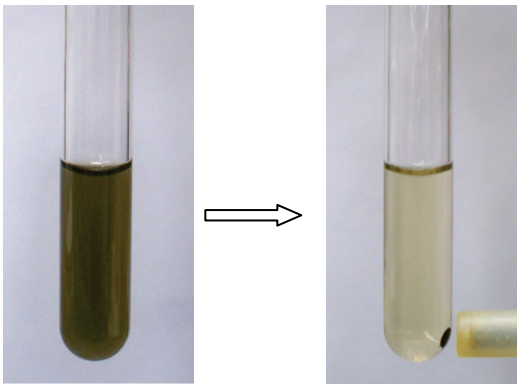

Before After

Figure 2-8. Magnetic separation of the catalyst from the reaction mixture, NaCl solution was added before applying the magnet.

While palladium-catalyzed Suzuki coupling reactions allow for successful synthesis of numerous compounds including pharmaceutically active ingredients, palladium is often retained in the isolated products. For pharmaceutical applications there are typically strict guidelines limiting heavy metal concentrations. The Pd limit in pharmaceutical substances mandated by European Agency for the Evaluation of Medicinal Products is 5 ppm.[49] For homogeneous palladium catalyzed reactions all of the palladium commonly remains in the reaction product after isolation, and it is very challenging and costly to remove. For heterogeneous catalysts, such as Pd on carbon and Pd bonded to polymer supports, the Pd content is often greatly reduced in the products, as most of the Pd remains bound to the support, which is removed by filtration. Unfortunately, leaching of the Pd from catalyst supports is possible and removal of residual palladium from products generated via heterogeneous catalysis can still be an issue. Adding to the appeal of the $Fe@Fe_xO_y$/Pd catalytic system, the residual Pd content in the crude solid product from the reaction of bromobenzene with phenylboronic acid is 0.31 ppm, which is far below the limit mandated by the European Agency for the Evaluation of Medicinal Products (i.e., 5 ppm). It is not clear how the $Fe@Fe_xO_y$ NPs retain Pd, however it is reasonable both surface –OH groups and Fe core play a role. It is useful to recall the mechanism by which Pd deposition onto $Fe@Fe_xO_y$ NPs occurs. In basic reaction conditions, the surface –OH groups are deprotonated and have a strong affinity to leached Pd species. In addition, if metallic Fe cores remain they have a demonstrated ability to reduce soluble Pd (II) species generated during the reaction. In the present

context it is useful to view Fe@Fe_xO_y NPs as "source" and "sink" for Pd in the Suzuki coupling reaction.

Catalyst recycling was also performed to evaluate the reusability of Fe@Fe_xO_y/Pd in the Suzuki-Miyaura coupling of bromobenzene with phenylboronic acid. After each cycle, the catalyst was separated from the reaction mixture by centrifugation, washed with distilled water and stored in an argon atmosphere between reactions. As summarized in Table 2-5, we observed only a slight loss of activity after the third reaction. A total turnover number (TON) of 906 was achieved, which is lower compared to most homogenous Pd catalysts with TONs of $> 10{,}000$.[50]

Table 2-5. A summary of catalyst reuse for Suzuki-Miyaura coupling reaction of bromobenzene with phenylboronic acid.[a]

Run	Time (h)	Yield (%)[b]	TOF (h^{-1})
1	4	95	47.5
2	4	93	46.5
3	4	94	47
4	4	88	44
5	4	83	41.5

[a]Reaction conditions: same as Table 2-1. [b]Isolated yield, average of two independent tests.

After 5 consecutive reactions (Table 2-5), the catalyst maintained size and morphology in TEM however particles appeared to be more agglomerated (Figure 2-9). No composition difference can be detected at the sensitivity of the EDX technique (Figure 2-10). In addition, the oxidation states of Pd, Fe and O remained unchanged even after 5 runs as confirmed by XPS (Figures 2-11, 2-12, 2-13). In Figure 2-11, we notice a reduced signal-to-noise ratio in the right

spectrum, which is caused by reduced sample amount after 5 reactions. In Figure 2-12, we note an increased Fe^{3+}/Fe^{2+} ratio after 5 reactions which likely arises from nanoparticle oxidation throughout.

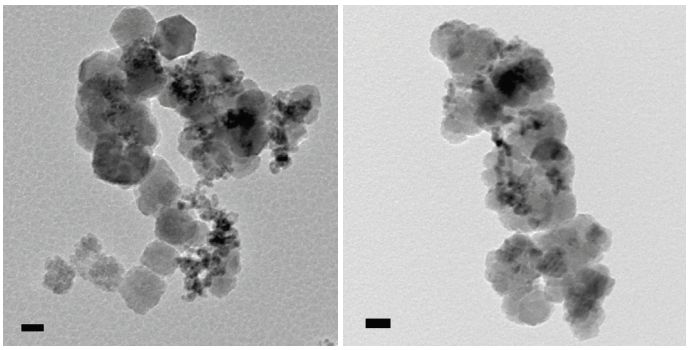

Figure 2-9. Bright-field TEM images of $Fe@Fe_xO_y/Pd$, left: before reaction; right: after 5 reactions, show no significant change in catalyst size and morphology. Scale bar: 20 nm.

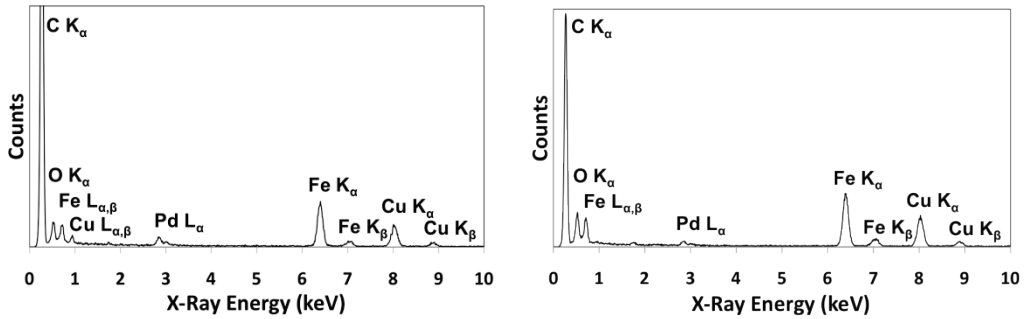

Figure 2-10. EDX spectra of $Fe@Fe_xO_y/Pd$, left: before reaction; right: after 5 reactions, show no significant change in catalyst composition.

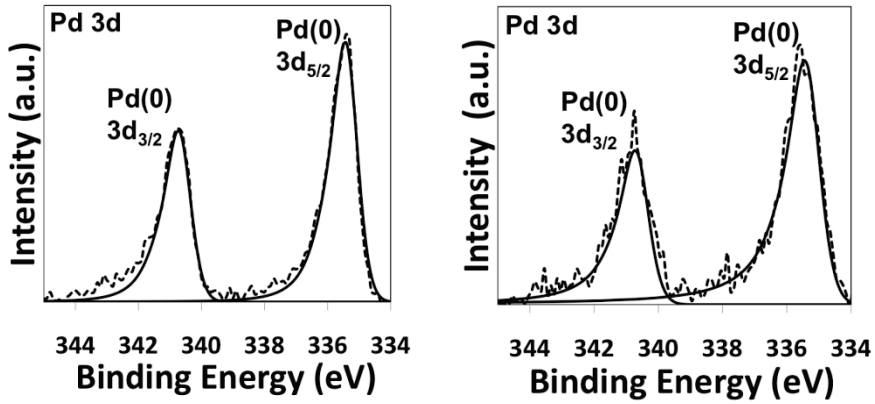

Figure 2-11. Shirley background-subtracted high-resolution Pd 3d region of the XP spectra of $Fe@Fe_xO_y/Pd$ (dotted line), left: before reaction; right: after 5

reactions. All spectra were calibrated to C 1s emission at 284.8 eV. The fitting (solid lines) indicates metallic Pd(0). FWHM range from 0.85 to 1.05. Note that reduced sample amount after reactions leads to reduced signal-to-noise ratio.

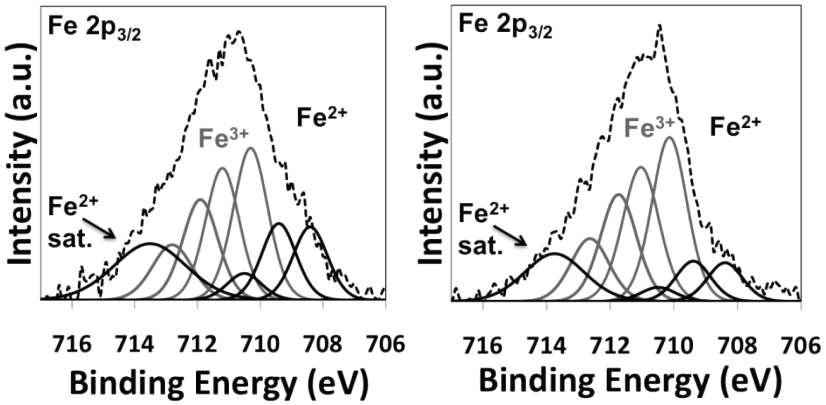

Figure 2-12. Shirley background-subtracted high-resolution Fe $2p_{3/2}$ region of the XP spectra of Fe@Fe_xO_y/Pd (dotted line), left: before reaction; right: after 5 reactions. All spectra were calibrated to C 1s emission at 284.8 eV. The fitting (solid lines) indicates the presence of mixed oxides Fe_3O_4 and FeOOH. A slight decrease in Fe(II) is observed after 5 reactions.

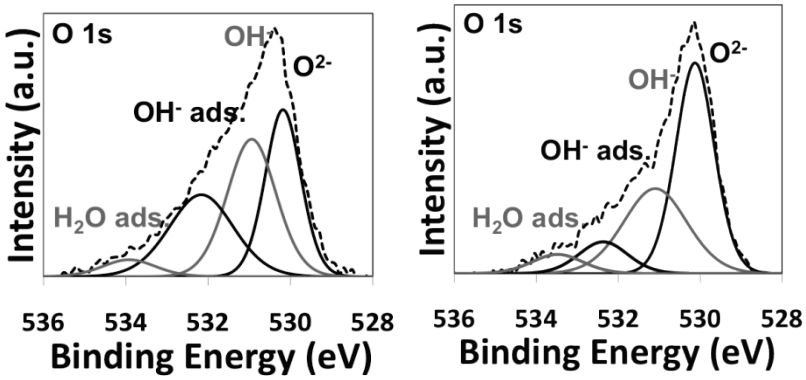

Figure 2-13. Shirley background-subtracted high-resolution O 1s region of the XP spectra of Fe@Fe_xO_y/Pd (dotted line), left: before reaction; right: after 5 reactions. All spectra were calibrated to C 1s emission at 284.8 eV. Solid lines show fits. The peak fit to crystalline OH^- confirms the presence of FeOOH alongside Fe_3O_4.

The mechanism of palladium-catalyzed cross couplings has been studied intensively. In general, Suzuki cross-coupling reactions catalyzed by Pd catalysts follow the "classic" mechanism summarized in Scheme 2-5.[51,52] It involves a

postulated molecular, homogeneous palladium species that cycles between Pd(0) and Pd(II) oxidation states during the course of the catalytic reaction. The reaction starts with oxidative addition of the aryl halide to Pd(0) to form Ar-Pd(II)-X (X = halide) complex. Ar-Pd(II)-X reacts with base to give Ar-Pd(II)-OH, followed by transmetallation of the aryl boron compound onto Pd to form Ar-Pd(II)-Ar' and $B(OH)_4^-$ under basic condition. Finally, reductive elimination of the desired product Ar-Ar' restores the original palladium catalyst. If there are ligands bonded to the palladium catalyst, they remain coordinated to Pd center throughout the entire catalytic cycle (ligands are not shown in Scheme 2-5 for clarity).

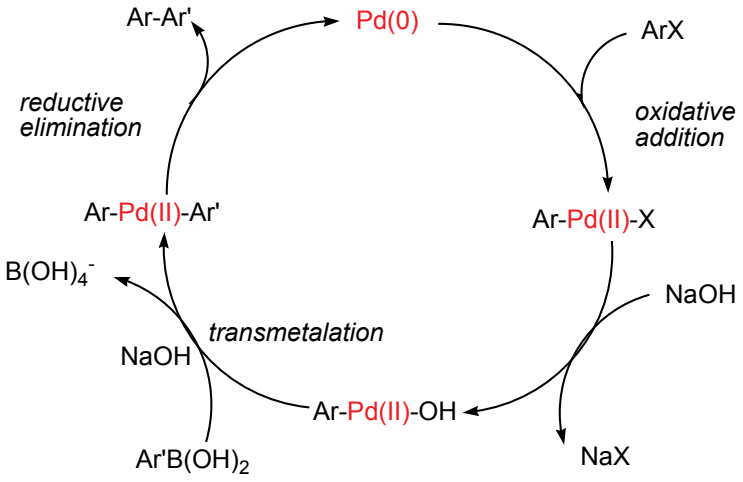

Scheme 2-5. The generally accepted "classic" mechanism of the Suzuki cross-coupling reaction catalyzed by Pd catalysts.

Recently, Amatore and Jutand reported the existence of an anionic version of the "classic" mechanism for homogenous palladium-catalyzed Heck and other coupling reactions.[53] The overall cycle is similar to the standard cycle discussed above however an anionic, penta-coordinated species ($[ArPdX(PPh_3)_2(OAc)]^-$) is

proposed to be the active Pd(II) intermediates.

The mechanism for reactions catalyzed by heterogeneous palladium is the subject of much scientific interest and the exact identity of the active species remains unclear (i.e., heterogeneous vs. quasi-homogeneous). It has been proposed the reaction can take place at the surface of solid metallic Pd as a heterogeneous reaction.[54,55] Alternatively, a quasi-homogeneous mechanism can occur, where Pd is dissolved in a colloidal[56,57] or molecular[58-63] form (e.g., by oxidative addition to the substrate) that is leached from the supported metallic Pd. Currently, it is widely accepted leached palladium species are the active catalysts in most coupling reactions employing solid-supported palladium.[51,52] Following reaction, the leached palladium is subsequently redeposited onto the support, which serves as a Pd reservoir. It is useful to look at a similar catalytic process, Heck reactions catalyzed by Pd/C, Pd/alumina, Pd on zeolites, or Pd on silicoaluminophosphates, Pd can dissolve and leach at the beginning of the reaction, it has been proposed that reactants probably act as ligands for the formation of complexes.[58-60,64-68] The concentration of Pd in solution was found to be highest at the beginning of the reaction and gradually dropped as the reaction progresses. As the reaction ends, most of the dissolved Pd is redeposited onto the support due to the lack of "reactant ligands".

For the present Fe@Fe_xO_y/Pd catalyst system, the leached palladium content in the filtrate from a one hour reaction of bromobenzene with phenylboronic acid was 1.87 ppm (i.e., 1.76% of initial catalyst loading, as determined by ICP-MS). In contrast, when the same quantity of Fe@Fe_xO_y/Pd was reacted for one hour in

the absence of bromobenzene and phenylboronic acid, only 0.15 ppm of Pd was detected. From this we conclude Pd leaching is facilitated by oxidative addition of bromobenzene to the Pd^0 surface.[58-63] Comparing the Pd content in the filtrate solutions from four hours (i.e., complete, 0.54 ppm) and one hour reactions (1.87 ppm) supports the proposal that leached Pd is redeposited onto $Fe@Fe_xO_y$ after reaction is completed. Reusing the filtrate with 0.54 ppm Pd as catalyst for the identical reaction results in 12% yield, strongly suggesting reactivity arises from the leached Pd for which $Fe@Fe_xO_y$/Pd NPs act as "source" and "sink".[58-63]

In the context of the generally accepted "classic" mechanism for the Suzuki coupling reaction (Scheme 2-5), it is unclear which step in the catalytic cycle is rate-determining. It depends upon many factors, including type of aryl halide (Cl, Br and I), catalyst, solvent and other reaction conditions. Our $Fe@Fe_xO_y$/Pd catalyst system has two metals Fe and Pd, and we are devoted to investigate the effect of Fe on catalytic activity of Pd. Due to communication between two transition metals, bimetallic NPs often show enhanced catalytic activity compared to one single metal,[69] so synergistic interaction between Fe and Pd may exist as well during the Suzuki coupling reaction. As we know, Fe has rather low electrochemical potential and thus strong electron-donating ability. In the four steps of the mechanism cycle for Suzuki coupling, it is most likely for Fe to have influence in the first step (i.e., oxidative addition) by supplying additional electron density to the surface Pd species.

Oxidative addition is a key step in many transition-metal catalyzed reactions, such as C-C coupling, hydrogenation, etc. It is a reaction involving the insertion

of a metal between two atoms that were previously bonded together, in which the metal oxidation state goes up. As shown in Scheme 2-6, the new M-X and M-Y bonds are formed using the electron pair of the X-Y bond and electron lone pair of the metal. The metal oxidation state increases (by +2, M^{2+}), while X and Y are formally reduced to X^-, Y^-.

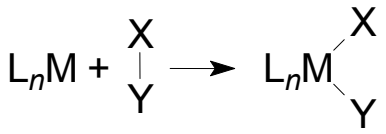

Scheme 2-6. Oxidative addition.

Oxidative addition is a reaction type rather than mechanism. Several different mechanisms are possible, including nucleophilic substitution (polar) mechanism, concerted (non-polar) mechanism and radical mechanism. Nucleophilic substitution mechanism, also called polar mechanism, suites for polar X-Y bonds, such as alkyl/aryl halides. It is very similar to an aliphatic nucleophilic substitution (S_N1 or S_N2) reaction. As shown in Scheme 2-7, metal initially acts as nucleophile to attack the electron deficient carbon. In the second step, the liberated halide anion binds to the metal. That doesn't happen in a normal nucleophilic substitution. In this case, the metal has empty d orbitals and is able to accept electron pair from the halide anion.

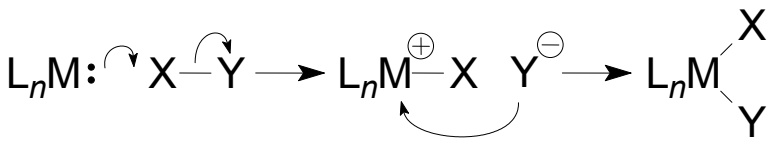

Scheme 2-7. Nucleophilic substitution mechanism for oxidative addition.

In the oxidative addition of the Suzuki coupling reaction catalyzed by our

$Fe@Fe_xO_y$/Pd catalyst system, nucleophilic substitution mechanism applies and Fe can donate electrons to surface Pd, which enhances nucleophilicity of Pd. The more nucleophilic the metal is, the greater its reactivity is in nucleophilic substitution of oxidative addition. For homogenous palladium-catalyzed Suzuki coupling, the nucleophilicity of palladium can be varied by changing the ligands. For heterogeous palladium catalyst, the nucleophilicity of palladium is hardly to tune because most of supports are insulators, such as zeolite, silica, and metal oxides. In the $Fe@Fe_xO_y$/Pd catalyst system, the metallic iron core can donate electrons to surface Pd, which may go through a few nanometer-thick iron oxide shell. This unique structure will enable us to adjust the catalytic activity by changing the electron-donating ability of the core.

To investigate the effect of Fe on the catalytic activity, we used different amounts of $Fe@Fe_xO_y$ to deposit Pd (Table 2-6). By increasing amount of $Fe@Fe_xO_y$, which can donate more electrons to surface Pd, thus the catalyst will supposed to be more active. Because aryl bromides and iodides are very active to participate in the coupling reactions with phenylboronic acid, it is hard to tell the difference of Pd activity. To find a suitable substrate which can differentiate the activity of catalysts with different amount of $Fe@Fe_xO_y$, we used less active aryl chlorides, such as chlorobenzene, 1-chloro-4-nitrobenzene and 1-chloro-4-acetylbenzene to couple with phenylboronic acid (Table 2-6).

From Table 2-6, there is no obvious tendency for the yield when the $Fe@Fe_xO_y$ amount was increased from 5 mg to 25 mg, then to 50 mg for three aryl chlorides. This result is unexpected, because we hope that the yield will increase when the

amount of $Fe@Fe_xO_y$ increases. It seems $Fe@Fe_xO_y$ has no substantial influence on Pd activity for Suzuki coupling.

Table 2-6. Effect of $Fe@Fe_xO_y$ on catalytic activity of palladium in the Suzuki coupling reaction[a]

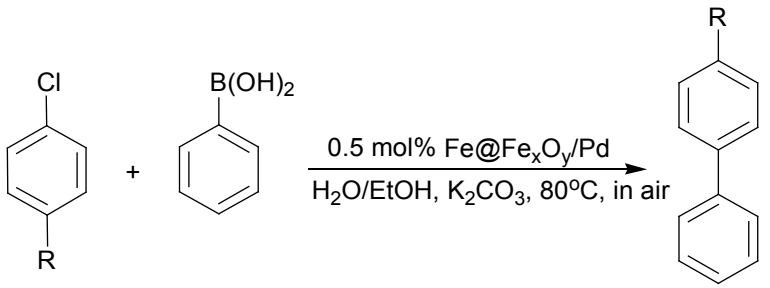

R	Yield (%)[b]		
	5 mg $Fe@Fe_xO_y$	25 mg $Fe@Fe_xO_y$	50 mg $Fe@Fe_xO_y$
-H	2.6	2.5	9.6
$-NO_2$	22.3	22.1	21.3
-COMe	15.7	14.2	15.0

[a]Reaction conditions: 2.0 mmol aryl chloride, 2.4 mmol phenylboronic acid, 5.0 mmol K_2CO_3, 0.5 mol% $Fe@Fe_xO_y$/Pd, H_2O/EtOH (1:1), 80 °C, 24 h. [b]GC yield.

Is it possible to activate inactive transition metal by increasing amount of Fe? Ni has appeared the perfect choice because of its similar but lower catalytic activity compared to Pd, and Ni is not active for Suzuki coupling even for iodobenzene. Activation of $Fe@Fe_xO_y$/Ni was attempted to catalyze coupling of iodobenzene and phenylboronic acid by increasing amount of $Fe@Fe_xO_y$. However, no biphenyl product was detected by GC-MS when $Fe@Fe_xO_y$ amount is up to 100 mg under the same reaction conditions as $Fe@Fe_xO_y$/Pd. So Ni is not activated to catalyze Suzuki coupling by increasing $Fe@Fe_xO_y$ amount. Recalling the mechanism cycle of Suzuki coupling reaction, it is hard to state which step is rate-determining; in fact depending upon the substrate, catalyst and solvent any of the four steps can be rate-determining. If one of the other three steps is rate-

determining, the $Fe@Fe_xO_y$ is not expected to exhibit an effect on the reaction rate even though it can donate electrons to the surface catalytic metal species, which can promote oxidative addition.

In conclusion, we have demonstrated $Fe@Fe_xO_y$ can be used as a versatile support for immobilizing catalytic metals. The immobilization is readily achieved via coordination of metal ions to the iron oxide surface and subsequent reduction of these coordinated ions to their metallic state by the iron core. As an example of their catalytic potential, $Fe@Fe_xO_y$ decorated with spectroscopically dectectable metallic Pd domains were evaluated and found to exhibit high catalytic activity toward Suzuki-Miyaura cross-coupling reactions in aqueous solution at room temperature in air. This catalytic system effectively couples the advantages of heterogeneous (e.g., low cost, air-stability, easy separation, and good reusability) and homogeneous systems (e.g., high yield), making it a promising material for practical application. Furthermore, $Fe@Fe_xO_y$/Pd has special retention ability for Pd species due to the established reducing nature and coordinating ability of the $Fe@Fe_xO_y$ support, which make leached Pd negligible. The effect of $Fe@Fe_xO_y$ on the catalytic activity of Pd and Ni was investigated by increasing amount of $Fe@Fe_xO_y$, however, no visible effect on activity of catalysts was found for the Suzuki coupling reactions. Ongoing investigations are aimed at other catalytic metals and metal combinations in an effort to demonstrate the versatility of the $Fe@Fe_xO_y$ support.

2.4 References

1. http://nobelprize.org/nobel_prizes/chemistry/laureates/2010/press.html, accessed July 28, 2011.
2. Miyaura, N.; Yamada, K.; Suzuki, A. *Tetrahedron Lett.* **1979**, *20*, 3437.
3. Miyaura, N.; Suzuki, A. *J. Chem. Soc. Chem. Commun.* **1979**, 866.
4. Ishiyama, T.; Abe, S.; Miyaura, N.; Suzuki, A. *Chem. Lett.* **1992**, 691.
5. Miyaura, N.; Yanagi, T.; Suzuki, A. *Synth. Commun.* **1981**, *11*, 513.
6. Miyaura, N.; Suzuki, A. *Chem. Rev.*, **1995**, *95*, 2457.
7. Garg, N. K.; Caspi, D. D.; Stoltz, B. M. *J. Am. Chem. Soc.* **2004**, *126*, 9552.
8. Baudoin, O.; Cesario, M.; Guenard, D.; Gueritte, F. *J. Org. Chem.* **2002**, *67*, 1199.
9. Thomson, R. H. *The Chemistry of Natural Products*, Blackie and Son, Glasgow, **1985**
10. Kotha, S.; Lahiri K.; Kashinath, D. *Tetrahedron,* **2002**, *58*, 9633.
11. Albaneze-Walker, J.; Murry, J. A.; Soheili, A.; Ceglia, S.; Springfield, S. A.; Bazaral, C.; Dormer P. G.; Hughes, D. L. *Tetrahedron*, **2005**, *61*, 6330.
12. K. Eicken, H. Rang, A. Harreus, N. Götz, E. Ammermann, G. Lorentz, and S. Strathmann, German Patent DE19531813, **1997**.
13. K. Eicken, M. Rack, F. Wetterich, E. Ammermann, G. Lorentz, and S. Strathmann, German Patent DE19735224, **1999**.
14. A. M. Rouhi, *Chem. & Eng. News* **2004**, *82* (36), Sept. 6, pp 49-58.
15. Kertesz, M.; Choi, C. H.; Yang, S. *Chem. Rev.* **2005**, *105*, 3448.
16. Nicolaou, K. C.; Bulger, P. G.; Sarlah, D. *Angew. Chem. Int. Ed.* **2005**, *44*, 4442-4489 and references therein.
17. Littke, A. D.; Dai, C.; Fu, G. C. *J. Am. Chem. Soc.* **2000**, *122*, 4020.
18. Yin, J.; Rainka, M. P.; Zhang, X.-X.; Buchwald, S. L. *J. Am. Chem. Soc.* **2002**, *124*, 1162.
19. Martin R.; Buchwald, S. L. *Acc. Chem. Res.* **2008**, *41*, 1461.
20. Navarro, O.; Kelly, R. A.; III; Nolan, S. P. *J. Am. Chem. Soc.* **2003**, *125*, 16194.
21. Hagen, J. *Industrial Catalysis: A Practical Approach*, 2nd Edition, Wiley-VCH, Weinheim, **2006**.
22. Yin, L,; Liebscher, J. *Chem. Rev.* **2007**, *107*, 133 and references therein.
23. Astruc, D.; Lu, F.; Aranzaes, J. R. *Angew. Chem., Int. Ed.* **2005**, *44*, 7852 and references therein.
24. Shiju, N. R.; Guliants, V. V. *Appl. Catal. A* **2009**, *356*, 1.
25. Jones, G. et al. *J. Catal.* **2008**, *259*, 147.
26. Bell, A. T. *Science* **2003**, *299*, 1688.
27. Gandhi, H. S.; Graham, G. W.; McCabe, R. W. *J. Catal.* **2003**, *216,* 433.
28. Zhang, W. *J. Nanopart. Res.* **2003**, *5*, 323.
29. Sheldon, R. A.; van Bekkum, H. *Fine Chemicals through Heterogeneous Catalysis*; Wiley: Weinheim, **2001**.
30. Lu, A.; Salabas, E. L.; Schuth, F. *Angew. Chem., Int. Ed.* **2007**, *46*, 1222.
31. Hu, A.; Yee, G. T.; Lin, W. *J. Am. Chem. Soc*. **2005**, *127*, 12486.
32. Baruwati, B.; Guin, D.; Manorama, S. V. *Org. Lett*. **2007**, *9*, 5377.

33. Stevens, P. D.; Fan, J.; Gardimalla, H. M. R.; Yen, M.; Gao, Y. *Org. Lett*. **2005**, *7*, 2085.
34. Zhu, Y.; Peng, S. C.; Emi, A.; Su, Z.; Monalisa; Kemp, R. A. *Adv. Synth. Catal.* **2007**, *349*, 1917.
35. Yi, D. K.; Lee, S. S.; Ying, J. Y. *Chem. Mater.* **2006**, *18*, 2459.
36. Macdonald, J. E.; Kelly, J. A.; Veinot, J. G. C. *Langmuir* **2007**, *23*, 9543.
37. Macdonald, J. E.; Veinot, J. G. C. *Langmuir* **2008**, *24*, 7169.
38. Zhou, S.; Johnson, M.; Veinot, J. G. C. *Chem. Commun.* **2010**, *46*, 2411-2413.
39. Li, X. Q.; Zhang, W. X. *Langmuir* **2006**, *22*, 4638-4642.
40. Wang, C.; Baer., D. R.; Amonette, J. E.; Engelhard, M. H.; Antony, J.; Qiang, Y. *J. Am. Chem. Soc.* **2009**, *131*, 8824-8832.
41. Wang, C.; Baer, D. R.; Thomas, L. E.; Amonette, J. E.; Antony, J.; Qiang, Y.; Duscher, G. *J. Appl. Phys.* **2005**, *98*, 094308.
42. Martin, J. E.; Herzing, A. A.; Yan, W.; Li, X.; Koel, B. E.; Kiely, C. J.; Zhang, W. *Langmuir* **2008**, *24*, 4329-4334.
43. Peng, Y.; Park, C.; Zhu, J.; White, R.; Laughlin, D. *J. Appl. Phys.* **2004**, *95*, 6798-6800.
44. Grosvenor, A. P.; Kobe, B. A.; Biesinger, M. C.; McIntyre, N. S. *Surf. Interface Anal.* **2004**, *36*, 1564.
45. Li, X.; Zhang, W. *J. Phys. Chem. C* **2007**, *111*, 6939-6946.
46. Sun, Y. P.; Li, X. Q.; Cao, J. S.; Zhang, W. X.; Wang, H. P. *Adv. Colloid Interface Sci.* **2006**, 120, 47-56.
47. http://www.modernmicroscopy.com/main.asp?article=71
48. Legare, P.; Fritsch, A. *Surf. Interface Anal.* **1990**, *15*, 698.
49. *Note for Guidance on Specific Limits for Residues of Metal Catalysts*, **2002**, http://www.emea.europa.eu/pdfs/human/swp/444600en.pdf
50. Farina, V. *Adv. Synth. Catal.* **2004**, *346*, 1553-1582.
51. Yin, L.; Liebscher, J. *Chem. Rev.* **2007,** *107*, 133 and references therein.
52. Phan, N. T. S.; Van Der Sluys, M.; Jones, C. W. *Adv. Synth. Catal.* **2006**, *348*, 609 and references therein.
53. Amatore, C.; Jutand, A. *Acc. Chem. Res.* **2000**, *33*, 314.
54. Augustine, R. L.; O'Leary, S. T. *J. Mol. Catal. A: Chem.* **1995**, *95*, 277 and references therein.
55. LeBlond, C. R.; Andrews, A. T.; Sun, Y. K.; Sowa, J. R. *Org. Lett.* **2001**, *3*, 1555.
56. Reetz, M. T.; Westermann, E. *Angew. Chem., Int. Ed.* **2000**, *39*, 165.
57. de Vries, J. G. *J. Chem. Soc., Dalton Trans.* **2006**, 421.
58. Seki, M. *Synthesis* **2006**, 2975.
59. Zhao, F.; Bhanage, B. M.; Shirai, M.; Arai, M. *Chem. Eur. J.* **2000**, *6*, 843.
60. Biffis, A.; Zecca, M.; Basato, M. *Eur. J. Inorg. Chem.* **2001**, 1131.
61. Zhao, F.; Shirai, M.; Arai, M. *J. Mol. Catal. A: Chem.* **2000**, *154*, 39.
62. Köhler, K.; Wagner, M.; Djakovitch, L. *Catal. Today* **2001**, *66*, 105.
63. Yu, K.; Sommer, W.; Richardson, J. M.; Weck, M.; Jones, C. W. *Adv. Synth. Catal.* **2005**, *347*, 161.
64. Davies, I. W.; Matty, L.; Hughes, D. L.; Reider, P. J. *J. Am. Chem. Soc.* **2001**, *123*, 10139.

65. Zhao, F.; Murakami, K.; Shirai, M.; Arai, M. *J. Catal.* **2000**, *194*, 479.
66. Okumura, K.; Nota, K.; Yoshida, K.; Niwa, M. *J. Catal.* **2005**, *231*, 245.
67. Pröckl, S. S.; Kleist, W.; Köhler, K. *Tetrahedron* **2005**, *61*, 9855.
68. Srivastava, R.; Venkatathri, N.; Srinivas, D.; Ratnasamy, P. *Tetrahedron Lett.* **2003**, *44*, 3649.
69. Wang, D.; Li, Y. *Adv. Mater.* **2011**, *23*, 1044-1060 and references therein.

Chapter 3: Synthesis of Fe-Pd Nano-structures and Their Catalytic Activity for Suzuki Cross-Coupling Reactions

3.1 Introduction

Metallic nanoparticles (NPs) constructed from more than one metal have been attracting increasing interest as a result of their multiple functionalities arising from different metals. Bimetallic NPs are emerging as a new class of useful materials that can exhibit hybrid properties associated with two constituent metals. While some bimetallic NPs do not show unexpected properties, frequently there is a substantial enhancement in specific physical and chemical properties arising from synergistic effects of combining these metals. A rich diversity of compositions, structures, and properties of bimetallic NPs has led to widespread applications in electronics, biosensing, and catalysis.[1-4] Combining metals offers an intriguing approach for tailoring the electronic and geometric structures to enhance the catalytic activity and selectivity. Bimetallic NPs are widely used as catalysts in a variety of industrially relevant reactions including catalytic reforming,[5-7] pollution control,[5] alcohol oxidation,[8] and fuel cells for energy conversion.[9-12] In all these cases, combining two metals enhanced catalytic activity and selectivity compared to monometallic counterparts.

There are many different types of bimetallic NPs. When considering mixing

pattern of two metals a variety of nanostructures can result depending upon reaction parameters. If one class of metal ion is reduced first a seed particle forms and the second metal deposits evenly on the seed to form a core-shell structure (Figure 3-1A). This is a classic example of heterogenous nucleation.[13] Heterostructures form when individual nucleation and growth of the two metals of choice occur and they share an interface during the growth process (Figure 3-1B). Alloy (Figure 3-1C) particles consist of a homogeneous mixture of two metals where metal-metal bonds form. Depending on relative size of mixing atoms, atom exchange happens when the atoms are relatively similar in size, where some of the atoms in the metallic crystals are replaced with atoms of the other constituent. If one type of atom is much smaller than the other, it may be trapped in the interstices between the atoms in the crystal matrix.[14]

(a) (b) (c)

Figure 3-1. Bimetallic NPs with three different structures, (a) core-shell; (b) heterostructure; (c) alloy. One sphere represents an atom, two types of atoms are depicted with different colours.

Alloy nanostructures can be differentiated from core-shell particles and heterostructures using powder X-ray diffraction (XRD). This is possible because core-shell and heterostructure compounds exhibit reflections characteristic of two constituent metals, while for alloys new reflections (usually between the original reflections arising from the two metals) appear, indicating new crystal structure.

3.1.1 Methods for Synthesis of Bimetallic NPs

In general, bimetallic NPs may be prepared in the solid, gas, or solution phases.[1,2,4] Metallurgical techniques are traditionally used for making bimetallic compounds, which melt two kinds of bulk metals under proper conditions. This solid state method requires high temperature and long annealing times; it is also difficult to obtain nanoscale bimetallic particles.[15,16] A typical gas phase synthesis employs molecular beam techniques (e.g., laser beam, pulsed arc, ion sputtering, magnetron sputtering).[17] Under these conditions, bulk metallic powders or two monometallic precursors are mixed and vaporized to produce gas phase atoms; collision and condensation of the atomic species and extrusion through a nozzle forms bimetallic particles.[18] A wide variety of bimetallic NPs (e.g., Au-Ag, Au-Pd, Au-Pt, Fe-Pd, Fe-Pt, Ni-Pd, Ni-Pt, and Fe-Ni alloys) have been prepared in this way.[19] Unfortunately, these gas phase preparations require complicated and costly apparatus and only yield small quantities of materials.

In this regard, solution-based methods provide clear advantages. The key issue that must be addressed is control of the nucleation and growth of two distinct metal species. Co-reduction is among the most common and straightforward methods for preparing bimetallic NPs, however appropriate selection of reducing agents is paramount if this method is to be fully exploited. Because redox potentials and chemical reactivities of metals (or metal precursors) differ great care must be exercised to control nucleation events. In general, the metal of higher redox potential is reduced first. When the second metal deposits on the surface of the preformed metal symmetrically, core-shell NPs are obtained. If the deposition

process only occurs preferentially on particular crystal faces or particle facets, heterostructure NPs will be obtained. Simultaneous reduction and nucleation lead to the formation of metal-metal bonds, alloyed NPs will be synthesized. Yang and co-workers synthesized truncated-octahedral alloyed Pt_3Ni nanocrystals (NCs) from $Pt(acac)_2$ and $Ni(acac)_2$ using borane-tert-butylamine complex and hexadecanediol as the reducing agents.[20] Butylamine is used to replace the capping agents in the surface treatment to create active electrocatalysts for oxygen reduction reaction (i.e., reduction from O_2 to H_2O). The co-reduction process in solution system is very effective in preparing high-quality bimetallic NPs with well defined structure, shape and size.

Thermal decomposition of organometallic compounds is another classic route to obtain highly monodisperse bimetallic NPs. A prototypical example of this type of synthesis was reported by Sun and coworkers.[21] This was the first synthetic report of monodisperse alloyed Fe-Pt NPs obtained from simultaneous thermal decomposition of iron pentacarbonyl ($Fe(CO)_5$) and reduction of platinum acetylacetonate ($Pt(acac)_2$) at 300 °C in a mixture of oleic acid and oleylamine (Scheme 3-1). The size and composition of the particles were controlled by varying the synthetic parameters such as molar ratio of stabilizers to metal precursors, molar ratio of two metal precursors.[21,22]

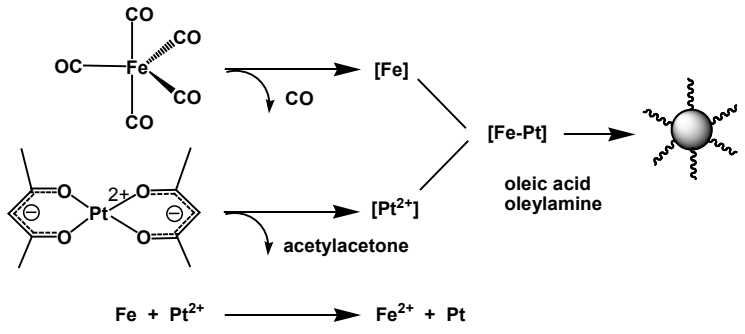

Scheme 3-1. Synthesis of alloyed Fe-Pt NPs using thermal decomposition.

Seeded-growth in solution provides a very effective route for generating bimetallic NPs with well-controlled morphologies (e.g., core-shell and heterostructures). When the second metal evenly deposits onto the surface of the preformed seed, core-shell structures will be obtained. Heterostructures are obtained if the deposition and growth of the second metal occur on a specific site or face of the seed. Xia et al.[13] used L-ascorbic acid and citric acid as reducing agents to control the growth of Au on cubic Pd seeds, and obtained Pd-Au core-shell and heterostructure nanocrystals (NCs), respectively (Figure 3-2).

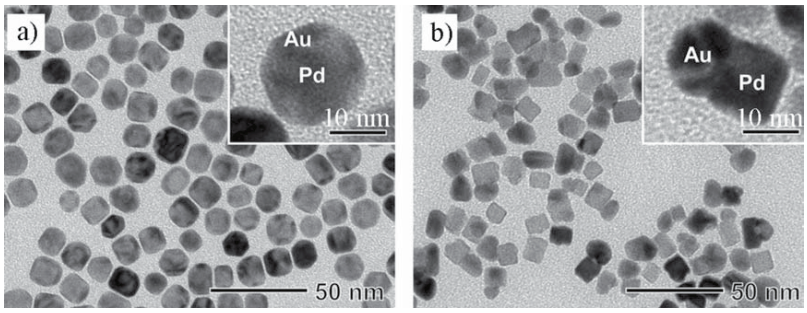

Figure 3-2. TEM images of a) Pd-Au core-shell and b) Pd-Au dimer NCs synthesized by seeded-growth, reproduced from ref. 13.

Galvanic displacement also provides a way to make bimetallic nanostructures. This method employs differences in the redox potential of the metals of choice. A prerequisite for galvanic displacement is the second metal ion must be reduced by the preformed metal. The preformed metal is a sacrificial template and is partially consumed. Successful synthesis of Co@Au core-shell nanospheres was achieved by a one-step galvanic displacement reaction between Co NPs and $AuCl_4^-$ ions in the presence of polyvinylpyrrolidone in aqueous solution (Figure 3-3).[23]

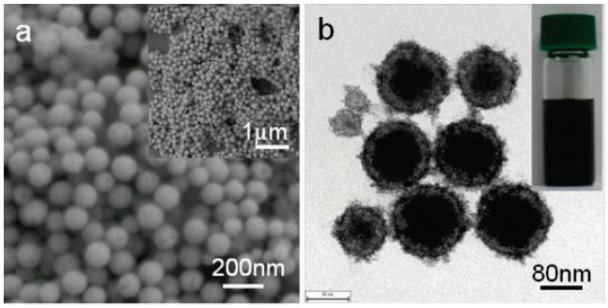

Figure 3-3. (a) SEM and (b) TEM images of Co@Au core-shell nanospheres synthesized by galvanic displacement, reproduced from ref. 23.

3.1.2 Catalytic Applications of Bimetallic NPs

As mentioned before, when compared to monometallic NPs, bimetallic NPs often show enhanced catalytic properties. Studies indicate the bimetallic NP composition, oxidation state, and morphology play a critical role in determining their catalytic properties. Li et al. showed improved catalytic efficiency of Au@Co core-shell bimetallic NPs for the CO oxidation reaction forming CO_2 compared to pure Au or Co NPs (Figure 3-4).[24]

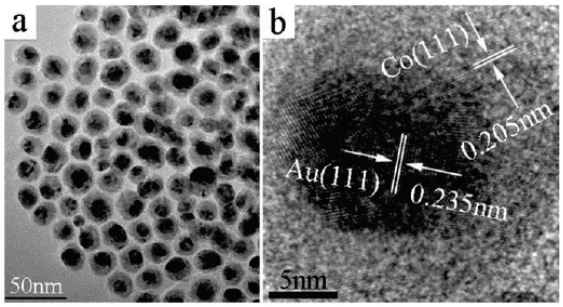

Figure 3-4. (a) TEM and (b) HRTEM images of Au@Co core-shell NPs, reproduced from ref. 24.

Another key example was reported by Hyeon and co-workers who synthesized bimetallic Pd/Ni NPs with Ni-rich cores and Pd-rich shells.[25] When tested for catalytic activity in Sonogashira coupling reactions, it was found that the catalytic

activity of the bimetallic Pd/Ni NPs far exceeded that of monometallic Pd NPs with similar size.

Stamenkovic and co-workers demonstrated that the nanocrystal Pt_3Ni (111) surface is 10-fold more active for the oxygen reduction reaction (i.e., reduction from O_2 to H_2O) than the corresponding Pt (111) surface and 90-fold more active than the state-of-the-art Pt/C catalysts for polymer electrolyte membrane fuel cells, because the Pt_3Ni (111) surface has an appropriate electronic structure and arrangement of surface atoms that greatly increases the number of active sites for oxygen adsorption.[26]

Xia and his colleagues synthesized Pd-Pt bimetallic nanodendrites consisting of a dense array of Pt branches on a Pd core, which were two and a half times more active for the oxygen reduction reaction than the state-of-the-art Pt/C catalyst and five times more active than the first-generation supportless Pt-black catalyst.[27]

In this chapter, we prepared three types of Fe-Pd alloy NPs using concomitant thermal decomposition of $Fe(CO)_5$ and reduction of $Pd(acac)_2$ in oleylamine with or without additional reducing agents. These as-synthesized Fe-Pd alloy NPs were characterized by TEM, XPS and XRD, and their catalytic activities were tested in Suzuki cross-coupling reactions.

3.2 Experimental Section

3.2.1 Chemicals

Iron (0) pentacarbonyl ($Fe(CO)_5$, 99.999%), palladium (II) acetylacetonate ($Pd(acac)_2$, 99%), oleylamine (technical grade, 70%), oleic acid (technical grade, 90%), 1-octadecene (technical grade, 90%), 1-adamantanecarboxylic acid (ACA,

99%), sodium sulfate (Na_2SO_4, ACS reagent,≥ 99%, anhydrous), all aryl halides and aryl boronic acids were purchased from Sigma-Aldrich. 1,2-hexadecanediol (>98%) was purchased from TCI and tri-n-butylphosphine (TBP, 99%) was purchased from Strem Chemicals, Inc. K_2CO_3 was purchased from Mallinckrodt. All reagents were used without further purification unless otherwise noted. Typically, in-house deionized water was employed for Suzuki coupling reactions, and 18.2 $M\Omega \cdot cm^{-1}$ Millipore water was used for ICP-MS studies.

3.2.2 Synthesis of Fe-Pd Nanodendrites (ND)-Method 1

The procedure for synthesis of Fe-Pd ND was adapted from a literature method for synthesizing FePt NPs.[28] $Pd(acac)_2$ (0.5 mmol, 152 mg), oleic acid (4 mmol, 1.27 ml), and oleylamine (4 mmol, 1.32 ml) were mixed with 10 ml of 1-octadecene in an argon atmosphere. The mixture was heated to 120 °C at a heating rate of 6-7 °C/min (oil bath). The flask was maintained at this temperature for 10 minutes to ensure the dissolution of $Pd(acac)_2$. Under a blanket of argon gas, 0.20 ml of $Fe(CO)_5$ was added. The solution was then heated to 200 °C at a heating rate of 5 °C/min, and kept at this temperature for 1 h. The heating source was then removed, and the solution was cooled to room temperature. A black product was precipitated by adding 10 ml of isopropyl alcohol, and the yellow-brown supernatant was decanted by applying a magnet. The black product was washed by isopropyl alcohol 15 ml×4 and dried *in vacuo* for 1 day to yield a dry powder. The dry powder was stored in an argon-filled glove box (0.6 ppm H_2O, 0.6 ppm O_2).

The composition of the as-synthesized NPs was analyzed by inductively coupled plasma mass spectrometry (ICP-MS), revealing composition is $FePd_3$.

3.2.3 Synthesis of Fe-Pd NPs (NP1, NP2)-Method 2

Fe-Pd NPs were prepared using a modified literature procedure.[29,30] All procedures were performed in an argon atmosphere. $Pd(acac)_2$ (0.08 g, 0.25 mmol), and 1-adamantanecarboxylic acid (ACA) (NP1, 0.27 g, 1.5 mmol; NP2 0.54 g, 3 mmol) were dissolved in 1 ml of tri-n-butylphosphine (TBP) to form solution (1) at room temperature. Subsequently, 0.14 ml (1 mmol) of $Fe(CO)_5$ was injected into the solution (1) to obtain orange stock solution (2). In a Schlenk flask, solution (3) consisting of 390 mg (1.5 mmol) 1,2-hexadecanediol and 17 ml oleylamine was heated to 120-180 °C for 60 min. Sequentially, the stock solution (2) was quickly injected into solution (3). The resulting reaction mixture was maintained at 120-180 °C for 1 hour, and then the reaction temperature was slowly increased (5 °C/min) and maintained at 280-300 °C for 2 hours. During heating, the reaction mixture slowly changed from orange to black, suggesting the formation of the nuclei. After two hours the reaction mixture was cooled to room temperature. The black precipitates were isolated from the solution by adding 30 ml acetone, and the yellow-brown supernatant was decanted by applying a magnet. The black product was washed by acetone 25 ml×4 and then dried *in vacuo* for 1 day to yield a dry powder. The dry powder was stored in an argon-filled glove box (0.6 ppm H_2O, 0.6 ppm O_2) until used in catalytic testing.

3.2.4 Determination of Fe and Pd Contents in Samples

The Fe and Pd contents were determined using inductively coupled plasma mass spectrometry (ICP-MS). NP samples were dissolved in concentrated nitric acid, and the solution was heated in a sand bath until no solid is present. The clear yellow/orange solution was quantitatively transferred to a 10 ml volumetric flask and analyzed by ICP-MS.

3.2.5 General Procedure for Evaluating Nanomaterial Catalytic Activity in Suzuki Cross-Coupling Reactions

For reactions performed in EtOH/H_2O (1:1), the aryl halide (2.0 mmol) and aryl boronic acid (2.4 mmol) were dissolved in 5 ml ethanol. ND or NP1 or NP2 (0.5 mol% Pd) were added to the ethanol solution. K_2CO_3 (5 mmol) in 5 ml deionized water was subsequently combined with the ethanol mixture and the mixture was sonicated for two minutes. The reaction mixture was subsequently stirred at room temperature (or 80 °C) in air for time listed in Table 3-1.

For reactions performed in dimethylformamide (DMF), ND, NP1, or NP2 (0.5 mol% Pd), aryl halide (2.0 mmol), aryl boronic acid (2.4 mmol) and K_2CO_3 (5 mmol) were added to a round bottom flask, and 10 ml DMF was added. The mixture was sonicated for two minutes before it was heated at 80 °C in air for time listed in Table 3-1.

Identical work-up procedures were used for the EtOH/H_2O and DMF reaction media. After reaction, the catalyst was separated by exposing the reaction mixture to a permanent magnet and the supernatant was decanted. The decantate was extracted with diethyl ether (4 × 25 ml) and the organic layers were combined, dried over anhydrous Na_2SO_4 and the solvent was removed on a rotary evaporator to yield the crude product. If necessary, the crude product was purified by column

chromatography on silica gel (petroleum ether/ethyl acetate) to give the desired products. Products were identified by GC-MS as well as ^{1}H and ^{13}C NMR. The catalyst was washed by acetone and dried before it was evaluated for reuse.

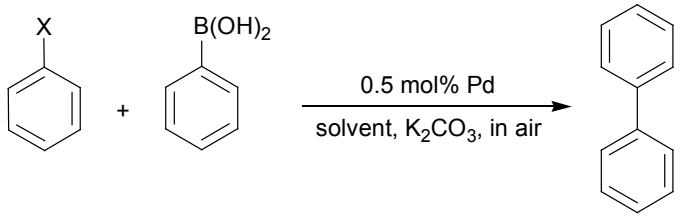

Scheme 3-2. Suzuki-Miyaura cross-coupling reactions.

Table 3-1. A summary of Suzuki-Miyaura cross-coupling reactions.

Entry	Catalyst	X	Temperature	Solvent	Time (h)	Yield (%)
1	ND	Br	r.t.	EtOH/H_2O	2	98
2	NP1	Br	r.t.	EtOH/H_2O	2	95
3	NP2	Br	r.t.	EtOH/H_2O	2	95
4	Pd/C	Br	r.t.	EtOH/H_2O	4	90
5	ND	Cl	r.t.	EtOH/H_2O	48	11
6	ND	Cl	r.t.	DMF	48	13
7	ND	Cl	80 °C	EtOH/H_2O	24	25
8	ND	Cl	80 °C	DMF	24	69
9	NP1	Cl	80 °C	DMF	24	52
10	NP2	Cl	80 °C	DMF	24	44
11	Pd/C	Cl	80 °C	DMF	24	27

3.2.6 Characterization Methods

^{1}H and ^{13}C NMR spectra were obtained for $CDCl_3$ solutions using a Varian Inova 400 spectrometer at 400 MHz and 100 MHz, respectively. Spectra were referenced to $CHCl_3$ (7.26 ppm) and $CDCl_3$ (77.06 ppm), respectively. Chemical shifts are recorded in parts per million (ppm, δ).

Gas chromatography-mass spectrometry (GC-MS) was performed using a Hewlett-Packard 5890 with a 5970 MSD using electron ionization. 1 μL of an acetone solution of the product was injected into a DB-5MS column with a 0.25 μm film. The carrier gas was helium at 1 ml/min. The injection port was at 280 °C and a linear temperature profile (50 °C - 280 °C at 10 °C /minute) was employed.

Transmission electron microscopy (TEM), energy dispersive X-ray spectroscopy (EDX), and selected area electron diffraction (SAED) were performed using a JEOL 2010 transmission electron microscope with an accelerating voltage of 200 keV and a LaB_6 thermionic emission filament. The instrument was fitted with an EDX detector for elemental analysis.

TEM samples were prepared by suspending particles in hexane by sonication and drop-coating the solution onto carbon-coated, 200-mesh Cu grids (SPI Supplies).

Powder X-ray diffraction (XRD) was performed using a Rigaku Geigerflex 2173 X-ray diffractometer equipped with a Co Kα radiation source (λ = 1.79 Å). The system is equipped with a graphite monochromator to filter the Kβ wavelengths. Bulk crystallinity was evaluated on finely ground samples mounted on an aluminum holder under a helium atmosphere.

X-ray photoelectron spectroscopy (XPS) was performed using an AXIS-165 XPS spectrometer from Kratos Analytical. The base pressure and operating pressure in the chamber were maintained at $\leq 10^{-7}$ Pa. A monochromatic Al Kα X-ray (λ = 8.34 Å) was used to irradiate the samples, and the spectra were obtained with an electron takeoff angle of 90°. Samples were pressed into carbon

tape. To control sample charging, the charge neutralizer filament was used during the experiment. The pass energy for the survey and the high-resolution spectra were 160 and 20 eV, respectively. Spectra were calibrated to the C 1s emission at 284.8 eV using CasaXPS (VAMAS) software. Following calibration, the background of each spectrum was subtracted using a Shirley-type background to remove most of the extrinsic loss structure. Fitting was carried out using 70% Lorentzian/30% Gaussian line shapes for metal zero-oxidation states, and Gaussian line shapes for higher oxidation states. Binding Energy values and orbital splitting were consistent with literature values obtained from the NIST database (http://srdata.nist.gov/xps/).

Inductively coupled plasma mass spectrometry (ICP-MS) was performed on a Perkin Elmer Elan 6000 ICP-MS. The flow rate on the instrument was 1 ml/min and dual detector mode was employed. A blank was subtracted after internal standard correction and the values reported are an average of three readings (35 sweeps per reading).

3.3 Results and Discussion

The synthesis of bimetallic Fe-Pd nanostructures was performed using a modified literature procedure previously reported for the synthesis of Fe-Pt[21,22,28] and Fe-Pd[29,30] NPs. We prepared Fe-Pd nanostructures by simultaneous thermal decomposition of iron pentacarbonyl ($Fe(CO)_5$) and reduction of palladium acetylacetonate ($Pd(acac)_2$) in the presence of oleic acid and oleylamine (Scheme 3-3). Oleic acid and oleylamine are used as stabilizers and their structures are shown in Scheme 3-4. In method 1, $Pd(acac)_2$ and excess $Fe(CO)_5$ are heated at

200 °C. Under these conditions, $Fe(CO)_5$ decomposes first to form Fe nuclei and subsequent/simultaneous decomposition and reduction of $Pd(acac)_2$ by preformed Fe atoms yields Fe-Pd nuclei. Further growth results formation of Fe-Pd NPs. In method 2, an additional reducing agent 1,2-hexadecanediol was introduced to accelerate conversion of $Pd(acac)_2$ to Pd atoms, which combine with Fe atoms from decomposition of $Fe(CO)_5$ to generate Fe-Pd nuclei. Again, further growth results formation of Fe-Pd NPs. The size of the particles can be controlled by varying molar ratio of stabilizer ACA to metal precursors.

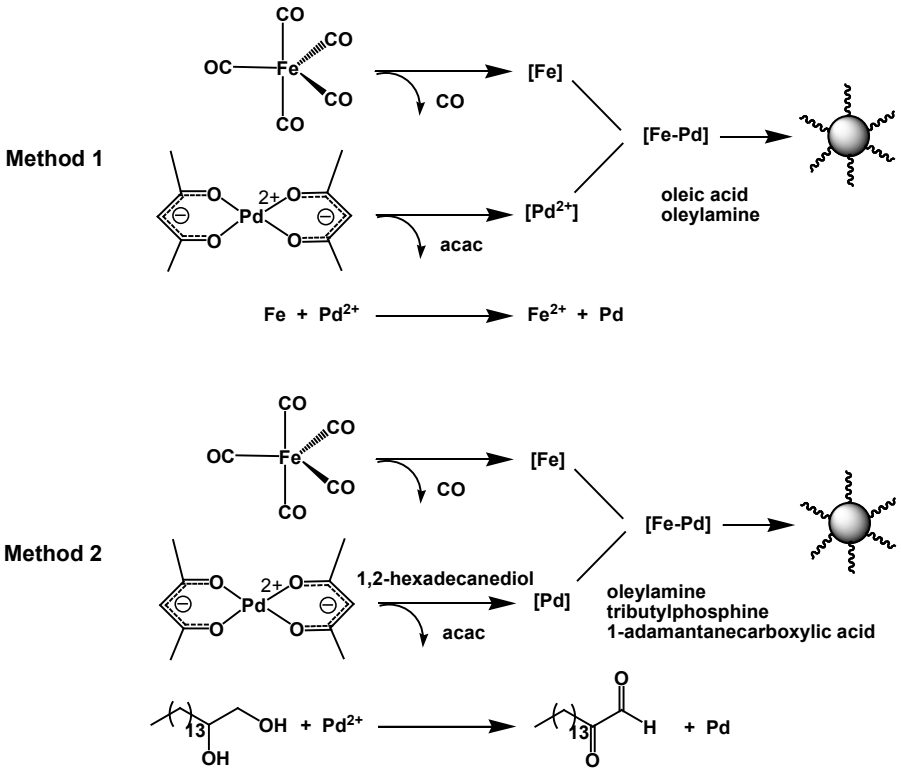

Scheme 3-3. Preparation of Fe-Pd nanostructures

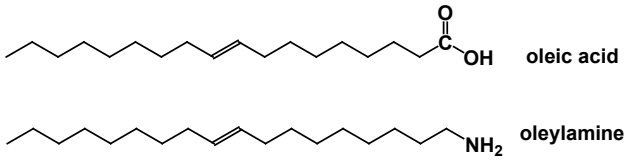

Scheme 3-4. Structures of oleic acid and oleylamine

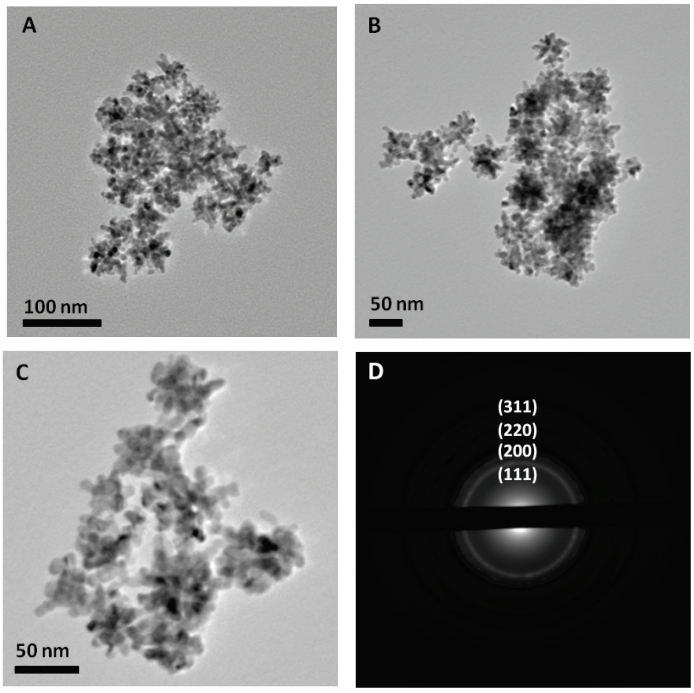

Figure 3-5. A-C: Bright-field TEM images of Fe-Pd "nanodendrites" (ND) prepared using method 1 outlined in Scheme 3-3. D: SAED pattern of ND.

Figures 3-5A and B show representative TEM images of nanostructures obtained from method 1. Clearly, the resulting NPs are dendritic. These "nanodendrites" (ND) tend to form agglomerates presumably due to their magnetic properties (Figures 3-5A, B).The average diameter of the ND is 51.6 nm, which was obtained by measuring the length from a branch edge to another one on the opposite side (Figure 3-6). The ND show a size distribution of 30-75 nm with >95% of the particles lying in the range of 35-70 nm (Figure 3-6). Higher

magnification TEM analysis of the ND (Figure 3-5C) shows they possess highly branched structures. Selected area electron diffraction (SAED) pattern (Figure 3-5D) clearly shows a well-defined ring pattern that is readily indexed to FePd alloy crystal planes.[31,32]

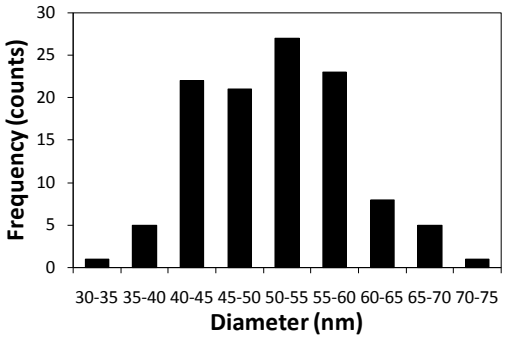

Figure 3-6. Size distribution histogram of ND (113 particles).

The presence of Fe and Pd in ND was confirmed using energy dispersive X-ray spectroscopy (EDX). The Cu and C peaks in the spectrum result from TEM grids (Figure 3-7).

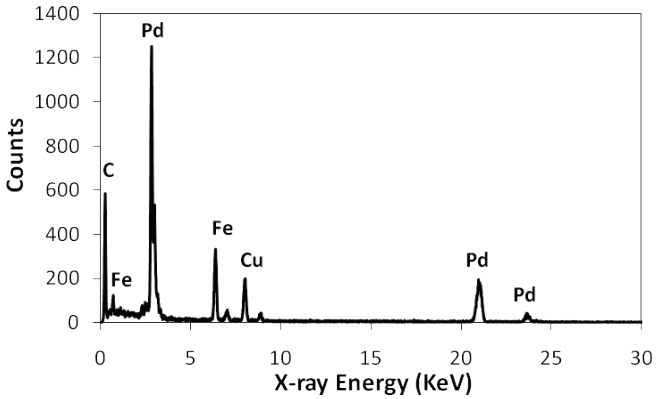

Figure 3-7. EDX spectrum of ND.

When method 2 was used, the as-prepared particles exhibit a pseudospherical morphology (Figures 3-8 NP1, 3-9 NP2). NP1 and NP2 were synthesized in the presence of 1.5 and 3 mmol of 1-adamantanecarboxylic acid (ACA), respectively

with other conditions the same. As expected NP2 are generally larger than NP1. In the synthesis of NP1 and NP2, tri-n-butylphosphine (TBP) and ACA were used as capping agents to tune the growth of nuclei. It has been proposed that the linear-shaped TBP forms a tight micelle structure and limits the growth of metal nuclei,[33] while ACA molecules with sterically bulky adamantyl end groups would repel each other and not have as strong coordination to the metal nuclei, leading to high surface free energy.[29,30] It has been observed that ACA tends to promote the growth of nuclei resulting in generally larger particles however the origins of this phenomenon remain unclear.[29,30,34,35] NP1 possess a broad size with an average diameter of 12.8 nm and distribution from 4-19 nm with 95% of the particles lying in the range of 7-19 nm (Figure 3-10 left). NP2 also show a wide size distribution with an average particle size of 17.7 nm and distribution from 10-26 nm with 95% of the particles lying in the range of 13-23 nm (Figure 3-10 right).

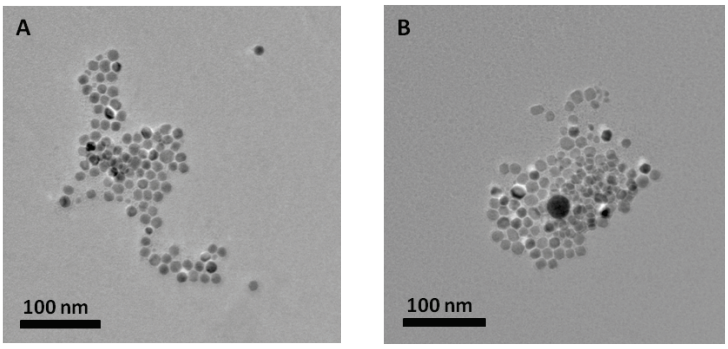

Figure 3-8. Bright-field TEM images of Fe-Pd NPs (NP1).

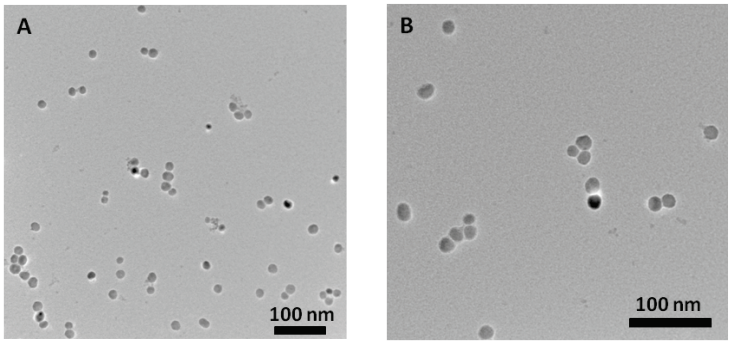

Figure 3-9. Bright-field TEM images of Fe-Pd NPs (NP2).

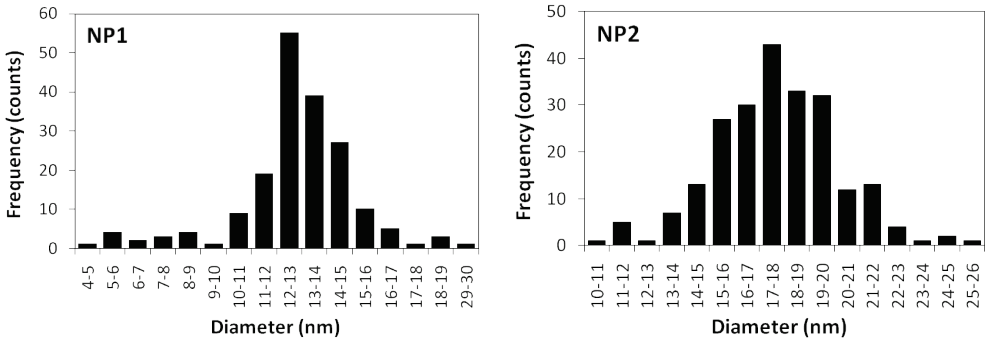

Figure 3-10. Size distribution histograms of NP1 (184 particles) and NP2 (225 particles).

For the synthesis of ND (method 1 in Scheme 3-3), no additional reducing agent was used. Under these conditions a limited number of nucleation sites are expected to form. As a result, particle growth will be limited to these sites and after consumption of the metal precursors relatively large particles will be obtained (Figure 3-5). In contrast, in the synthesis of NP1 and NP2, 1, 2-hexadecanediol was added to the reaction mixture smaller particles are obtained (method 2 in Scheme 3-3). Diols (e.g., ethylene glycol and 1, 2-hexadecanediol) have been widely used as reducing agents to generate noble metal NPs. Under these conditions, diols are oxidized to ketones and/or aldehydes.[36-40] Clearly, the additional reducing agent leads to facile reduction of $Pd(acac)_2$ and produces more

nucleation sites. The growth of these sites is limited by the concentration of the metal precursors present in solution. This process leads to a greater number of nuclei that in turn consume the metal precursors leading to smaller particles (Figures 3-8 and 9).

A typical EDX spectrum of NP1 and NP2 is shown in Figure 3-11. Both NP1 and NP2 are made up of Fe, Pd, O and P. O is due to oxidation when samples were exposed to air and from oxygen-containing capping agents (i.e., oleic acid and ACA). P arises from the tri-n-butylphosphine (TBP) capping agent. C and Cu are from TEM grids.

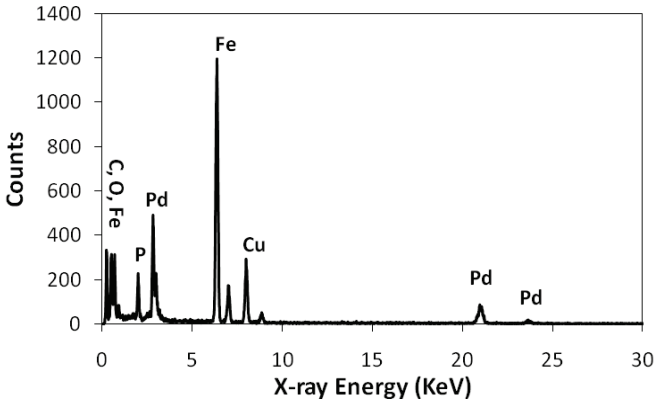

Figure 3-11. A typical EDX spectrum of NP1 and NP2.

The X-ray diffraction (XRD) patterns of ND, NP1 and NP2 all show diffraction patterns readily indexed to the crystalline FePd alloy (Figure 3-12).[41] For ND, only reflections arising from the FePd alloy are noted. For NP1 and NP2, there are obvious reflections corresponding to crystalline Fe_3O_4 (and/or Fe_2O_3),[42,43] indicating the presence of substantial Fe_3O_4 (and/or Fe_2O_3). Presumably the iron oxide was formed from oxidation of iron when samples were exposed to air during handling and analysis.

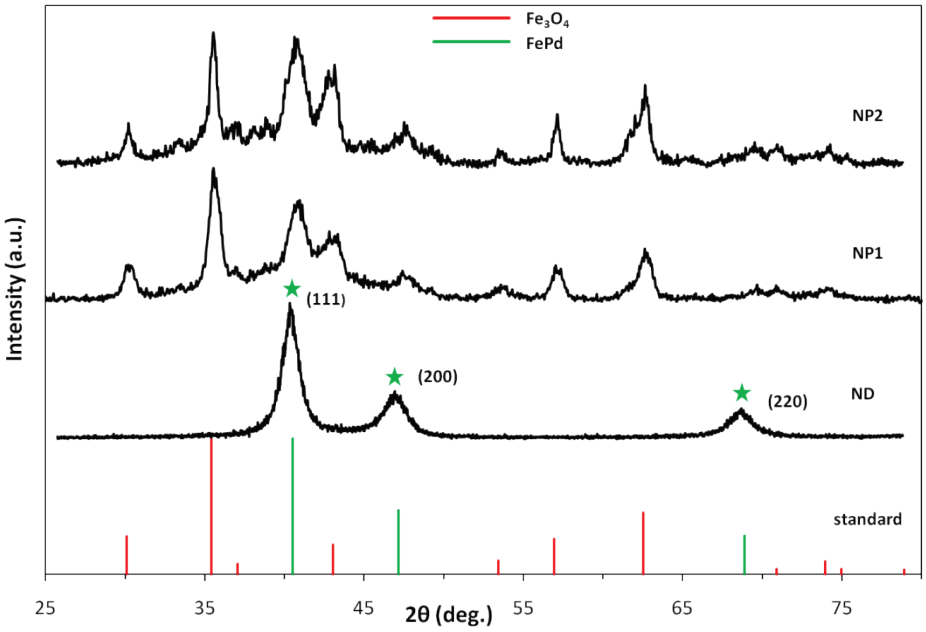

Figure 3-12. XRD patterns of ND, NP1 and NP2 compared to FePd and Fe_3O_4 standards. XRD was performed on an X-ray diffractometer equipped with a Co Kα radiation source (λ = 1.79 Å), and data were converted to those corresponding to Cu Kα radiation source (λ = 1.54 Å) for comparison purpose.

X-ray photoelectron spectroscopy (XPS) was performed to evaluate the oxidation state of palladium and iron species in these samples. Figure 3-13 shows Pd 3d region of XP spectra of the three samples. Each shows emissions within 335.3-335.8 eV in Pd $3d_{5/2}$ region, indicating the majority of Pd is present as Pd(0).[44,45] A shift in the Pd 3d emission of ND to lower binding energy compared to those of NP1 and NP2 is observed and may arise from larger nanodomains in ND in addition to electron contribution from iron.[46]

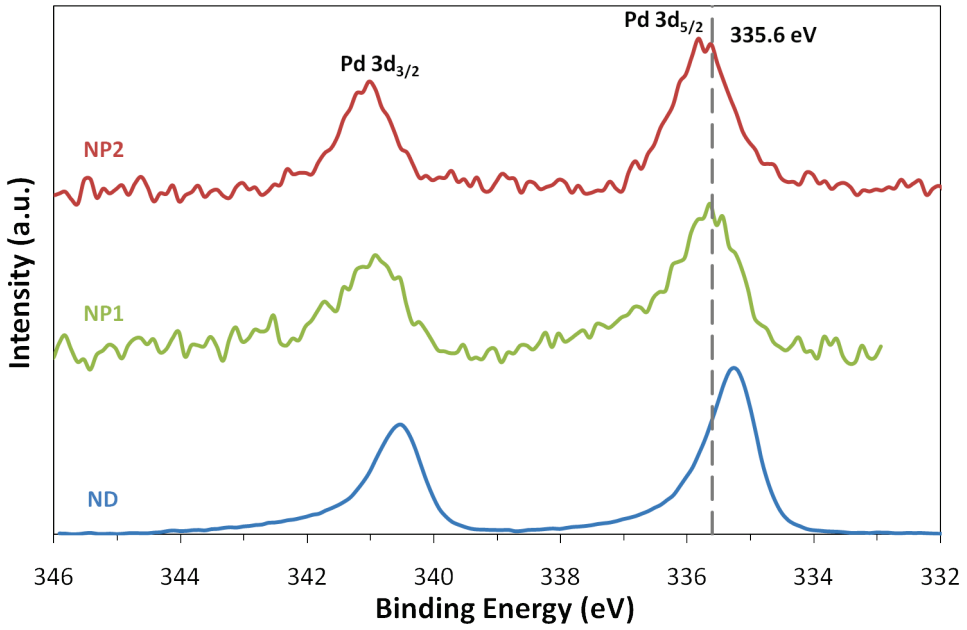

Figure 3-13. Shirley background-subtracted high-resolution Pd 3d region of the XP spectra of ND, NP1 and NP2, the dotted line at 335.6 eV indicates emission arising from Pd(0).

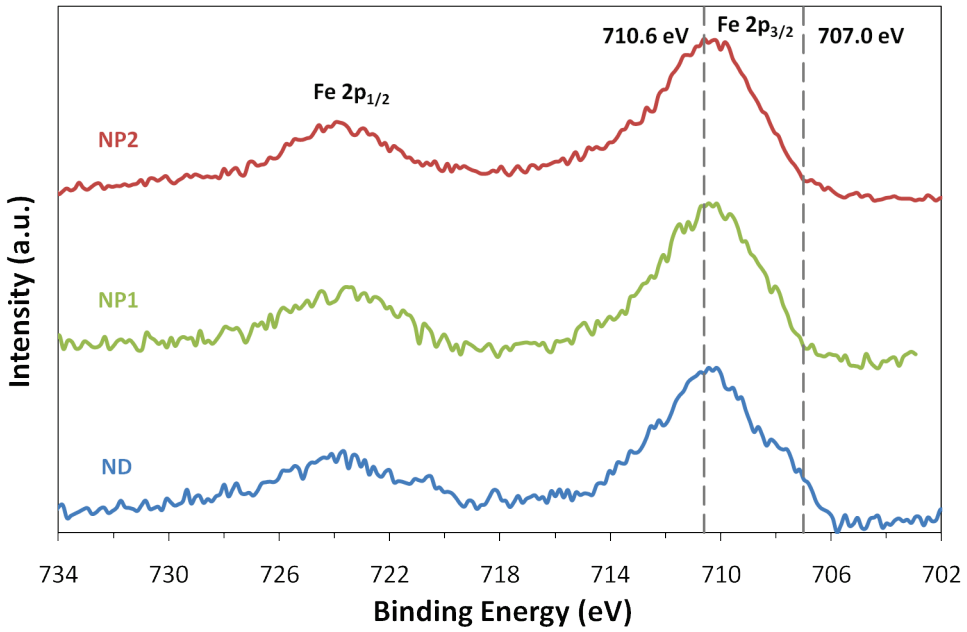

Figure 3-14. Shirley background-subtracted high-resolution Fe 2p region of the XP spectra of ND, NP1 and NP2, the dotted lines at 707.0 and 710.6 eV indicate emissions arising from Fe(0) and Fe(II, III), respectively.

In the Fe 2P region of XP spectra (Figure 3-14), three samples show emissions at approximately 710.6 eV in Fe $2p_{3/2}$ region, indicating coexistence of Fe(0), Fe_3O_4 and Fe_2O_3 in the samples.[47,48] While no iron oxide reflections are observed in the XRD pattern of ND, XPS indicates some oxidation has occurred. From this we conclude oxidation of the Fe in the ND leads to the formation of non-crystalline iron oxides.

ICP-MS confirmed the compositions of these nanostructures. Table 3-2 summarizes the Fe/Pd atomic ratios and Pd weight percents (wt. %) for ND, NP1 and NP2. The majority of Pd is present in its metallic form for all samples (Figure 3-13). From XPS analysis above (i.e., Figure 3-14) the line shapes inidicate Fe(0), Fe(II) and Fe(III) are present in all samples.

Table 3-2. Fe and Pd content in the samples[a]

Samples	Weight (mg)	Fe (ppm)	Pd (ppm)	Atomic ratio	Pd wt. %
ND	8	115	645	1 : 3	80.6
NP1	18.4	860	271	6 : 1	14.7
NP2	14.3	665	276	4.6 : 1	19.3

[a]Samples were dissolved in concentrated nitric acid and then analyzed by ICP-MS (unit: ppm, i.e., μg/g, 10 ml solution).

The as-synthesized ND, NP1 and NP2 were used as catalysts in Suzuki-Miyaura cross-coupling reactions (Scheme 3-5). As shown in Table 3-3, entries 1-4, they all exhibit higher catalytic activity than commercial palladium on carbon (Pd/C 10 wt.%, Aldrich 205699) for the cross-coupling reaction of bromobenzene and phenylboronic acid. In light of the high yields (i.e., > 95%) with bromobenzene it was not readily possible to evaluate the origins of the improved

reactivity of the Fe containing nanomaterials. For this reason, we chose to explore activity of ND, NP1 and NP2 in Suzuki cross-coupling reactions employing the generally inactive chlorobenzene. At room temperature low yields of coupling product were obtained with chlorobenzene substrate using ND catalyst in EtOH/H_2O (1:1) or DMF (Table 3-3, entries 5, 6). Because the relative inactivity of chlorobenzene toward the Suzuki cross-coupling reaction arises from the comparatively strong C-Cl bond, we chose to explore reactions at slightly elevated temperatures (i.e., 80 °C). When reactions were performed at 80 °C in DMF, chlorobenzene was coupled to phenylboronic acid with substantial yields when we used ND, NP1 and NP2 as catalysts (Table 3-3, entries 8-10). ND shows the highest activity (i.e., 69%, Table 3-3, entry 8). This higher activity may arise as a result of two contributing factors, a higher specific surface area due to its highly branched structure and a greater availability of electrons at the Pd center (XPS in Figure 3-13) leading to easier oxidative addition. In contrast, no product was detected for the same reaction at 80 °C using the Pd/C as catalyst. ND also showed much higher activity in DMF than that in EtOH/H_2O (1:1) (Table 3-2, entries 7, 8). This may result from the interaction of surface capping agents on the ND which are capped with long-chain carbon surfactants (i.e., oleic acid and oleylamine) and are well more dispersed in DMF compared to EtOH/H_2O (1:1).

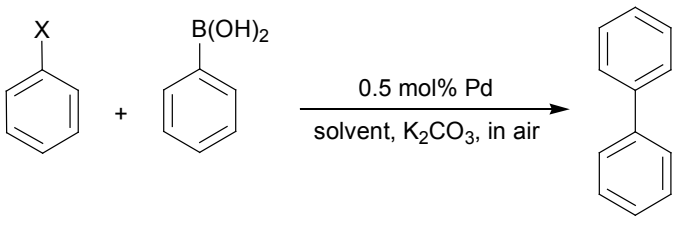

Scheme 3-5. Suzuki-Miyaura coupling reactions

Table 3-3. A summary of Suzuki-Miyaura coupling reactions.[a]

Entry	Catalyst	X	Temperature	Solvent	Time (h)	Yield (%)
1	ND	Br	r.t.	EtOH/H_2O	2	98
2	NP1	Br	r.t.	EtOH/H_2O	2	95
3	NP2	Br	r.t.	EtOH/H_2O	2	95
4	Pd/C	Br	r.t.	EtOH/H_2O	4	90
5	ND	Cl	r.t.	EtOH/H_2O	48	11
6	ND	Cl	r.t.	DMF	48	13
7	ND	Cl	80 °C	EtOH/H_2O	24	25
8	ND	Cl	80 °C	DMF	24	69
9	NP1	Cl	80 °C	DMF	24	52
10	NP2	Cl	80 °C	DMF	24	44
11	Pd/C	Cl	80 °C	DMF	24	27

[a]Reaction conditions: 2.0 mmol aryl halide, 2.4 mmol aryl boronic acid, 5.0 mmol K_2CO_3, 0.5 mol% Pd (relative to aryl halide). [b]Isolated yield.

To further evaluate the activity of ND toward coupling of chlorobenzene with phenylboronic acid in DMF, the ND catalyst was isolated from the reaction mixture using a permanent magnet (Figure 3-15), washed repeatedly with acetone (a minimum of three times) and dried in vacuum. The dried catalyst was reused for the identical reaction under identical conditions.

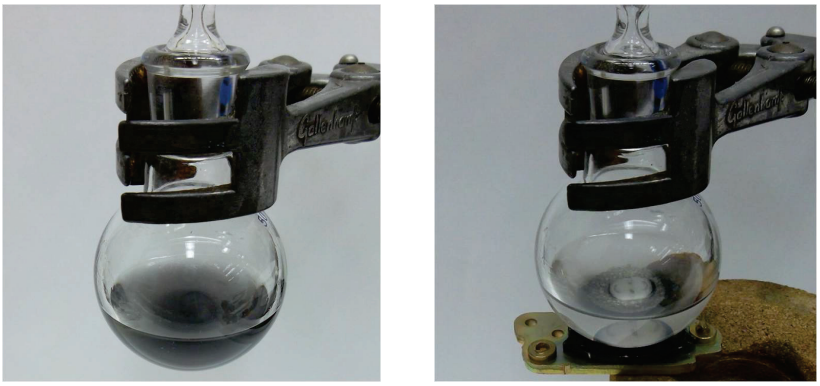

Figure 3-15. Catalyst separation, white powder in the bottom is K_2CO_3.

Yield data obtained from the repeated use of the ND catalyst are presented in Table 3-4. While a slight loss of activity is observed it is reasonable this results from material handling during catalyst recycling. A total turnover number (TON) of 478 was achieved, which is lower compared to most homogenous Pd catalysts with TONs of > 10,000. [49] In fact, ICP-MS analysis of reaction crude products indicates a slightly less catalyst remained following each reaction (Table 3-5).

Table 3-4. ND reuse for Suzuki-Miyaura coupling reaction of bromobenzene with phenylboronic acid.

Run	Time (h)	Yield (%)
1	24	69
2	24	62
3	24	57
4	24	51

Table 3-5. ICP-MS analysis of biphenyl product using ND as catalyst

Recycle	Percent of the lost (%)	Percent of the left (%)
1	8.3	91.7
2	7.5	84.2
3	7.4	76.8
4	7.8	69.0

[a]Samples were dissolved in concentrated nitric acid and then analyzed by ICP-MS (unit: ppm, i.e., μg/g, 10 ml solution).

In conclusion, three Fe-Pd nanostructures have been synthesized - ND, NP1 and NP2 by simultaneous thermal decomposition of $Fe(CO)_5$ and reduction of $Pd(acac)_2$. ND exhibit a dendritic strucutre with an average diameter of 51.6 nm, while NP1 and NP2 exhibit a pseudospherical morphology with average

diameters of 12.8 nm and 17.7 nm, respectively. All three samples contain crystalline FePd alloy confirmed by XRD and iron oxides were formed due to exposure to air. Improved catalytic activity in Suzuki coupling reactions relative to commercial Pd/C was demonstrated and ND exhibited the highest activity which we attribute to their highly branched structures and a greater availability of electrons at the Pd center. ND were recycled by applying a permanent magnet followed by decanting the reaction mixture. The ND catalyst was effectively reused three times with certain loss of activity which is readily attributed to material handling limitations.

3.4 References

1. Cortie, M. B.; McDonagh, A. M. *Chem. Rev.* **2011**, *111*, 3713-3735.
2. Ferrando, R.; Jellinek, J.; Johnston, R. L. *Chem. Rev.* **2008**, *108*, 845-910.
3. Lu, L.; Eychmüller, A. *Acc. Chem. Res.* **2008**, *41*, 244-253.
4. Wang, D.; Li, Y. *Adv. Mater.* **2011**, *23*, 1044-1060.
5. Somorjai, G. A. *Introduction to Surface Chemistry and Catalysis*; Wiley-VCH: New York, **1994**, 500–512.
6. Huber, G. W.; Shabaker, J. W.; Dumesic, J. A. *Science* **2003**, *300*, 2075.
7. Burda, C.; Chen, X. B.; Narayanan, R.; El-Sayed, M. A. *Chem. Rev.* **2005**, *105*, 1025.
8. Enache, D. I.; Edwards, J. K.; Landon, P.; Solsona-Espriu, B.; Carley, A. F.; Herzing, A. A.; Watanabe, M.; Kiely, C. J.; Knight, D. W.; Hutchings, G. J. *Science* **2006**, *311*, 362.
9. Huber, G. W.; Shabaker, J. W.; Dumesic, J. A. *Science* **2003**, *300*, 2075.
10. Alayoglu, S.; Nilekar, A. U.; Mavrikakis, M.; Eichhorn, B. *Nat. Mater.* **2008**, *7*, 333
11. Kowal, A.; Li, M.; Shao, M.; Sasaki, K.; Vukmirovic, M. B.; Zhang, J.; Marinkovic, N. S.; Liu, P.; Frenkel, A. I.; Adzic, R. R. *Nat. Mater.* **2009**, *8*, 325.
12. Kolb, G. *Fuel Processing: for Fuel Cells*; Wiley-VCH: Weinheim, Germany, **2008**.
13. Lim, B.; Kobayashi, H.; Yu, T.; Wang, J.; Kim, M. J.; Li, Z. Y.; Rycenga, M.; Xia, Y. *J. Am. Chem. Soc.* **2010**, *132*, 2506.
14. Dossett, J. L.; Boyer, H. E. *Practical Heat Treating*, ASM International, **2006**, 1-14.
15. Novet, T.; Johnson, D. C. *J. Am. Chem. Soc.* **1991**, *113*, 3398.
16. Suryanarayana, C. *Prog. Mater. Sci.* **2001**, *46*, 1.
17. Binns, C. *Surf. Sci. Rep.* **2001**, *44*, 1.
18. Muñoz-Flores, B. M.; Kharisov, B. I.; Jiménez-Pérez, V. M.; Martínez, P. E.; López, S. T. *Ind. Eng. Chem. Res.* **2011**, *50*, 7705-7721.
19. Abdelsayed, V.; Glaspell, G.; Nguyen, M.; Howe, J. M.; El-Shall, M. S. *Faraday Discuss.* **2008**, *138*, 163-180.
20. Wu, J. B.; Zhang, J. L.; Peng, Z. M.; Yang, S. C.; Wagner, F. T.; Yang, H. *J. Am. Chem. Soc.* **2010**, *132*, 4984.
21. Sun, S.; Murray, C. B.; Weller, D.; Folks, L.; Moser, A. *Science* **2000**, *287*, 1989-1992.
22. Chen, M.; Liu, J. P.; Sun, S. *J. Am. Chem. Soc.* **2004**, *126*, 8394-8395.
23. Lu, Y.; Zhao, Y.; Yu, L.; Dong, L.; Shi, C.; Hu, M. J.; Xu, Y. J.; Wen, L. P.; Yu, S. H. *Adv. Mater.* **2010**, *22*, 1407-1411.
24. Wang, D.; Li, Y. *J. Am. Chem. Soc.* **2010**, *132*, 6280-6281.
25. Son, S. U.; Jang, Y.; Park, J.; Na, H. B.; Park, H. M.; Yun, H. J.; Lee, J.; Hyeon, T. *J. Am. Chem. Soc.* **2004**, *126*, 5026.
26. Stamenkovic, V. R.; Fowler, B.; Mun, B. S.; Wang, G.; Ross, P. N.; Lucas, C. A.; Marković, N. M. *Science* **2007**, *315*, 493.

27. Lim, B.; Jiang, M.; Camargo, P. H. C.; Cho, E. C.; Tao, J.; Lu, X.; Zhu, Y.; Xia, Y. *Science* **2009**, *324*, 1302-1305.
28. Mazumder, V.; Chi, M.; More, K. L.; Sun, S. *J. Am. Chem. Soc.* **2010**, *132*, 7848-7849.
29. Hou, Y.; Kondoh, H.; Kogure, T.; Ohta, T. *Chem. Mater.* **2004**, *16,* 5149-5152.
30. Hou, Y.; Kondoh, H.; Ohta, T. *J. Nanosci. Nanotechnol.* **2009**, *9*, 202-208.
31. Chbihi, A.; Sauvage, X.; Genevois, C.; Blavette, D.; Gunderov, D.; Popov, A. G. *Adv. Eng. Mater.* **2010**, *12*, 708-713.
32. Saravanan, P.; Srinivasa Rao, K.; Sivaprahasam, D.; Chandrasekaran, V. *Intermetallics* **2010**, *18*, 2262-2265.
33. Peng, X.; Wickham, J.; Alivisatos, A. P. *J. Am. Chem. Soc*. **1998**, *120*, 5343.
34. Chen, M.; Nikles, D. E. *Nano Lett.* **2002**, *2*, 211.
35. Suslick, K. S.; Fang, M.; Heyon, T. *J. Am. Chem. Soc*. **1996**, *118*, 11960.
36. Xiong, Y.; Chen, J.; Wiley, B.; Xia, Y.; Aloni, S.; Yin, Y. *J. Am. Chem. Soc.* **2005**, *127*, 7332.
37. Xiong, Y.; Xia, Y. *Adv. Mater*. **2007**, *19*, 3385.
38. Wiley, B.; Sun, Y.; Xia, Y. *Acc. Chem. Res.* **2007**, *40*, 1067.
39. Wu, J.; Zhang, J.; Peng, Z.; Yang, S.; Wagner, F.; Yang, H. *J. Am. Chem. Soc.* **2010**, *132*, 4984.
40. Zhang, Q.; Xie, J.; Yang, J.; Lee, J. Y. *ACS Nano* **2009**, *3*, 139.
41. Massalski, T. B. *Binary Alloy Phase Diagrams*, 2nd edition, ASM International, Materials Park, Ohio, **1990**, *2*, 1749-1751.
42. Wang, C.; Baer., D. R.; Amonette, J. E.; Engelhard, M. H.; Antony, J.; Qiang, Y. *J. Am. Chem. Soc.* **2009**, *131*, 8824-8832.
43. Peng, Y.; Park, C.; Zhu, J.; White, R.; Laughlin, D. *J. Appl. Phys.* **2004**, *95*, 6798-6800.
44. Hillebrecht, F. U.; Fuggle, J. C.; Bennett, P. A.; Zolnierek, Z. *Phys. Rev. B* **1982**, *27*, 2179.
45. Kumar, G.; Blackburn, J. R.; Albridge, R. G.; Moddeman, W. E.; Jones, M. M. *Inorg. Chem.* **1972**, *11*, 296.
46. Schildenberger, M.; Prins, R.; Bonetti, Y. C. *J. Phys. Chem. B* **2000**, *104*, 3250.
47. Grosvenor, A. P.; Kobe, B. A.; Biesinger, M. C.; McIntyre, N. S. *Surf. Interface Anal.* **2004**, *36*, 1564.
48. Li, X.; Zhang, W. *J. Phys. Chem. C* **2007**, *111*, 6939-6946.
49. Farina, V. *Adv. Synth. Catal.* **2004**, *346*, 1553-1582.

Chapter 4: Conclusions and Future Work

Work described in this thesis has focused on synthesis, characterization and catalytic applications of iron-containing nanoparticles (NPs) in Suzuki-Miyaura cross-coupling reactions. This chapter will summarize conclusions and outline some future work directions.

4.1 Pd Decorated Iron/Iron Oxide NPs for Suzuki Cross-Coupling Reactions (Chapter 2)

4.1.1 Conclusions

In Chapter 2, we have found and demonstrated iron/iron oxide NPs ($Fe@Fe_xO_y$) can be used as a versatile support for immobilizing catalytic metals.[1,2,3] The immobilization is readily achieved via coordination of metal ions to the iron oxide surface and subsequent reduction of these coordinated ions to their metallic state by the iron core. As a result, $Fe@Fe_xO_y$ particle surfaces bear spectroscopically detectable zero valent metals. Uniquely, our approach does not use any external reducing reagents or post-synthetic NP surface modification because of the established reducing nature and coordinating ability of the $Fe@Fe_xO_y$ support. We prepared palladium "decorated" $Fe@Fe_xO_y$ NPs ($Fe@Fe_xO_y$/Pd) to explore their catalytic capabilities toward Suzuki-Miyaura cross-coupling reactions. They were evaluated and found to exhibit high catalytic activity in a series of Suzuki cross-

coupling reactions in aqueous solution at room temperature in air, which is higher than commercially available catalyst Pd/C. The Fe@Fe_xO_y/Pd system effectively couples the advantages of heterogeneous (e.g., low cost, air-stability, easy separation, and good reusability) and homogeneous systems (e.g., high yield), making it a promising material for practical application. Furthermore, Fe@Fe_xO_y/Pd has special retention ability for Pd species due to the established reducing nature and coordinating ability of the Fe@Fe_xO_y support, which makes leached Pd negligible. The effect of Fe@Fe_xO_y on the catalytic activity of Pd and Ni was investigated by increasing amount of Fe@Fe_xO_y while keeping Pd and Ni the same and no evident activity increase of catalysts was found for the Suzuki cross-coupling reactions. This may be because the accelerated oxidative addition is not rate-determining step.

4.1.2 Future Work

Highlighting the versatility of our method of depositing metals onto Fe@Fe_xO_y, in principle it is possible to deposit any transition metal with a redox potential more positive than that of iron (e.g., Co, Ni, Cu, Pd, Au, Ag, Pt, Rh and Ru).[1,2] The deposition is easily controlled, making metal loading amount exquisitely tunable and surface immobilization of more than one metal possible. Each transition metal has catalytic activity toward some characteristic reactions, e.g., Au has substantial activities in CO oxidation and selective alkene oxidation,[4,5] and Ru and Rh have high catalytic activity for various hydrogenation reactions.[6,7] We can explore to catalyze these reactions using Fe@Fe_xO_y decorated with relevant transition metals. Furthermore, metal combinations are of interest because they

may exhibit superior catalytic activities to monometallic counterparts arising from synergistic interaction of constituent metals.[8,9]

4.2 Catalytic Activity of Fe-Pd Nanostructures for Suzuki Cross-Coupling Reactions (Chapter 3)

4.2.1 Conclusions

In Chapter 3, we have synthesized three Fe-Pd nano-structures—"nanodendrites" (ND), nanoparticles (NP1 and NP2) by simultaneous thermal decomposition of $Fe(CO)_5$ and reduction of $Pd(acac)_2$.[10,11] ND exhibit a dendritic structure with an average diameter of 51.6 nm, while NP1 and NP2 exhibit a pseudospherical morphology with average diameters of 12.8 nm and 17.7 nm, respectively. The three nanostructures all contain crystalline FePd alloy confirmed by XRD and iron oxides were formed due to exposure to air. XPS show these nanostructures have characteristic emissions of Pd (0), and ND have a shift to lower binding energy compared to ND1 and ND2, which arises from more iron (0) in ND. We demonstrated they have higher catalytic activity than commercial Pd/C toward Suzuki cross-coupling reactions, and ND have highest activity among them. This higher reactivity of ND may arise as a result of two contributing factors, a higher specific surface area due to its highly branched structure and a greater availability of electrons at the Pd center confirmed by XPS leading to easier oxidative addition. ND were recycled by applying a permanent magnet followed by decanting the reaction mixture. The ND catalyst was effectively reused three times with certain loss of activity which is readily attributed to material handling limitations.

4.2.2 Future Work

Many factors such as surfactant choice, concentration ratios, reaction times and temperature have been identified to influence particle size and morphology in the synthesis of iron-containing nanoparticles using thermal decomposition of $Fe(CO)_5$ and corresponding organometallic compounds.[12,13] Our group found the presence of water increases nucleation events by lowering the activation energy for $Fe(CO)_5$ decomposition through water-gas-shift chemistry, which produces smaller particles.[14] Therefore, water concentration should be monitored and controlled for the consistency of results. Selection of surfactants is another experiment we will consider next, because different surfactants have different binding abilities to particle surface, which will influence nucleation and growth processes. Synthesis of bimetallic nanoparticles using other solution-based synthetic methods such as co-reduction,[15] seeded growth[16] and noble metal induced reduction[17] will be explored, and their catalytic and physical properties will be evaluated.

4.3 Iron-Containing NPs for Fischer-Tropsch Synthesis and Hydrogenation Reactions (Future Work)

The presented approach for "decorating" $Fe@Fe_xO_y$ NPs with various metals is exceptionally versatile. It offers the opportunity to combine the properties of numerous transitional metals, provides a non-innocent catalytic support and allows for convenient catalyst recovery and reuse. In the following section a series of potential catalytic applications (e.g., Fischer-Tropsch synthesis, hydrogenation of aromatic compounds) of materials prepared using the general procedure

described earlier in this thesis are outlined.

4.3.1 Fischer-Tropsch Synthesis

The Fischer-Tropsch synthesis (FTS) offers the possibility of converting a mixture of carbon monoxide and hydrogen (syngas) into a series of hydrocarbons.[18] FTS has received much attention because of ever increasing crude oil prices, the need to minimize environmental impact of fossil fuels and the need to meet energy requirements with sustainable sources. Syngas is readily produced from natural gas,[19,20] coal[21] and biomass[22] through steam reforming, partial or autothermal oxidation, or gasification processes, and its conversion to hydrocarbons is an attractive alternative to petroleum-derived fuels and chemicals if suitable cost-effective catalysts can be developed. The hydrocarbons from FTS are clean high-value transportation fuels free from sulfur and nitrogen making them more environmentally benign than petroleum-based fuels obtained from standard sources.[23,24] FTS generates a wide range of products, including alkanes and alkenes as well as some oxygenates (e.g., primarily alcohols) and can be represented as following equations.

$$nCO + (2n + 1)\,H_2 \longrightarrow C_nH_{2n+2} + nH_2O \qquad \textbf{Equation 4-1}$$

$$nCO + 2nH_2 \longrightarrow C_nH_{2n} + nH_2O \qquad \textbf{Equation 4-2}$$

$$nCO + 2nH_2 \longrightarrow C_nH_{2n+1}OH + (n-1)H_2O \qquad \textbf{Equation 4-3}$$

The catalytic synthesis of hydrocarbons from carbon monoxide and hydrogen mixtures can be dated back to the beginning of 20th century. In 1902, Sabatier et al. synthesized methane from a mixture of CO and H_2 using cobalt and nickel

catalysts. During the period from 1920s to 1930s, Franz Fischer and Hans Tropsch developed a process for the synthesis of hydrocarbons from coal.[25-27] They combined coal with steam which reacted to give a gaseous mixture of carbon monoxide and hydrogen and then converted the mixture to hydrocarbons over iron and/or cobalt catalysts. In 1926, Fischer and Tropsch obtained liquid hydrocarbons at low pressures (P = 1-10 atm) and low temperatures (T = 180-200 °C).[27]

The commercialization of FTS began in 1936 in Germany, and many FT plants have been built for the production of fuels.[28,29] In 1938, Germany had a capacity of 660 000 tons of primary products per year. When the supply of petroleum was plentiful, most of the world's FTS plants were inactive as a result of financial limitations. However South Africa's desire for energy independence and the low quality of its coal prompted extensive development of FTS. South African Synthetic Oil Limited (SASOL) built its first FTS plant in Sasolburg in 1955. SASOL's second and third FTS plants began production in Secunda in 1980 and 1982, respectively.[30] The 1970s energy crises revitalized synthetic fuel research and development. In 1993, the Shell FTS plant came into operation in Malaysia with a capacity of 12 500 barrels per day (bpd).[29] In 2007, Sasol Oryx started a 34 000 bpd plant.[31]

All group VIII metals have noticeable activity in FTS in the order ruthenium followed by iron, nickel, and cobalt.[32] Ruthenium is the most active catalyst for FTS, but high costs and the limited reserves hinder its industrial-scale application. Nickel catalysts preferentially afford low molecular weight hydrocarbons (e.g.,

methane) when industrially practical conditions are employed. Cobalt and iron were proposed by Fischer and Tropsch as the first catalysts and have been used in industry for hydrocarbon synthesis. While cobalt catalysts are more costly than their iron-based counterparts, however they are generally more active and more selective to the preparation of linear long-chain hydrocarbons; furthermore, and they are more resistant to deactivation by water. Fe catalysts are active under wider ranges of temperatures and H_2/CO ratios without significant decrease in linear long-chain hydrocarbons.

Based upon these points, a bimetallic catalyst made up of Co and Fe with nanoscale dimensions could combine the benefits of these two metals. In Chapter 2, we have demonstrated our ability to deposit transition metals onto iron oxide capped iron nanoparticles (Fe@Fe_xO_y NPs) via coordination of metal ions to the iron oxide surface followed by reduction of these coordinated ions to their metallic state by the iron core.[1-3] Co can be deposited onto Fe@Fe_xO_y using this approach, because Co has a more positive redox potential than that of Fe.[1,2] In this context we have prepared cobalt decorated Fe@Fe_xO_y NPs (Fe@Fe_xO_y/Co NPs) via reduction of $Co(NO_3)_2$ by Fe@Fe_xO_y NPs in an aqueous solution and performed preliminary catalytic applications of Fe@Fe_xO_y/Co NPs in FTS. The details of these reactions are provided in Appendix.

The syngas used for these preliminary investigations had a H_2/CO ratio close to that produced from biomass (i.e., 1.0).[33] These early reactions provided a wide product distribution, and C_5 – C_{30} hydrocarbons were formed. Unfortunately, only liquid products were analyzed because a GC column suitable for

characterizing gaseous products was not available. The liquid product distributions are shown in Table 4-1. It is notable that C_5 – C_{12} hydrocarbons (i.e., gasoline fraction) made up the vast majority (83.6 mol%) of the liquid products, followed by 14.4 mol% of C_{13} – C_{20} hydrocarbons (i.e., diesel fuel fraction). Heavy hydrocarbons ($C_{\geq 21}$) were suppressed and only 2.0 mol% of them was detected in the organic phase. The catalyst was recycled and reused to examine its stability. After reaction, a magnet was used to retain the catalyst, and liquid product was decanted. The catalyst was dried *in vacuo* before reuse. From Table 4-1, we can see the activity and selectivity of the reused catalyst was almost maintained except a little increase in C_{13} – C_{20} fraction and decrease in C_5 – C_{12} fraction. All of GC data are included in Appendix in the last part of thesis.

Table 4-1. Fe@Fe_xO_y/Co for FTS [a]

Catalysts	CO conv. (%)	Liquid product selectivity (mol%) [b]		
		C_5-C_{12}	C_{13}-C_{20}	$C_{\geq 21}$
Fe@Fe_xO_y/Co	66	83.6	14.4	2.0
Reuse	64	75.9	22.5	1.6

[a]Reaction conditions: H_2/CO (1:1 ratio), catalyst (114.7 mg Fe@Fe_xO_y/Co, 12.8 wt.% Co), P = 290 psi = 2 MPa, 503 K, 96 h. [b]GC results.

Clearly this preliminary study has demonstrated cobalt decorated Fe@Fe_xO_y NPs is an active and selective Fischer-Tropsch catalyst for the formation of C_5 – C_{12} hydrocarbons, which constitute gasoline. Syngas from biomass has H_2/CO ratio close to 1.0 as we used, revealing FTS is a very effective way to produce fuels from biomass. In addition, the catalyst is readily stable and reusable. Ongoing investigations will focus on exploring the influence of particle structure,

syngas composition and establishing procedures for evaluating the makeup of gaseous reaction products.

4.3.2 Hydrogenation of Aromatic Compounds

4.3.2.1 Hydrogenation of Benzene

Aromatic compounds have relatively long environmental lifetimes, exhibit mutagenic activity and been identified as carcinogens.[34,35] Hydrogenation of benzene to cyclohexane is important, cyclohexane being a key intermediate in the production of the nylon precursor adipic acid.[36] Developing effective catalysts for hydrogenation of benzene is of interest because it is related to the production of low-aromatic gasoline and diesel fuels[37] and the industrial demands for cyclohexane. However, hydrogenation of benzene is notably more difficult compared to olefin hydrogenation due to the resonance stability of the aromatic ring.[38] Consequently, hydrogenation of benzene is conventionally performed at high temperatures and H_2 pressures (i.e., $\geq$ 100 °C and 50 atm H_2).[39]

Ru and Rh are the most active catalysts for hydrogenation of benzene.[40,41] In attempts to combine the benefits of these metals with iron-containing supports, nanomaterials were prepared using two methods, direct reduction and thermal decomposition. Direct reduction exploits the established reducing power of Fe@Fe_xO_y NPs. As is the case throughout this thesis, Ru and Rh cations coordinate to the surface of the Fe@Fe_xO_y particles and are subsequently reduced to their metallic state.[1-3] Ru and Rh decorated Fe@Fe_xO_y were prepared by combining an aqueous solution of $RuCl_3$ and $RhCl_3$ with Fe@Fe_xO_y NPs. This procedure yielded bimetallic Fe@Fe_xO_y/RuRh NPs. Our alternative approach

employed simultaneous thermal decomposition of $Fe(CO)_5$ and $Ru_3(CO)_{12}$ to prepare FeRu NPs.[42] Bright-field TEM images of FeRu NPs are shown in Figure 4-1. The spherical particles have a core-shell structure with an average diameter of 13 nm.

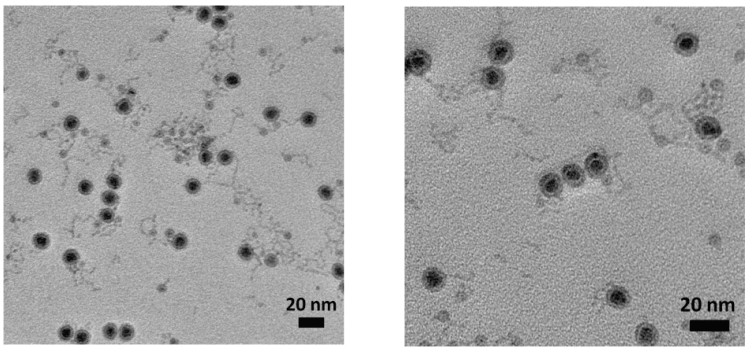

Figure 4-1. Bright-field TEM images of FeRu NPs.

Fe@Fe_xO_y/RuRh, Fe@Fe_xO_y/Rh and FeRu NPs were tested for hydrogenation of benzene under high pressure at an elevated temperature. Preliminary results are provided in Table 4-2. Fe@Fe_xO_y/RuRh (0.5 mol% Ru, 0.5 mol% Rh) catalyzed the hydrogenation of benzene under 50 psi at 80 °C forming cyclohexane as only product with a yield of 76 %. The turn over frequency (TOF) for the present Fe@Fe_xO_y/RuRh catalyst under these conditions was 4.75. When Fe@Fe_xO_y/Rh (0.05 mol% Rh) was used under 45 psi at 80 °C, the yield of cyclohexane was 22% after 89 h and the TOF was 4.94. Because TOF is relative low compared to literature values,[40,41] the influence of reaction pressure was explored. At a higher temperature (i.e., 100 psi, 110 °C) the FeRu catalyst obtained from the carbonyl decomposition afforded a TOF of 15.6 h^{-1}, which may be attributed from the harsher conditions.

Based upon the present results for hydrogenation of benzene, these catalysts hold promise. Ongoing investigations will include more detailed material characterization, evaluation of the role of surface modification and tailoring of NP composition.

Table 4-2. Hydrogenation of benzene

Catalyst	Pressure (psi)	Temperature (°C)	Time (h)	Yield (%)[d]	TOF (h^{-1})
$Fe@Fe_xO_y/RuRh$[a]	50	80	16	76	4.75
$Fe@Fe_xO_y/Rh$[b]	45	80	89	22	4.94
$Fe@Fe_xO_y$	45	80	89	0	0
FeRu[c]	100	110	50	39	15.6

[a]0.5 mol% Ru, 0.5 mol% Rh relative to benzene. [b]0.05 mol% Rh relative to benzene. [c]0.05 mol% Ru. [d]yield of clyclohexane, from ^{1}HNMR integration.

4.3.2.2 Hydrogenation of Nitrobenzene

As an extension of the studies of benzene hydrogenation outlined above, the catalytic hydrogenation of nitrobenzene was investigated. This process is industrially important to the production of aniline; approximately 85% of global aniline is produced in this way.[43] Aniline is used in the synthesis of methylene diphenyl diisocyanate (MDI), and as an additive for rubber processing. It is also an important intermediate in the production of pharmaceuticals, pesticides, herbicides, dyes and pigments.[44-46] Commercially, hydrogenation of nitrobenzene is carried out at 473 K in the vapor phase over a nickel or copper based catalyst.[36] Liquid-phase hydrogenation of nitrobenzene is also performed using noble metal

catalysts (Pd, Pt, Ru), but the common drawback is the hydrogenation requires high pressure and/or high temperature.[47-50] Therefore, it is desirable to develop catalysts for the selective hydrogenation of nitrobenzene to produce aniline under mild conditions.[51-54]

Using the palladium decorated Fe@Fe_xO_y NPs (Fe@Fe_xO_y/Pd NPs) described in Chapter 2 we performed preliminary testing of Fe@Fe_xO_y/Pd NPs as catalyst for hydrogenation of nitrobenzene. In addition, the Fe-Pd nanodentrites (Fe-Pd ND) described in Chapter 3 was also used in the hydrogenation of nitrobenzene. For comparison purpose, commercial 10 wt.% Pd/C (Aldrich) was also studied. Plots showing reaction pressure versus reaction time for these reactions are shown from Figure 4-2 to Figure 4-4.

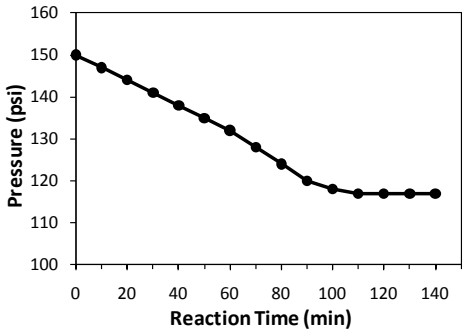

Figure 4-2. Graph of pressure versus reaction time for the hydrogenation of nitrobenzene, 0.1mol % Fe@Fe_xO_y/Pd, 145 psi (RT), 80 °C.

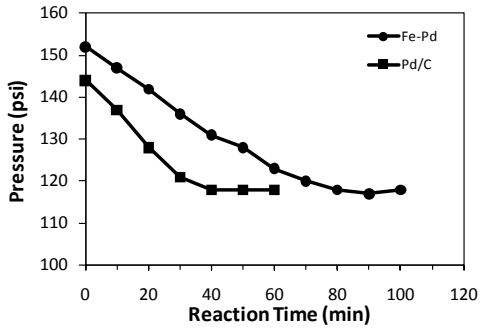

Figure 4-3. Graph of pressure versus reaction time for the hydrogenation

of nitrobenzene, 0.1mol % Pd, 145 psi (RT), 80 °C.

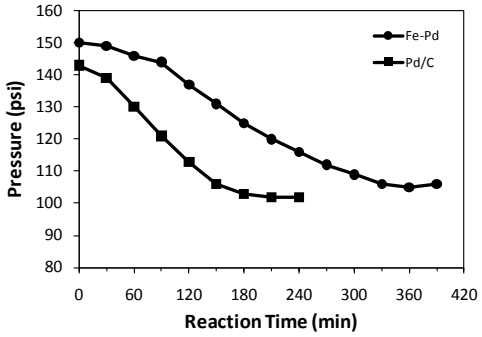

Figure 4-4. Graph of pressure versus reaction time for the hydrogenation of nitrobenzene, 0.1mol % Pd, 145 psi (RT), 35 °C.

Table 4-3 lists data for the reactions from Figure 4-2 to Figure 4-4. When the reactions were performed under 145 psi at 80 °C, the activity sequence is Pd/C > Fe-Pd ND > Fe@Fe_xO_y/Pd (see Figure 4-2, 3 and TOF in Table 4-3). When the reactions were performed at lower temperature (35 °C), the activity decreased, but Pd/C is still higher than Fe-Pd ND (see Figure 4-4 and TOF in Table 4-5).

Table 4-3. Hydrogenation of nitrobenzene using Pd catalysts

Catalyst	Pressure (psi)	Temperature (°C)	Time (min)	Yield (%)[d]	TOF (min^{-1})
Fe@Fe_xO_y/Pd[a]	145	80	110	97	8.8
Fe@Fe_xO_y	145	80	960	0	0
Fe-Pd ND[b]	145	80	80	94	11.8
Pd/C[c]	145	80	40	93	23.3
Fe-Pd ND	145	35	330	94	2.8
Pd/C	145	35	180	92	5.1

[a]0.1 mol% Pd relative to nitrobenzene. [b]0.1 mol% Pd relative to benzene. [c]0.1 mol% Pd, 10 wt.% Pd/C. [d]aniline, GC yield.

4.4 References

1. Macdonald, J. E.; Kelly, J. A.; Veinot, J. G. C. *Langmuir* **2007**, *23*, 9543.
2. Macdonald, J. E.; Veinot, J. G. C. *Langmuir* **2008**, *24*, 7169.
3. Zhou, S.; Johnson, M.; Veinot, J. G. C. *Chem. Commun.* **2010**, *46*, 2411-2413.
4. Min, B. K.; Friend, C. M. *Chem. Rev.* **2007**, *107*, 2709-2724.
5. Pina, C. D.; Falletta, E.; Prati, L.; Rossi, M. *Chem. Soc. Rev.* **2008**, *37*, 2077-2095.
6. Su, F.; Lv, L.; Lee, F. Y.; Liu, T.; Cooper, A. I.; Zhao, X. S. *J. Am. Chem. Soc.* **2007**, *129*, 14213-14223.
7. Roucoux, A.; Nowicki, A.; Philippot K. *Nanoparticles and Catalysis,* edited by Astruc D., Chapter 11, Wiley-VCH, Weinheim, 2008, 349-387.
8. Stamenkovic, V. R.; Fowler, B.; Mun, B. S.; Wang, G.; Ross, P. N.; Lucas, C. A.; Markovic, N. M. *Science* **2007**, *315*, 493.
9. Lim, B.; Jiang, M.; Camargo, P. H. C.; Cho, E. C.; Tao, J.; Lu, X.; Zhu, Y.; Xia, Y. *Science* **2009**, *324*, 1302-1305.
10. Mazumder, V.; Chi, M.; More, K. L.; Sun, S. *J. Am. Chem. Soc.* **2010**, *132*, 7848-7849.
11. Y. Hou, H. Kondoh, T. Kogure, T. Ohta, *Chem. Mater.* **2004**, *16,* 5149-5152.
12. Chen, M.; Liu, J. P.; Sun, S. *J. Am. Chem. Soc.* **2004**, *126*, 8394-8395.
13. Teng, X. W.; Yang, H. *J. Mater. Chem.* **2004**, *14*, 774-779.
14. Macdonald, J. E.; Brooks C. J.; Veinot, J. G. C. *Chem. Commun.* **2008**, 3777-3779.
15. Lim, B.; Wang, J.; Camargo, P. H. C.; Cobley, C. M.; Kim, M. J.; Xia, Y. *Angew. Chem. Int. Ed.* **2009**, *48*, 6304.
16. Lim, B.; Kobayashi, H.; Yu, T.; Wang, J.; Kim, M. J.; Li, Z. Y.; Rycenga, M.; Xia, Y. *J. Am. Chem. Soc.* **2010**, *132*, 2506.
17. Wang, D. S.; Peng, Q.; Li, Y. D. *Nano Res.* **2010**, *3*, 574.
18. Khodaov, A. Y.; Chu, W.; Fongarland, P. *Chem. Rev.* **2007**, *107*, 1692-1744.
19. Iglesia, E. *Appl. Catal., A* **1997**, *161*, 59-78.
20. Schulz, H. *Appl. Catal., A* **1999**, *186*, 3-12.
21. Dry, M. E. *Catal. Today* **2002**, *71*, 227-241.
22. Tijmensen, M. J. A.; Faaij, A. P. C.; Hamelinck, C. N.; van Hardeveld, M. R. M. *Biomass Bioenergy* **2002**, *23*, 129-152.
23. Eilers, J.; Posthuma, S. A.; Sie, S. T. *Catal. Lett.* **1990**, *7*, 253-270.
24. Knottenbelt, C. *Catal. Today* **2002**, *71*, 437-445.
25. Fischer, F.; Tropsch, H. *Brennst. Chem.* **1923**, *4*, 276-285.
26. Fischer, F.; Tropsch, H. *Brennst. Chem*. **1926**, *7*, 97-116.
27. Fischer, F.; Tropsch, H. *Ber. Dtsch. Chem. Ges*. **1926**, *59*, 830.
28. Dry, M. E. *Catal. Today* **2002**, *71*, 227-241.
29. Dry, M. E. *Handbook of Heterogeneous Catalysis*, Vol. 6, Wiley-VCH: Weinheim, **2008**, 2965-2994.
30. van Dyk, J. C.; Keyser, M. J.; Coertzen, M. *Int. J. Coal Geol.* **2006**, *65*, 243.
31. Remans, T. J.; Jenzer, G.; Hoek, A. *Handbook of Heterogeneous Catalysis*, Vol. 6, Wiley-VCH, Weinheim, **2008**, 2994–3010.

32. Vannice, M. A. *J. Catal.* **1975**, *37*, 449-461.
33. Tomishige, K.; Asadullah, M.; Kunimori, K. *Catal. Today* **2004**, *89*, 389-403.
34. Chang, C.-T.; Chen, B.-Y. *J. Hazard. Mater.* **2008**, *153*, 1262.
35. Johnson, E. S.; Langård, S.; Lin, Y. S. *Sci. Total Environ.* **2007**, *374*, 183.
36. Arpe, H. J.; Weissermel, K. *Industrial Organic Chemistry*, 4th edition; Wiley-VCH: New York, 2003.
37. Enya, T.; Suzuki, H.; Watanabe, T.; Hirayama, T.; Hisamatsu, Y. *Environ. Sci. Technol.* **1997**, *31*, 2772.
38. Widegren, J. A.; Finke, R. G. *J. Mol. Catal. A: Chem.* **2003**, *191*, 187.
39. Augustine, R. L. *Heterogeneous Catalysis for the Synthetic Chemistry*; Marcel Dekker: New York, 1996.
40. Zahmakıran, M.; Tonbul, Y.; Özkar, S. *J. Am. Chem. Soc*. **2010**, *132*, 6541-6549.
41. Pan, H. B.; Wai, C. M. *J. Phys. Chem. C* **2009**, *113*, 19782-19788.
42. Peng, S.; Wang, C.; Xie, J.; Sun, S. *J. Am. Chem. Soc*. **2006**, *128*, 10676-10677.
43. Travis, A. S. *The Chemistry of Functional Groups: The Chemistry of Anilines*, Wiley-VCH: Weinheim, 2007, 715-782
44. Blaser, H. U. *Science.* **2006**, *313*, 312.
45. Corma, A.; Concepcion, P.; Serna, P. *Angew. Chem. Int. Ed.* **2007**, *46*, 7266.
46. Meng, X.; Cheng, H.; Akiyama, Y.; Hao, Y.; Qiao, W.; Yu, Y.; Zhao, F.; Fujita, S. I.; Arai, M. *J. Catal.* **2009**, *264*, 1.
47. Garcia, R.; Besson, M.; Gallezot, P. *Appl. Catal. A* **1995**, *127*, 165-176.
48. Zhao, F. Y.; Ikushima, Y.; Arai, M. *J. Catal.* **2004**, *224*, 479-483.
49. Nadgeri, J. M.; Telkar, M. M.; Rode, C. V. *Catal. Commun.* **2008**, *9*, 441-446.
50. Yu, Z. K.; Liao, S. J.; Xu, Y.; Yang, B.; Yu, D. R. *J. Mol. Catal. A: Chem.* **1997**, *120*, 247-255.
51. Li, C. H.; Yu, Z. X.; Yao, K. F.; Ji, S. F.; Liang, J. *J. Mol. Catal. A: Chem.* **2005**, *226*, 101-105.
52. Xia, C.; Liu, Y.; Zhou, S.; Yang, C.; Liu, S.; Xu, J.; Yu, J.; Chen, J.; Liang, X. *J. Hazard Mater.* **2009**, *169*, 1029-1033.
53. Maegawa, T.; Akashi, A.; Yaguchi, K.; Iwasaki, Y.; Shigetsura, M.; Monguchi, Y.; Sajiki, H. *Chemistry* **2009**, *15*, 6953-6963.
54. Jurcík, V.; Nolan, S. P.; Cazin, C. S. *Chemistry* **2009**, *15*, 2509-2511.

Appendix

NMR Data

The ^{1}H NMR and ^{13}C NMR data of all products in Table 2-3 are listed below. All NMR and GC spectra of products are listed in the Appendix.

Biphenyl. ^{1}H NMR (400 MHz, $CDCl_3$): δ 7.66 (d, J = 8.4 Hz, 4H), 7.49 (t, J = 7.5 Hz, 4H), 7.39 (t, J = 7.4 Hz, 2H); ^{13}C NMR (100 MHz, $CDCl_3$): δ 141.3, 128.8, 127.3, 127.2.

2-Methylbiphenyl. ^{1}H NMR (400 MHz, $CDCl_3$): δ 7.50-7.46 (m, 2H), 7.41 (t, J = 7.6 Hz, 3H), 7.35-7.30 (m, 4H), 2.35 (s, 3H); ^{13}C NMR (100 MHz, $CDCl_3$): δ 142.0, 141.9, 135.4, 130.4, 129.8, 129.2, 128.1, 127.3, 126.8, 125.8, 20.5.

2-Methoxybiphenyl. ^{1}H NMR (400 MHz, $CDCl_3$): δ 7.57 (d, J = 7.0 Hz, 2H), 7.45 (t, J = 7.4 Hz, 2H), 7.38-7.34 (m, 3H), 7.09-7.01 (m, 2H), 3.84 (s, 3H); ^{13}C NMR (100 MHz, $CDCl_3$): δ 156.5, 138.6, 130.9, 130.8, 129.6, 128.6, 128.0, 126.9, 120.9, 111.3, 55.6.

3-Methoxybiphenyl. ^{1}H NMR (400 MHz, $CDCl_3$): δ 7.65 (d, J = 8.4 Hz, 2H), 7.49 (t, J = 7.2 Hz, 2H), 7.41 (m, 2H), 7.25 (d, J = 7.7 Hz, 1H), 7.20 (s, 1H), 6.96 (d, J = 8.2 Hz, 1H), 3.91 (s, 3H); ^{13}C NMR (100 MHz, $CDCl_3$): δ 160.0, 142.8, 141.2, 129.8, 128.8, 127.5, 127.2, 119.7, 113.0, 112.7, 55.3.

4-Methoxybiphenyl. ^{1}H NMR (400 MHz, $CDCl_3$): δ 7.60-7.55 (m, 4H), 7.44 (t, J = 7.6 Hz, 2H), 7.33 (t, J = 7.4 Hz, 1H), 7.01 (d, J = 8.9 Hz, 2H), 3.88 (s, 3H); ^{13}C NMR (100 MHz, $CDCl_3$): δ 159.2, 140.8, 133.8, 128.7, 128.2, 126.7, 126.6,

114.2, 55.4.

4-Acetylbiphenyl. ^{1}H NMR (400 MHz, $CDCl_3$): δ 8.04 (d, *J* = 8.0 Hz, 2H), 7.69 (d, *J* = 8.0 Hz, 2H), 7.63 (d, *J* = 7.5 Hz, 2H), 7.48 (t, *J* = 7.4 Hz, 2H), 7.41 (t, *J* = 7.1 Hz, 1H), 2.64 (s, 3H); ^{13}C NMR (100 MHz, $CDCl_3$): δ 197.7, 145.8, 139.9, 135.9, 129.0, 128.9, 128.2, 127.3, 127.2, 26.7.

4-Nitrobiphenyl. ^{1}H NMR (400 MHz, $CDCl_3$): δ 8.30 (d, *J* = 8.8 Hz, 2H), 7.74 (d, *J* = 8.8 Hz, 2H), 7.63 (d, *J* = 6.9 Hz, 2H), 7.53-7.44 (m, 3H); ^{13}C NMR (100 MHz, $CDCl_3$): δ 147.6, 147.1, 138.8, 129.1, 128.9, 127.8, 127.4, 124.1.

^{1}H and ^{13}C NMR Spectra

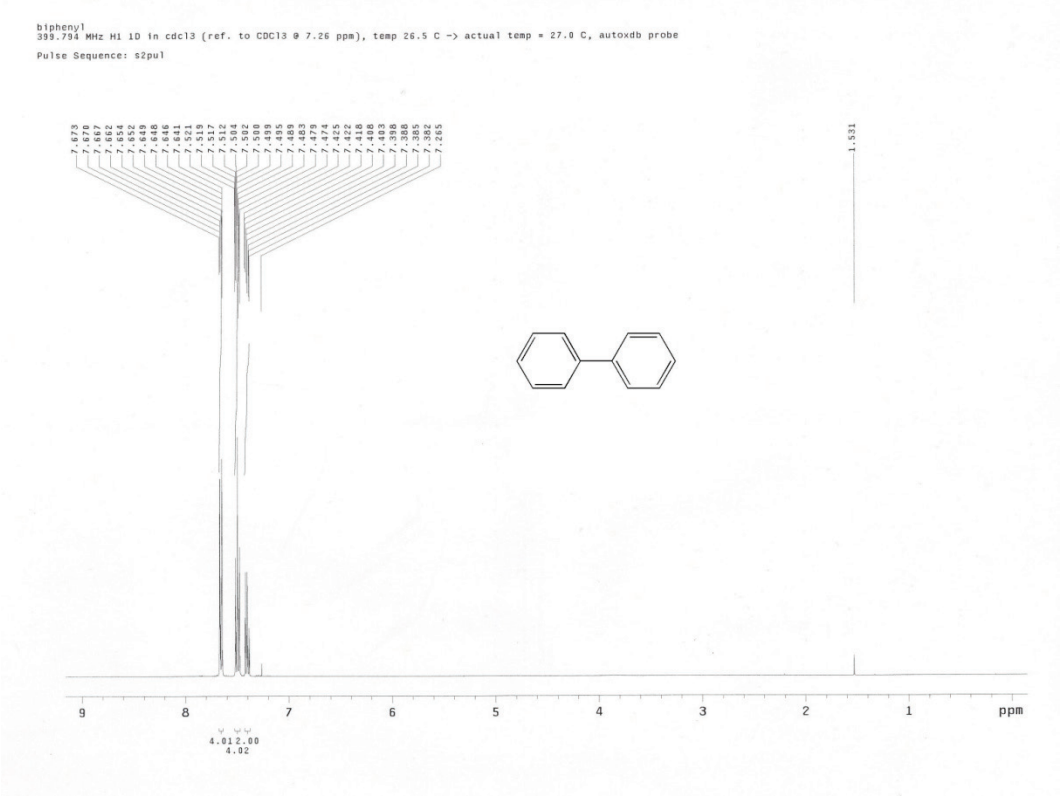

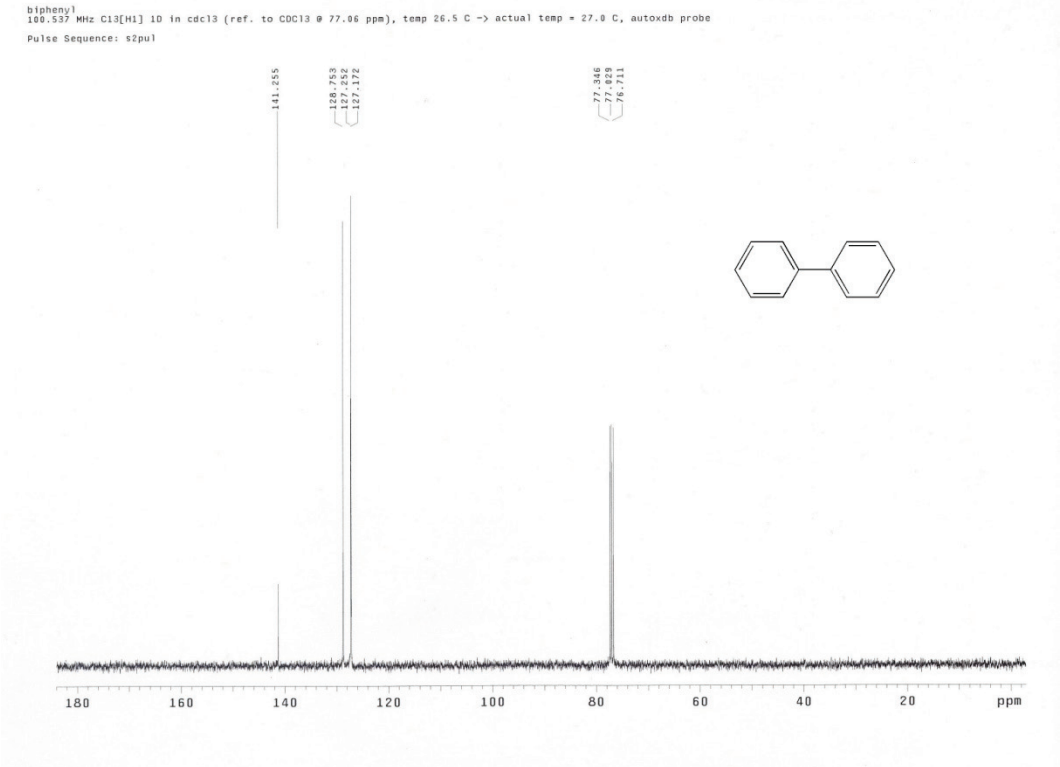

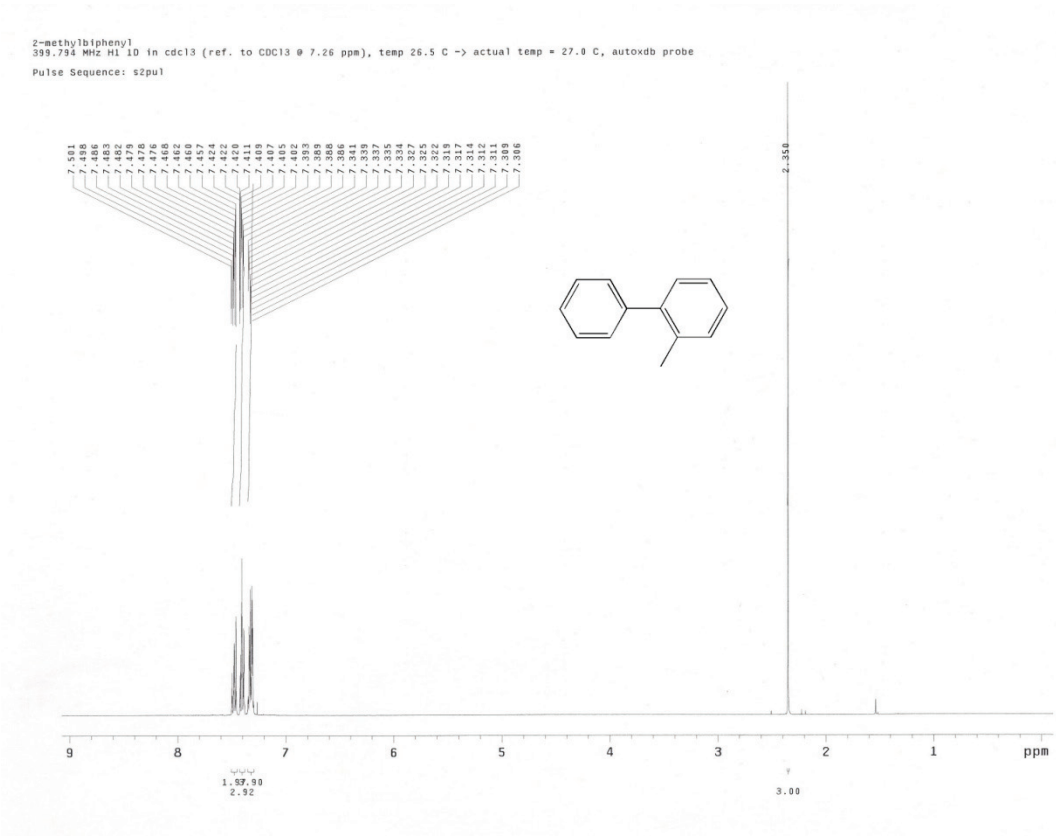
2-methylbiphenyl
399.794 MHz H1 1D in cdcl3 (ref. to CDCl3 @ 7.26 ppm), temp 26.5 C -> actual temp = 27.0 C, autoxdb probe
Pulse Sequence: s2pul
7.501
7.498
7.486
7.483
7.482
7.478
7.476
7.468
7.462
7.460
7.457
7.424
7.422
7.420
7.411
7.409
7.407
7.405
7.402
7.393
7.389
7.388
7.386
7.341
7.339
7.337
7.335
7.334
7.327
7.325
7.322
7.319
7.317
7.314
7.312
7.311
7.309
7.306
2.350
9
8
7
6
5
4
3
2
1
ppm
1.97
1.90
2.92
3.00

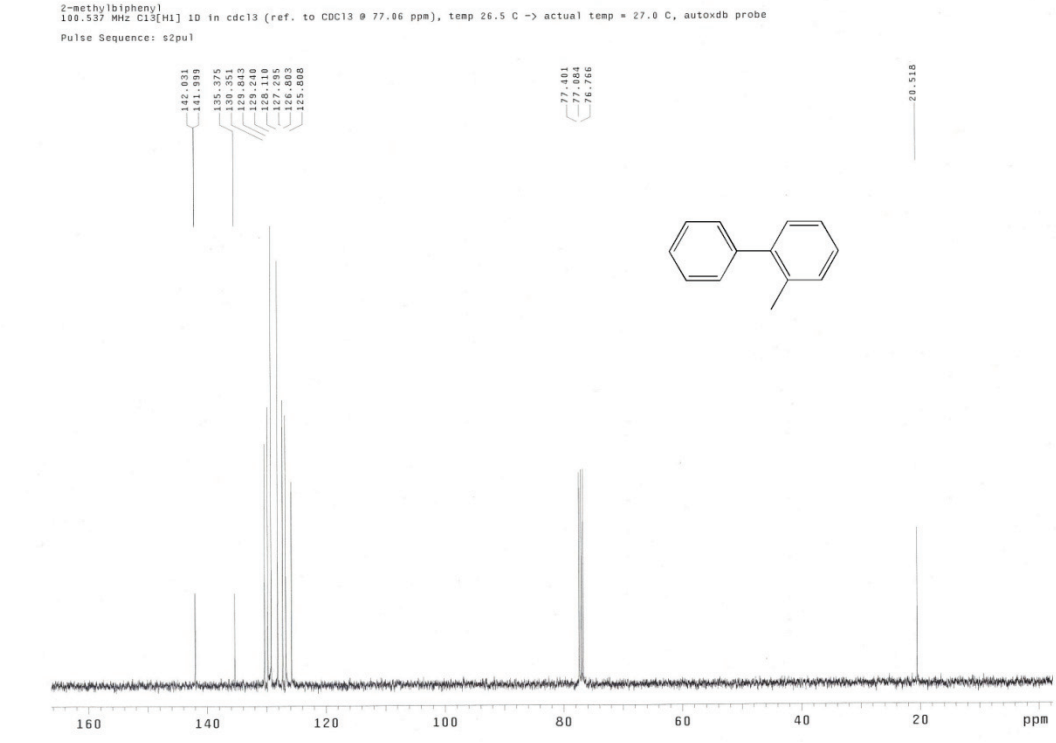
2-methylbiphenyl
100.537 MHz C13[H1] 1D in cdcl3 (ref. to CDCl3 @ 77.06 ppm), temp 26.5 C -> actual temp = 27.0 C, autoxdb probe
Pulse Sequence: s2pul
142.031
141.999
135.375
130.351
129.615
129.240
128.110
127.295
126.803
125.808
77.401
77.084
76.766
20.518
160
140
120
100
80
60
40
20
ppm

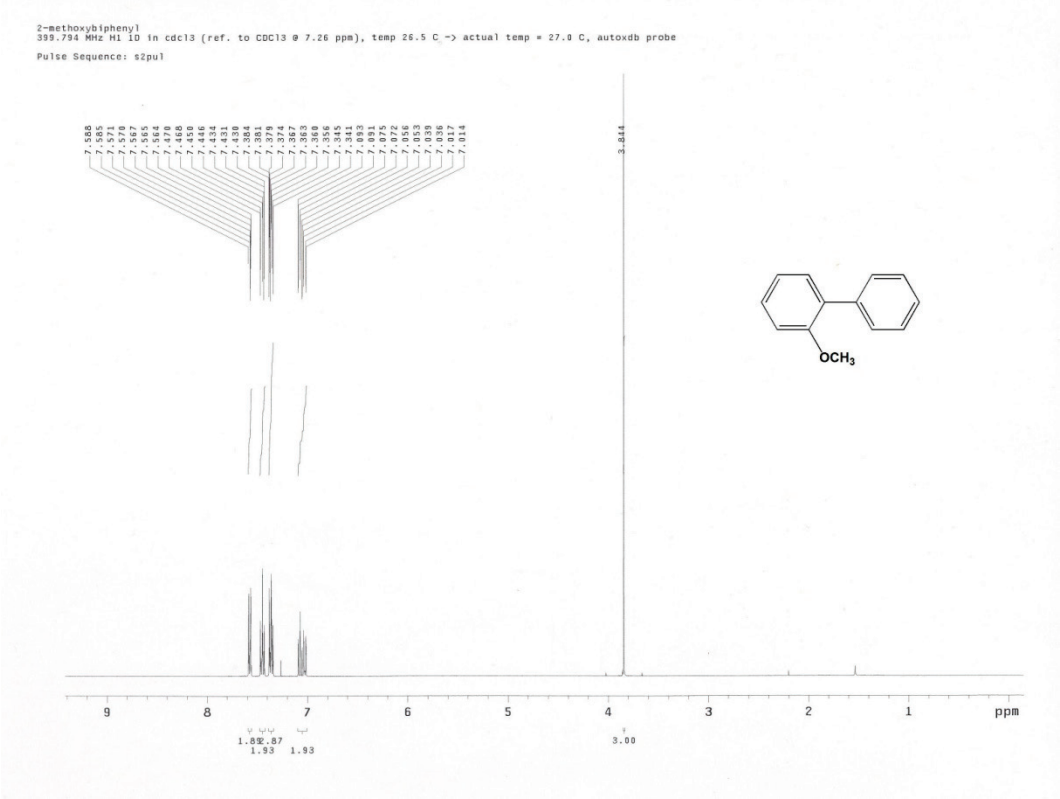
2-methoxybiphenyl
399.794 MHz H1 1D in cdcl3 (ref. to CDCl3 @ 7.26 ppm), temp 26.5 C -> actual temp = 27.0 C, autoxdb probe
Pulse Sequence: s2pul
7.588
7.585
7.571
7.570
7.567
7.565
7.564
7.470
7.468
7.450
7.446
7.434
7.431
7.430
7.384
7.381
7.378
7.374
7.367
7.363
7.360
7.356
7.345
7.341
7.093
7.091
7.075
7.072
7.056
7.053
7.039
7.036
7.017
7.014
3.844
OCH3
9
8
7
6
5
4
3
2
1
ppm
1.85
2.87
1.93
1.93
3.00

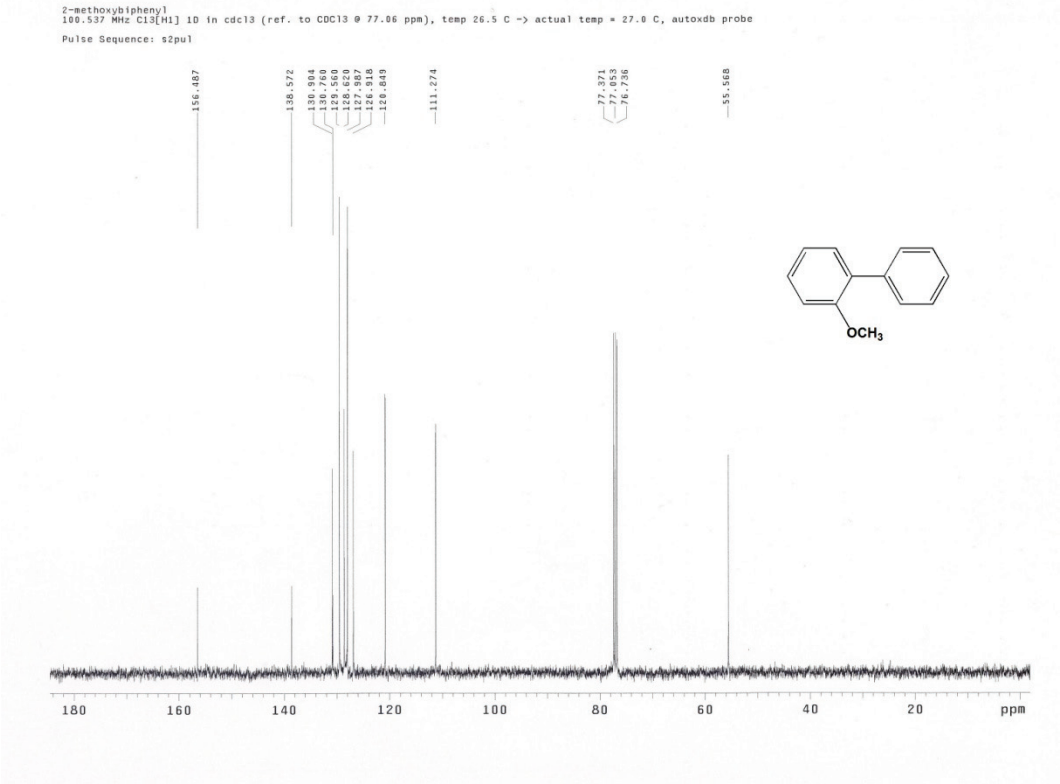
2-methoxybiphenyl
100.537 MHz C13[H1] 1D in cdcl3 (ref. to CDCl3 @ 77.06 ppm), temp 26.5 C -> actual temp = 27.0 C, autoxdb probe
Pulse Sequence: s2pul
156.487
138.572
130.904
130.760
129.560
128.620
127.987
126.918
120.849
111.274
77.371
77.053
76.736
55.568
OCH3
180
160
140
120
100
80
60
40
20
ppm

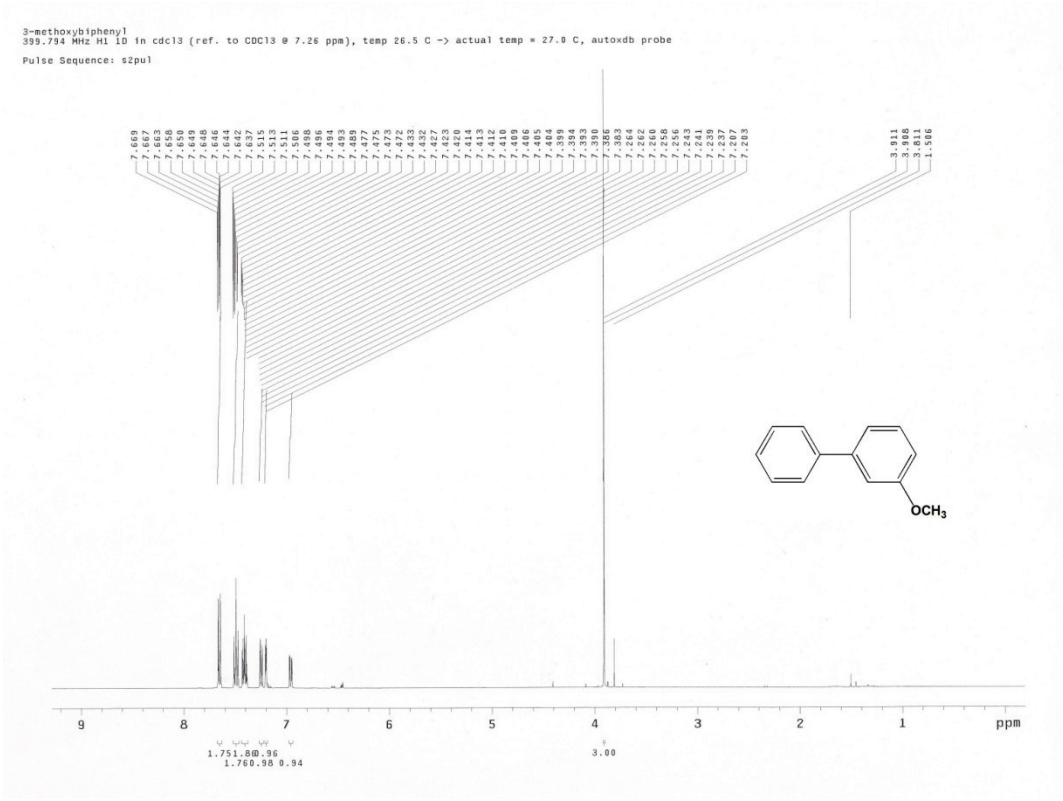
3-methoxybiphenyl
399.794 MHz H1 1D in cdcl3 (ref. to CDCl3 @ 7.26 ppm), temp 26.5 C -> actual temp = 27.0 C, autoxdb probe
Pulse Sequence: s2pul
7.669
7.667
7.663
7.658
7.650
7.649
7.648
7.646
7.644
7.642
7.637
7.515
7.513
7.511
7.506
7.498
7.496
7.494
7.489
7.485
7.477
7.475
7.473
7.472
7.438
7.432
7.427
7.423
7.420
7.414
7.413
7.412
7.410
7.409
7.406
7.405
7.404
7.399
7.394
7.393
7.390
7.386
7.383
7.264
7.262
7.260
7.258
7.256
7.243
7.241
7.239
7.237
7.207
7.203
3.911
3.908
3.811
1.986
OCH3
9
8
7
6
5
4
3
2
1
ppm
1.751.80 0.96
1.760.98 0.94
3.00

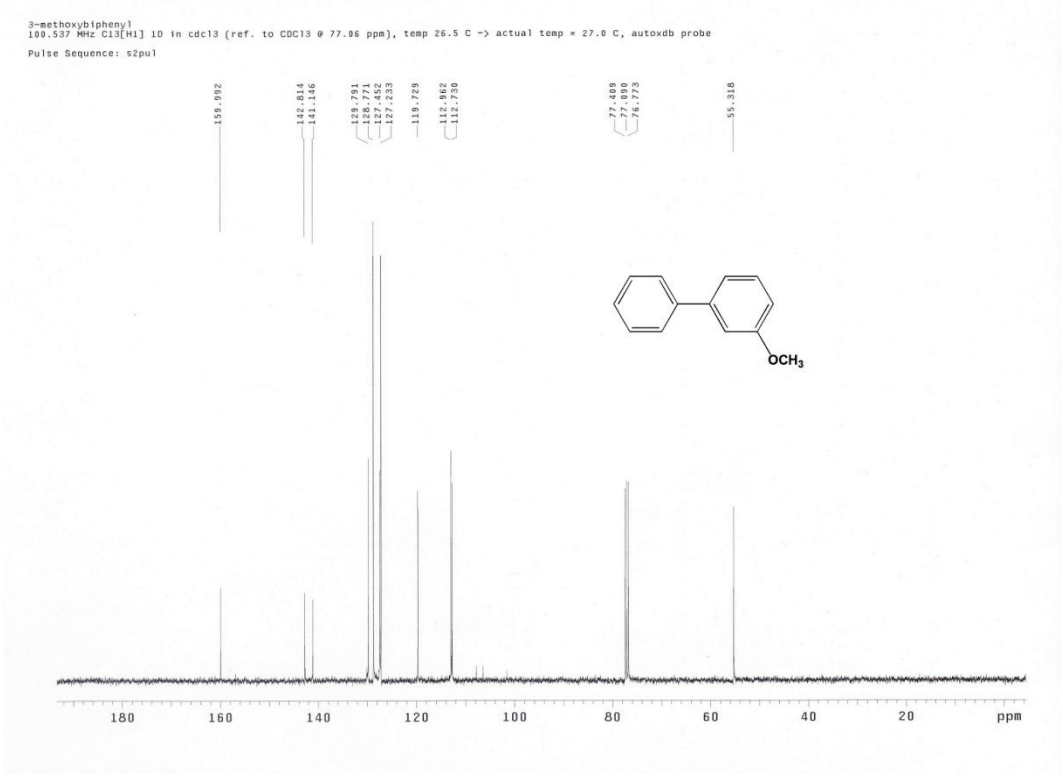
3-methoxybiphenyl
100.537 MHz C13[H1] 1D in cdcl3 (ref. to CDCl3 @ 77.06 ppm), temp 26.5 C -> actual temp = 27.0 C, autoxdb probe
Pulse Sequence: s2pul
159.992
142.814
141.146
129.791
128.771
127.452
127.233
119.729
112.962
112.730
77.409
77.090
76.773
55.318
OCH3
180
160
140
120
100
80
60
40
20
ppm

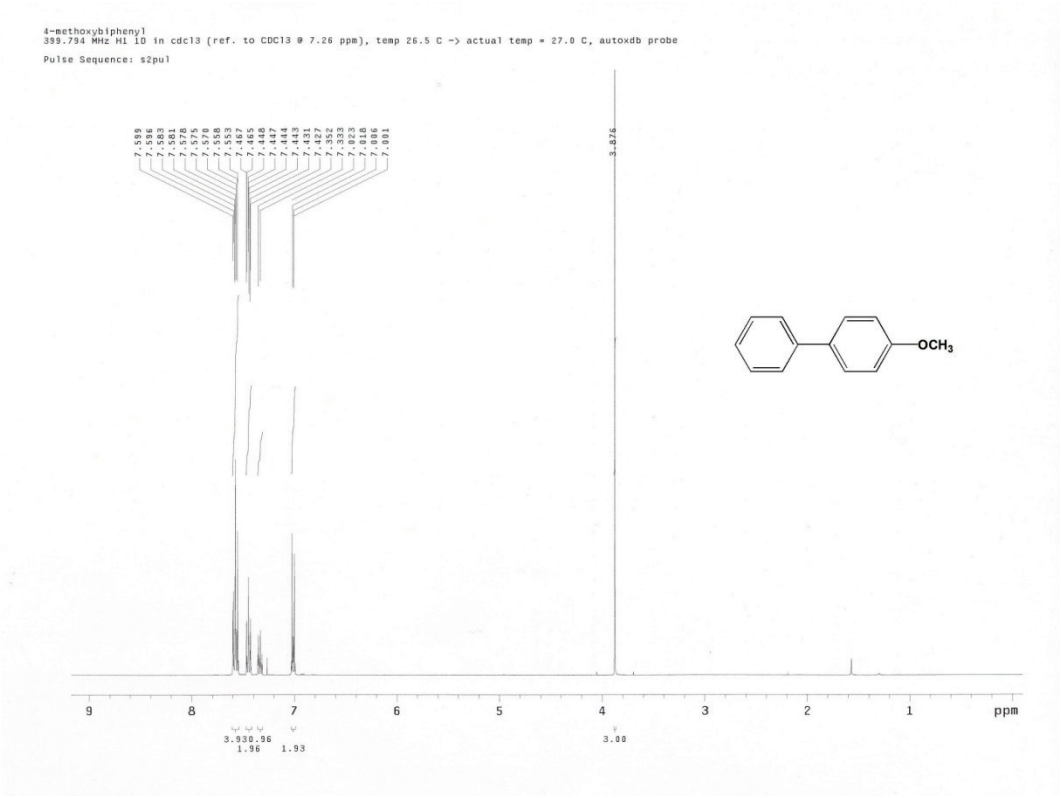
4-methoxybiphenyl
399.794 MHz H1 1D in cdcl3 (ref. to CDCl3 @ 7.26 ppm), temp 26.5 C -> actual temp = 27.0 C, autoxdb probe
Pulse Sequence: s2pul
7.599
7.596
7.583
7.581
7.578
7.575
7.570
7.558
7.553
7.467
7.465
7.448
7.447
7.444
7.443
7.431
7.427
7.352
7.333
7.023
7.018
7.006
7.001
3.876
OCH3
9
8
7
6
5
4
3
2
1
ppm
3.93
0.96
1.96
1.93
3.00

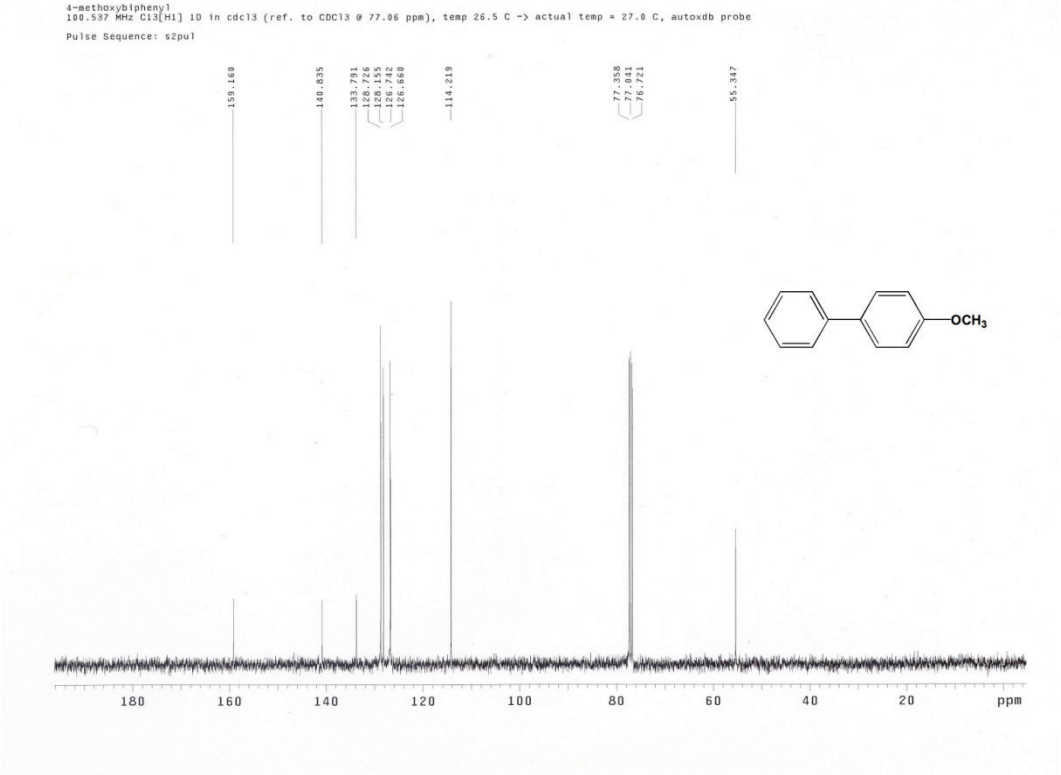
4-methoxybiphenyl
100.537 MHz C13[H1] 1D in cdcl3 (ref. to CDCl3 @ 77.06 ppm), temp 26.5 C -> actual temp = 27.0 C, autoxdb probe
Pulse Sequence: s2pul
159.160
140.835
133.791
128.726
128.155
126.742
126.660
114.219
77.358
77.041
76.721
55.347
OCH3
180
160
140
120
100
80
60
40
20
ppm

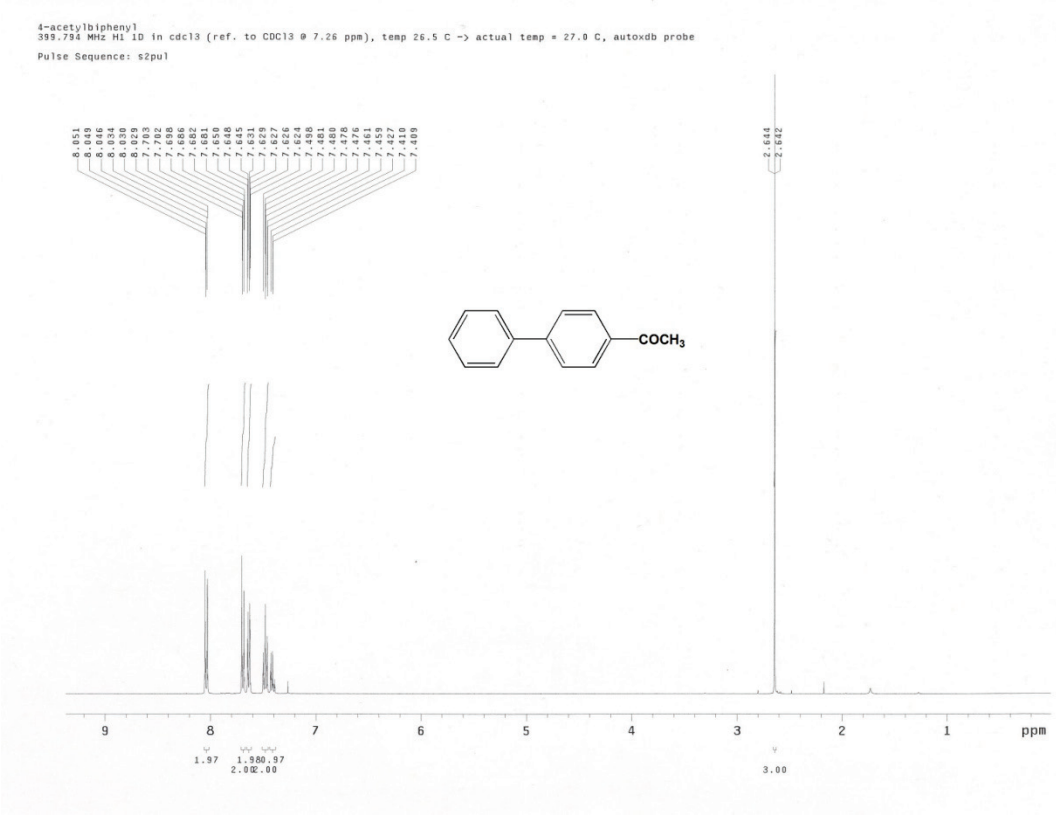
4-acetylbiphenyl
399.794 MHz H1 1D in cdcl3 (ref. to CDCl3 @ 7.26 ppm), temp 26.5 C -> actual temp = 27.0 C, autoxdb probe
Pulse Sequence: s2pul
8.051
8.048
8.046
8.034
8.030
8.029
7.703
7.702
7.698
7.686
7.682
7.681
7.650
7.648
7.646
7.631
7.629
7.627
7.626
7.624
7.498
7.481
7.480
7.478
7.476
7.461
7.459
7.427
7.410
7.409
2.644
2.642
COCH3
9
8
7
6
5
4
3
2
1
ppm
1.97
1.98
0.97
2.00
2.00
3.00

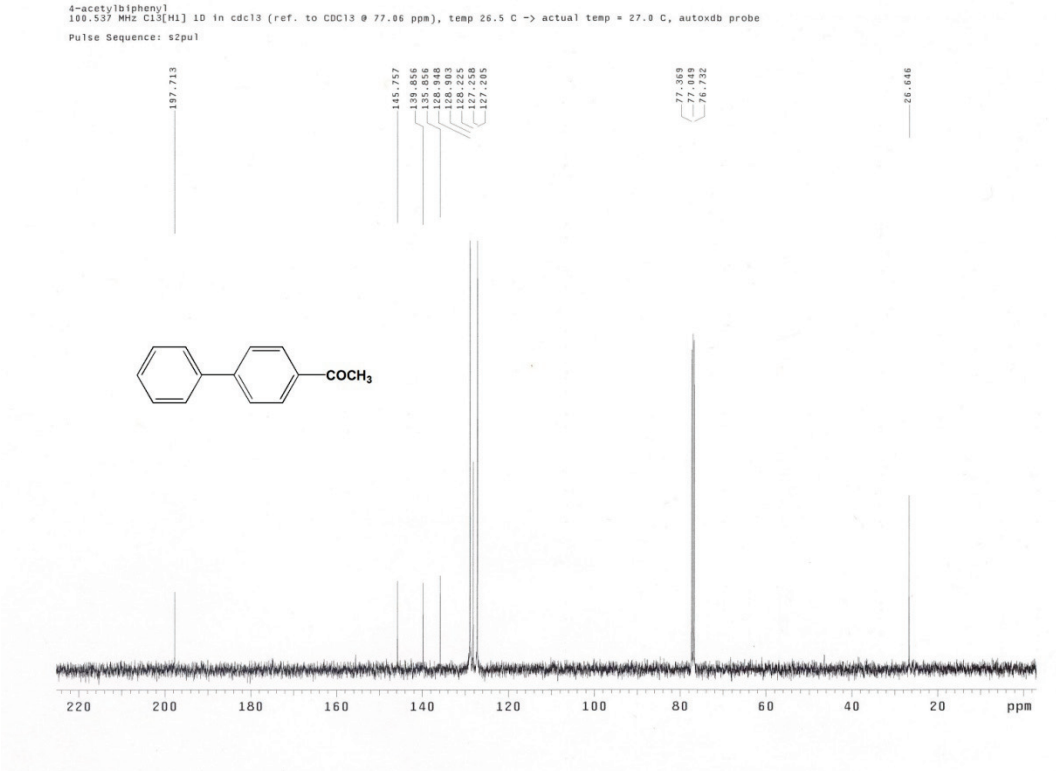
4-acetylbiphenyl
100.537 MHz C13[H1] 1D in cdcl3 (ref. to CDCl3 @ 77.06 ppm), temp 26.5 C -> actual temp = 27.0 C, autoxdb probe
Pulse Sequence: s2pul
197.713
145.757
139.856
135.656
128.948
128.993
128.225
127.258
127.205
77.369
77.049
76.732
26.646
COCH3
220
200
180
160
140
120
100
80
60
40
20
ppm

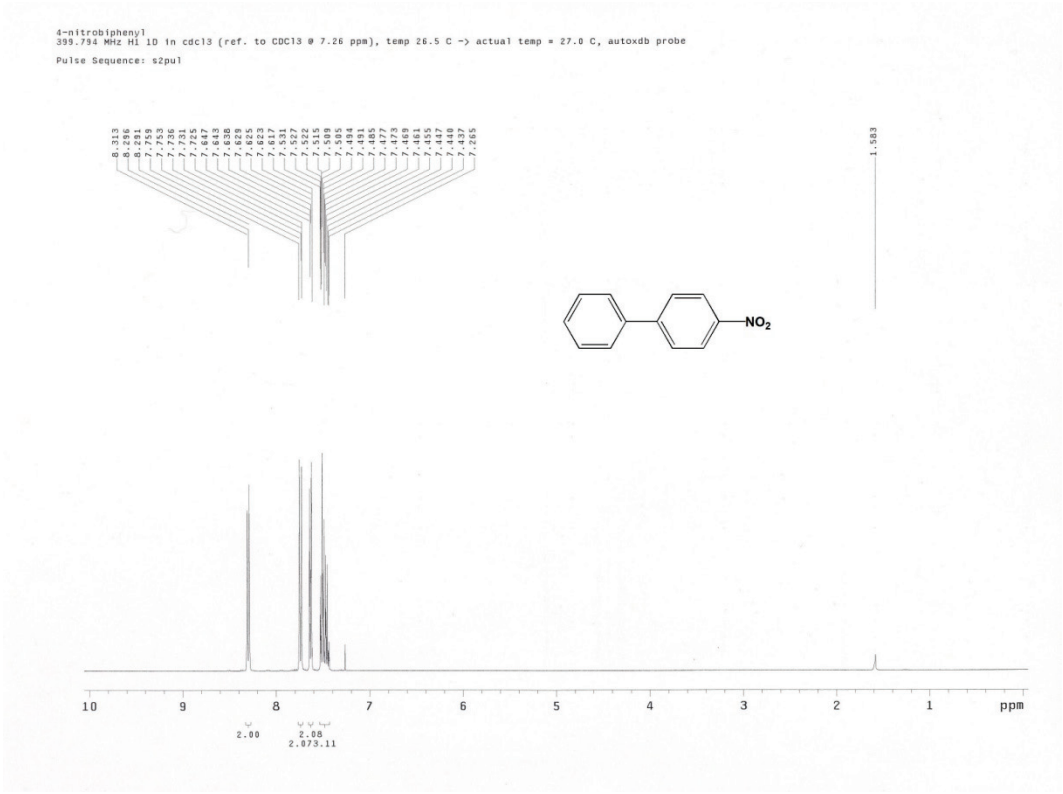
4-nitrobiphenyl
399.794 MHz H1 1D in cdcl3 (ref. to CDCl3 @ 7.26 ppm), temp 26.5 C -> actual temp = 27.0 C, autoxdb probe
Pulse Sequence: s2pul
8.313
8.296
8.291
7.759
7.753
7.736
7.731
7.725
7.647
7.643
7.638
7.629
7.625
7.623
7.617
7.531
7.527
7.522
7.515
7.508
7.505
7.494
7.491
7.485
7.477
7.473
7.469
7.461
7.455
7.447
7.440
7.437
7.265
1.583
NO2
10
9
8
7
6
5
4
3
2
1
ppm
2.00
2.08
2.073.11

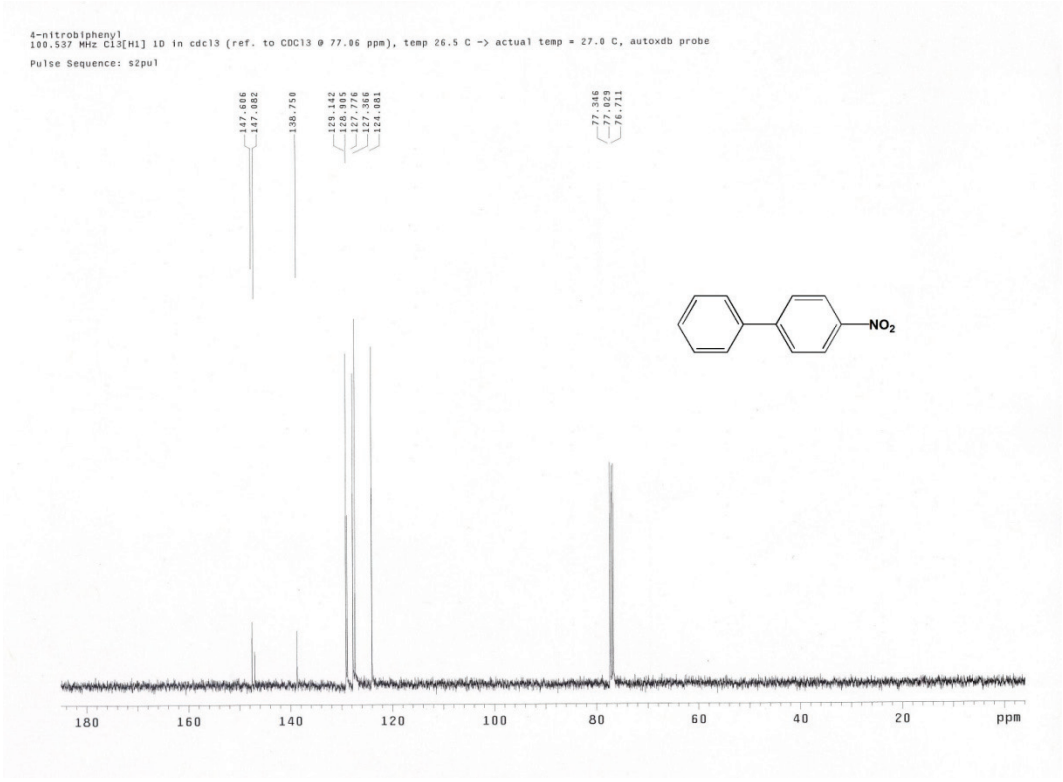
4-nitrobiphenyl
100.537 MHz C13[H1] 1D in cdcl3 (ref. to CDCl3 @ 77.06 ppm), temp 26.5 C -> actual temp = 27.0 C, autoxdb probe
Pulse Sequence: s2pul
147.606
147.082
138.750
129.142
128.795
124.776
127.366
124.081
77.346
77.059
76.711
NO2
180
160
140
120
100
80
60
40
20
ppm

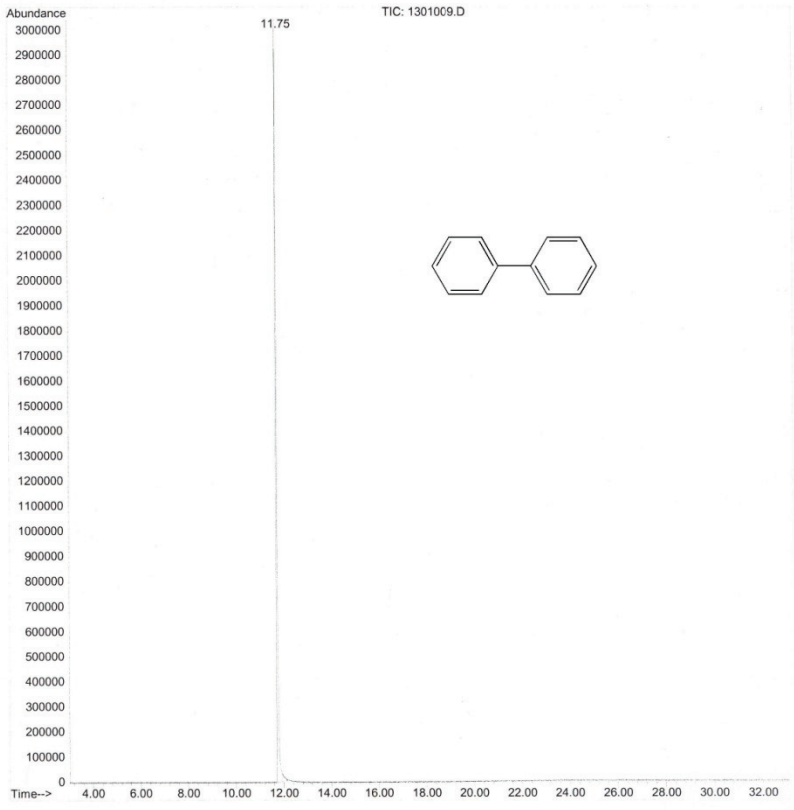

Library Searched : C:\DATABASE\WILEY138.L
Quality : 95
ID : 1,1'-Biphenyl

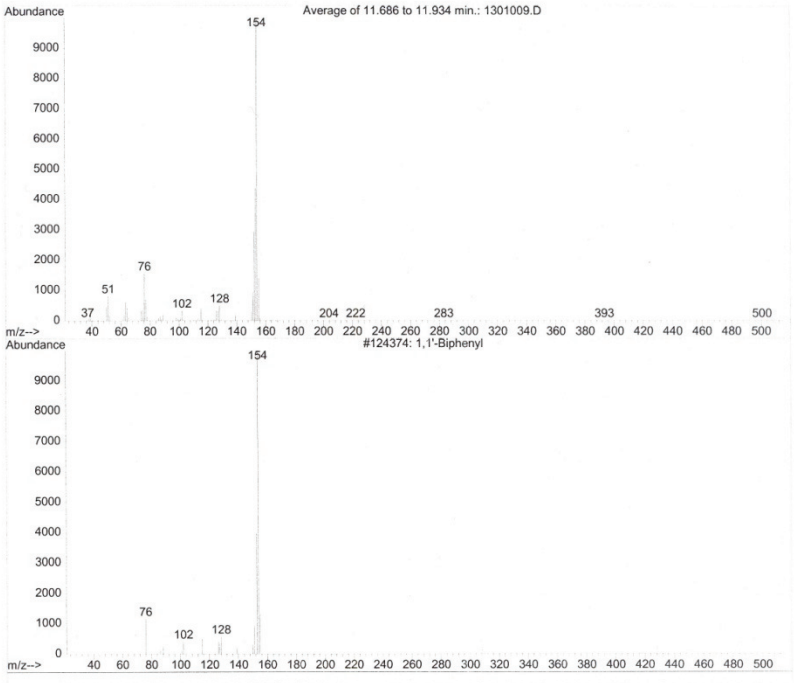

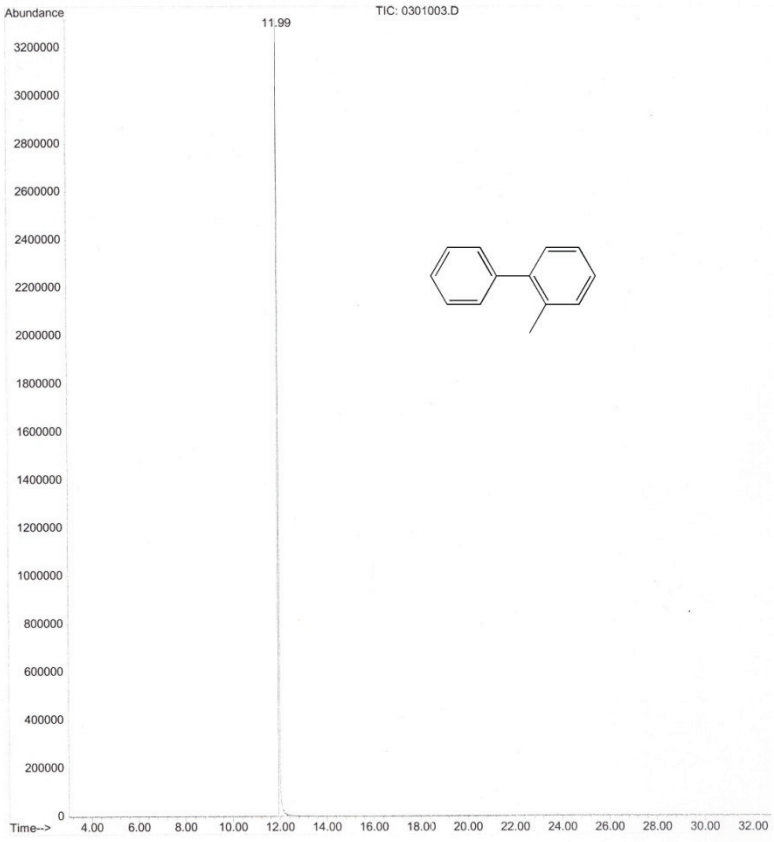

Library Searched : C:\DATABASE\WILEY138.L
Quality : 92
ID : 1,1'-Biphenyl, 2-methyl-

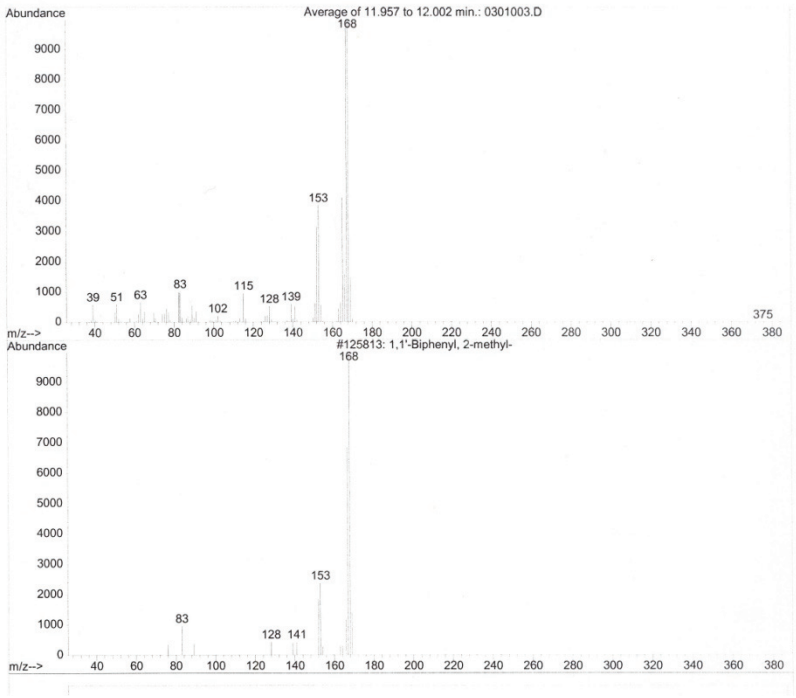

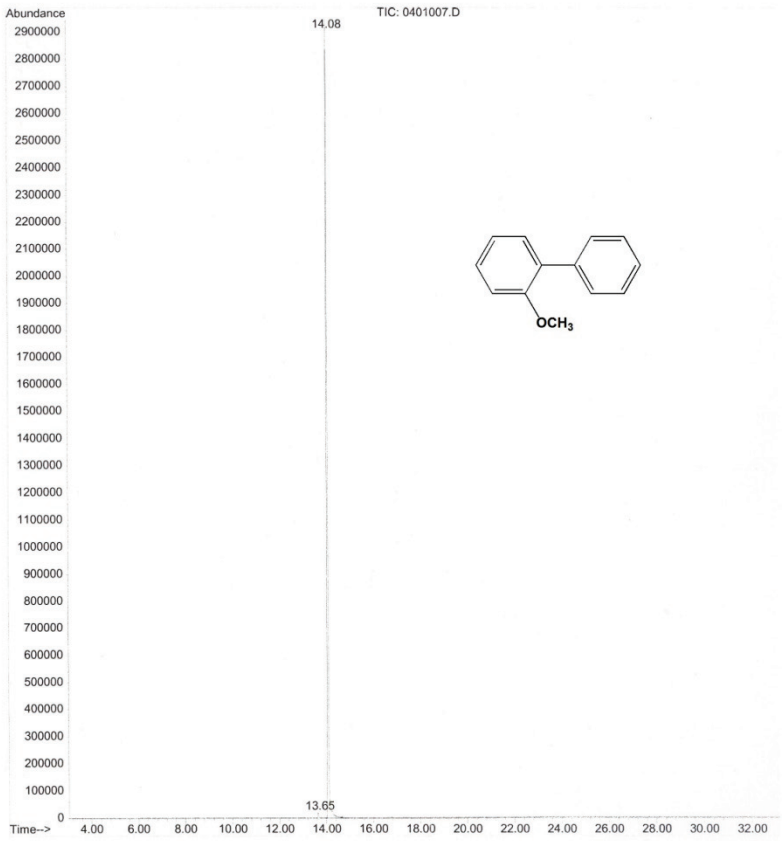

Library Searched : C:\DATABASE\WILEY138.L
Quality : 95
ID : 1,1'-Biphenyl, 2-methoxy-

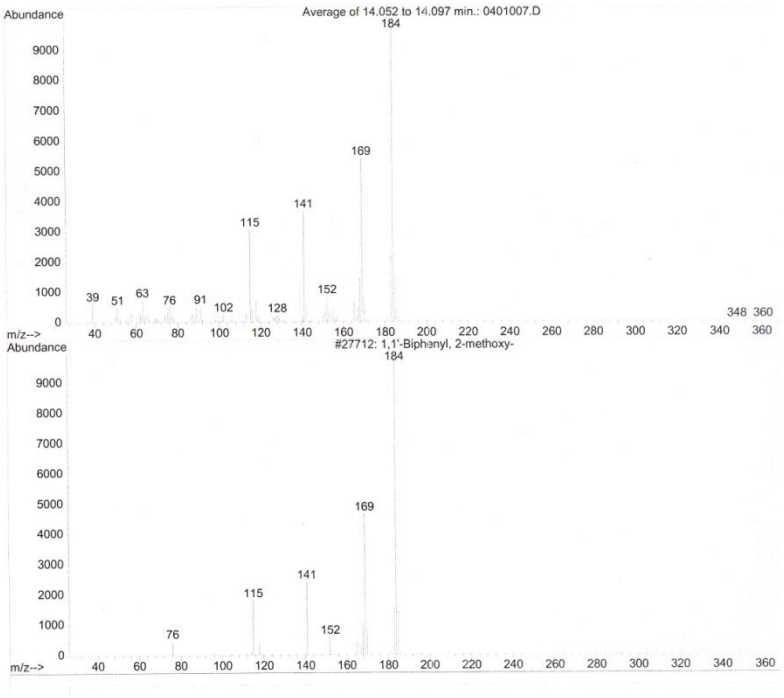

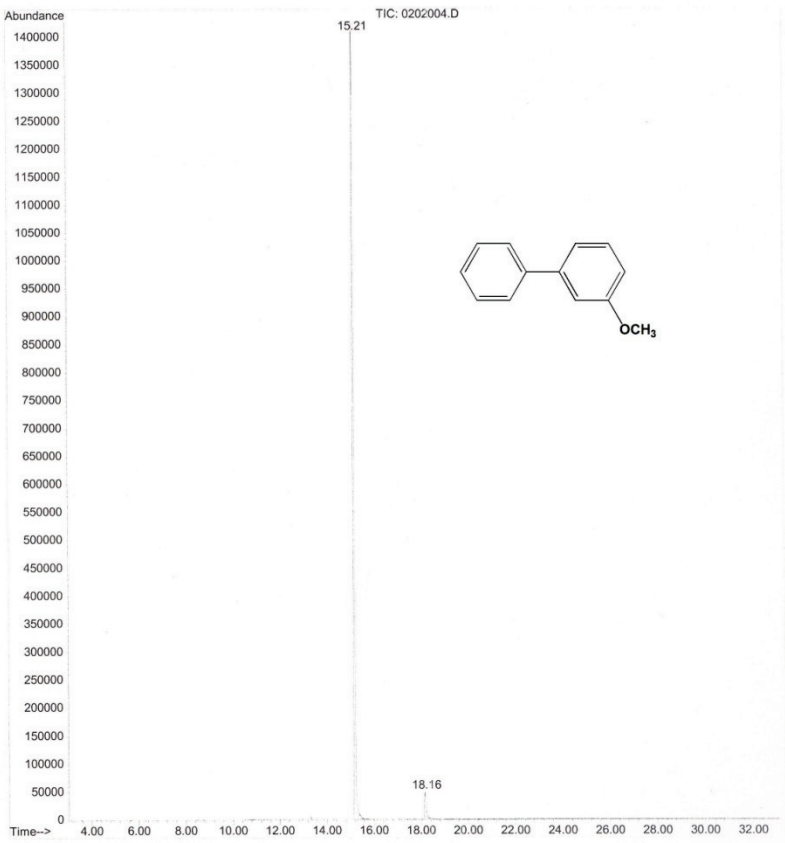

Library Searched : C:\DATABASE\WILEY138.L
Quality : 94
ID : 1,1'-Biphenyl, 3-methoxy-

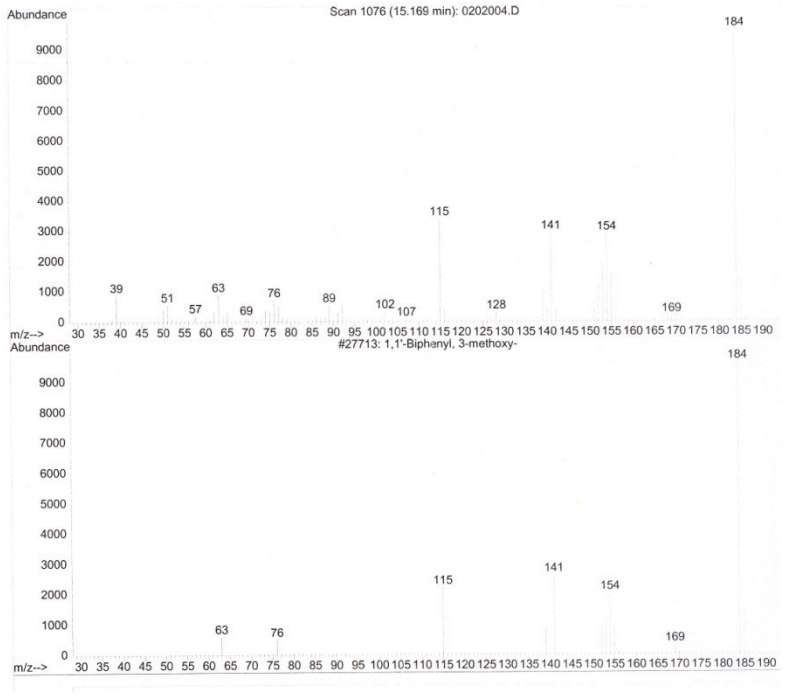

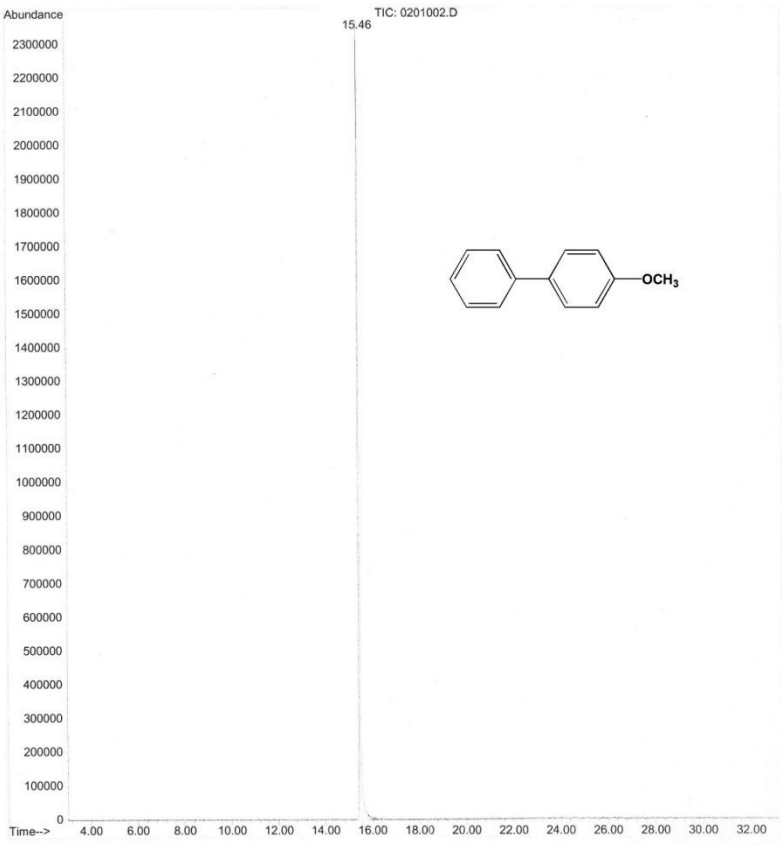

Library Searched : C:\DATABASE\WILEY138.L
Quality : 97
ID : 1,1'-Biphenyl, 4-methoxy-

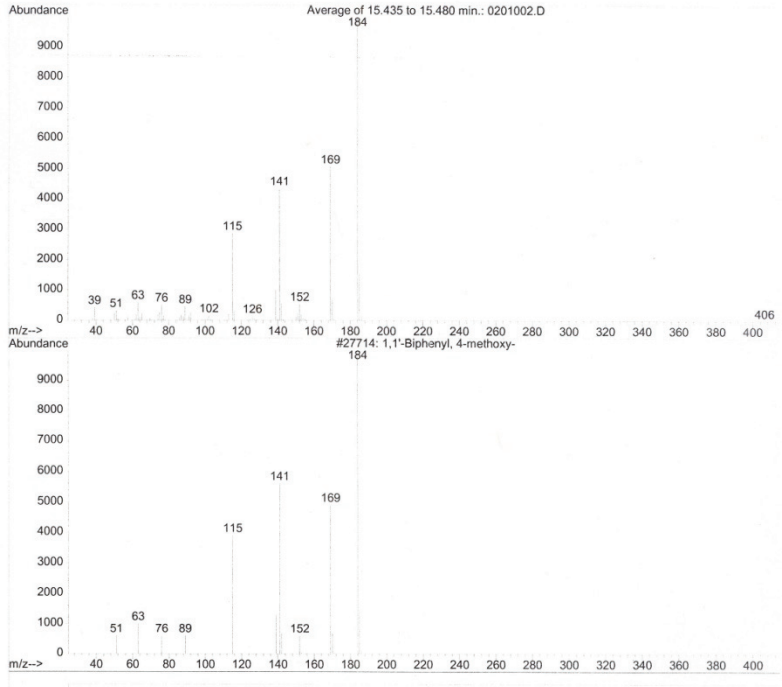

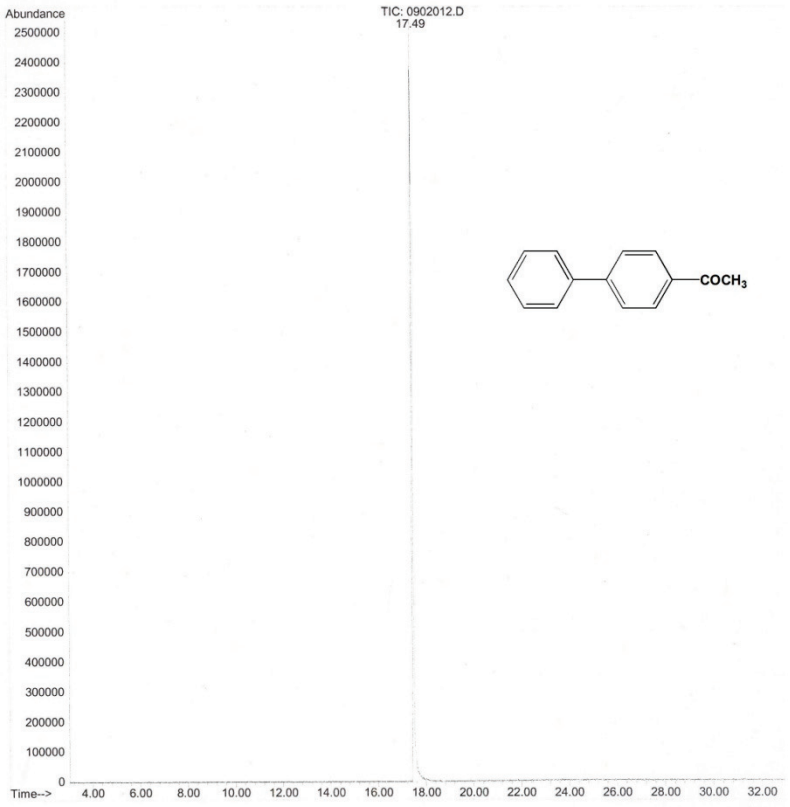
TIC: 0902012.D
17.49
Abundance
Time-->
COCH3

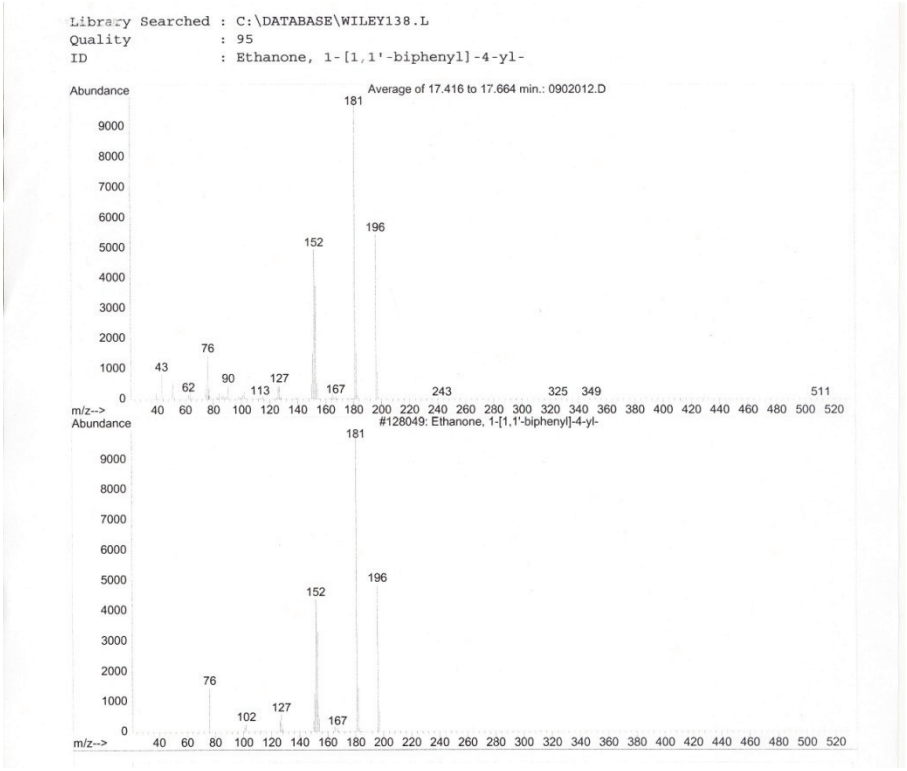
Library Searched : C:\DATABASE\WILEY138.L
Quality : 95
ID : Ethanone, 1-[1,1'-biphenyl]-4-yl-
Average of 17.416 to 17.664 min.: 0902012.D
#128049: Ethanone, 1-[1,1'-biphenyl]-4-yl-
Abundance
m/z-->

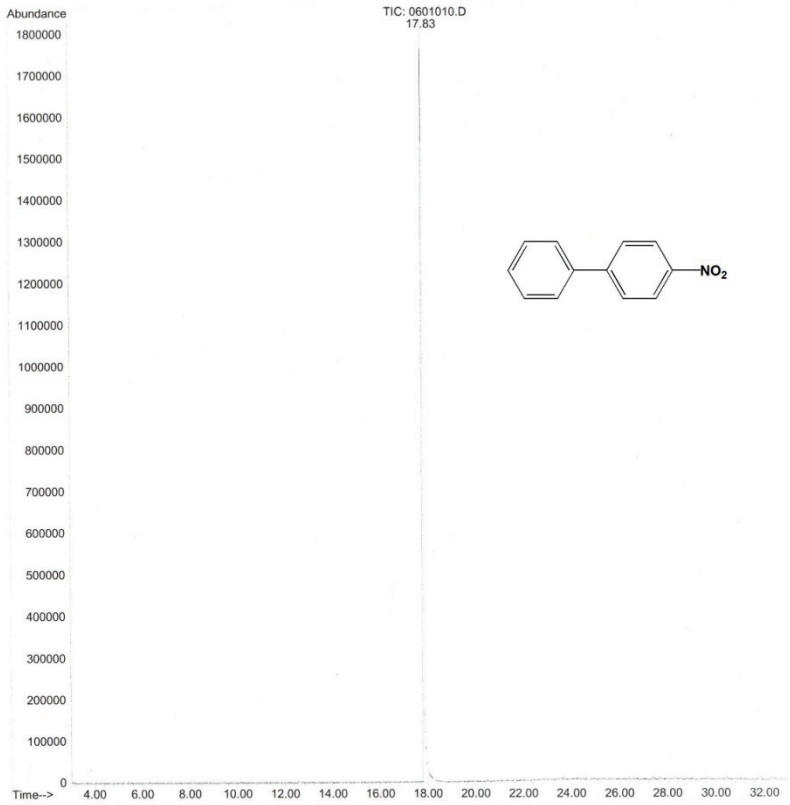

Library Searched : C:\DATABASE\WILEY138.L
Quality : 98
ID : 1,1'-Biphenyl, 4-nitro-

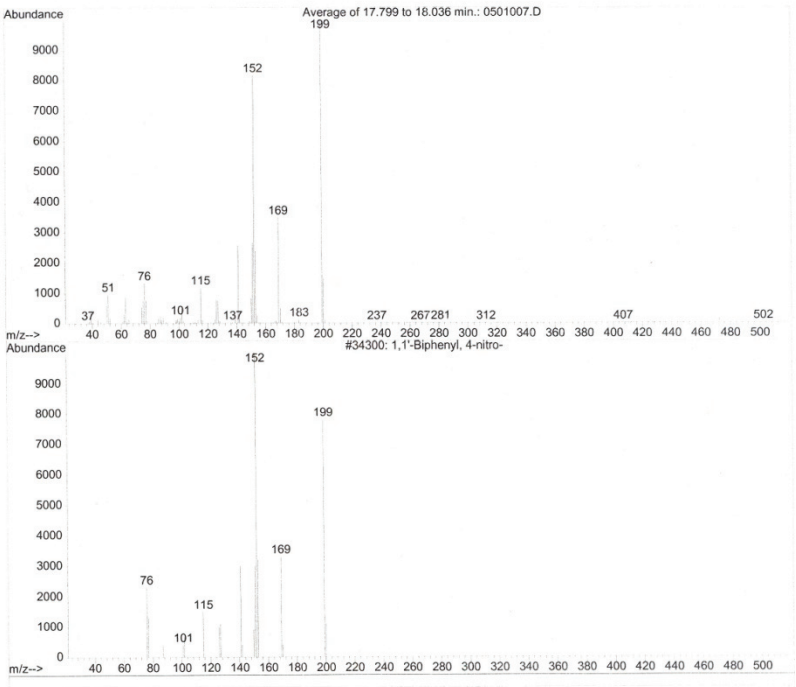

Experimental Details for Section 4.3

Preparation of Fe-Ru NPs by Thermal Decomposition

The procedure for synthesis of Fe-Ru NPs was adapted from a literature method for synthesizing Fe NPs. 20 mL of 1-octadecene (ODE) and oleylamine (0.9 mmol, 0.3 mL) were mixed and degassed under Ar at 120 °C for 30 minute. The temperature was then raised to 180 °C, and under a blanket of Ar, $Fe(CO)_5$ (1.52 mmol, 0.2 mL) was added. 10 minutes later, $Ru_3(CO)_{12}$ (0.1 mmol, 64.5 mg) in 2 mL oleylamine was added. The mixture was kept at 180 °C for 20 minutes before it was cool down to room temperature. 30 mL of absolute ethanol (degassed with Ar at least 10 min) was added to precipitate the product, and the supernatant was decanted by applying a magnet. The black precipitate was washed with degassed absolute ethanol under Ar (15 mL×4) and dried *in vacuo* overnight.

General Procedure for Fischer-Tropsch Synthesis

The freshly prepared $Fe@Fe_xO_y$/Co NPs (0.25 mmol Co on 0.1 g $Fe@Fe_xO_y$) were dispersed in 20 mL of cyclohexane in a beaker, which was then placed into a 1 L stainless steel autoclave (Parr Inst.) The autoclave was purged three times and then refilled with 290 psi (2.0 MPa) of CO and H_2 mixture (1:1, Praxair). The autoclave was heated and kept at 230 °C until the total pressure decreased to ~205 psi (or ~100 psi at room temperature, corresponding to a CO conversion of ~65%). The reaction was monitored by the pressure drop. After reaction, the autoclave was cooled to room temperature. The products formed two layers and the top

liquid layer containing hydrocarbon products were collected and analyzed by GC-MS.

General Procedure for Hydrogenation of Aromatics

The catalytic reactions were carried out at 80 °C under an initial pressure of 45 psi at room temperature in a 200 ml stainless steel autoclave (Parr Instrument) In a typical hydrogenation experiment, the Fe@Fe_xO_y/Rh catalyst was added into a 20 mL vial and then 1mL of benzene was added. The vial was put into an autoclave, and the autoclave was purged three times with hydrogen to remove the air inside. Hydrogen was charged into the autoclave until the desired pressure was reached, and the autoclave was sealed and placed in an oil bath. The reaction mixture was then stirred (500 rpm) at 80 °C under 45 psi of hydrogen pressure. The reaction was followed by monitoring the pressure change. At the end of the reaction, the autoclave was cooled to room temperature. Products were analyzed by GC-MS and ^{1}H NMR.

Hydrogenation of nitrobenzene followed same procedure as above.

GC Spectra for FTS

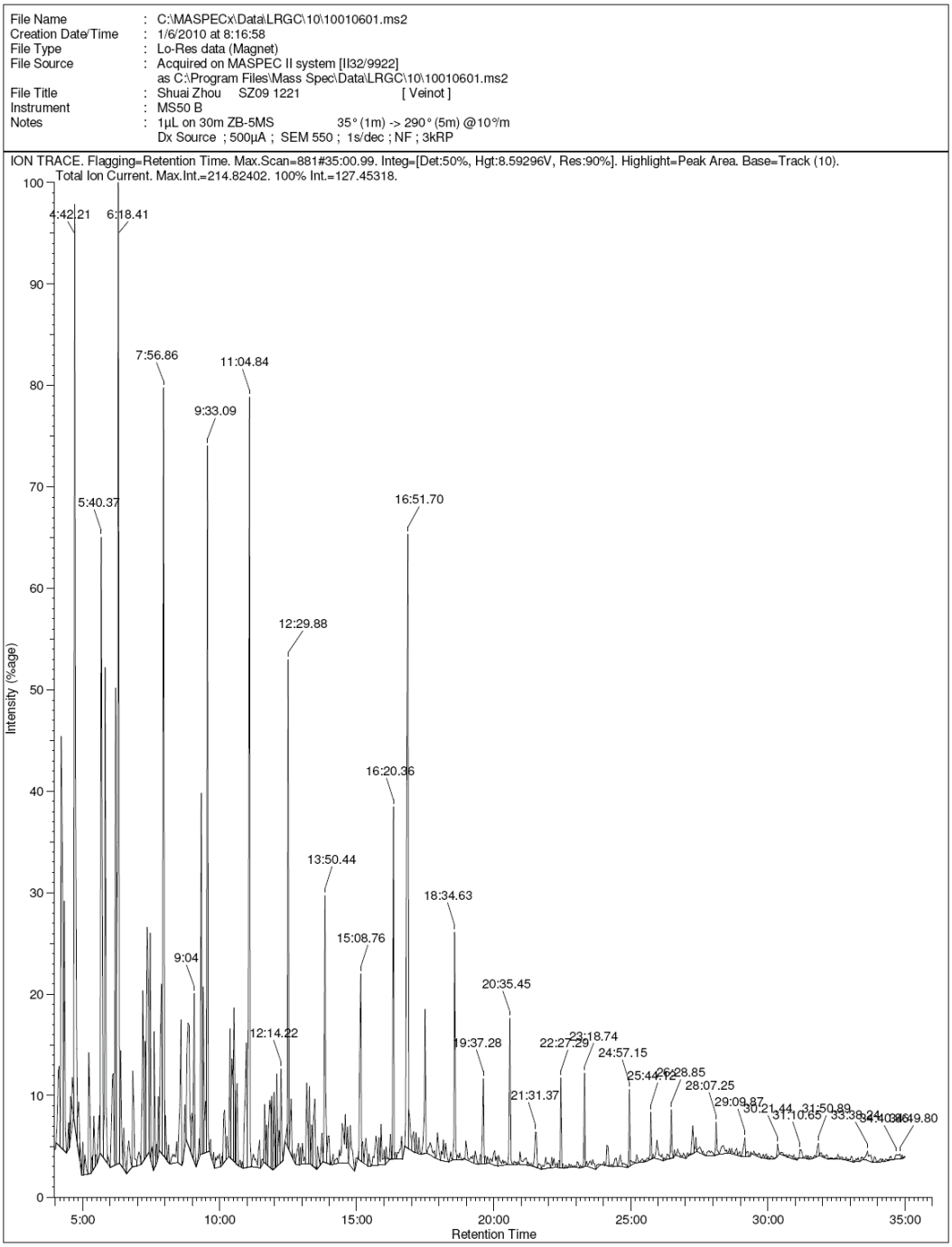

File Name	:	C:\MASPECx\Data\LRGC\10\10010801.ms2
Creation Date/Time	:	1/8/2010 at 11:08:12
File Type	:	Lo-Res data (Magnet)
File Source	:	Acquired on MASPEC II system [II32/9922] as C:\Program Files\Mass Spec\Data\LRGC\10\10010801.ms2
File Title	:	Shuai Zhou SZ100107 [Veinot]
Instrument	:	MS50 B
Notes	:	1µL spless on 30m ZB-5MS 35° (1m) -> 290°(20m) @10°/m Dx Source ; 500µA ; SEM 550 ; 1s/dec ; NF ; 3kRP